REAL TIME SENSOR BASED

MOTION PLANNING

SOSODORO

NATIONAL UNIVERSITY OF SINGAPORE

2003

REAL TIME SENSOR BASED

MOTION PLANNING

SOSODORO

(B.S., ITB)

A THESIS SUBMITTED

FOR THE DEGREE OF MASTER OF ENGINEERING

DEPARTMENT OF MECHANICAL ENGINEERING

NATIONAL UNIVERSITY OF SINGAPORE

2003

Acknowledgment

I feel indebted to my supervisor Assoc. Prof. Marcelo H Ang Jr., without whom this work would not be possible. I would like to express sincere appreciation and gratitude to him for the guidance and invaluable advice. I am grateful to him for sharing knowledge that strengthens and widens my foundation in Mechatronics.

I am also grateful to Prof. Poo Aun Neow and Dr. Etienne Burdet for their generous advice, discussions, and suggestions.

I wish to express my special thanks to Mr. Yee Choon Seng, Ms. Xi Wei Ya, Ms. Ang, Ms. Ooi, lab. technicians, and all colleagues at the Control & Mechatronics Lab. and Center of Intelligent Products & Manufacturing Systems for their generous assistance, advice, and encouragement.

Least but not last, I dedicate this work for my beloved parents and my Allah for everything.

Table of Content

List of Tables

List of Pictures

Summary

Motion planning is one of the principal elements in a robotic system. It opens areas of interests especially when it is associated with sensor-based applications. Dedicated works mainly concern on global optimal solution using what so called on-line trajectory planners. The methods however often require massive computational power and thus limit its practical scope. A simpler optimality paradigm, i.e. kinematic optimality, opens possibility to study a more applicable sensor based motion planning profile. It also offers faster process and system optimality. The algorithms developed in this study apply conditionals to select the required motion parameter and are able to equivalently generate the optimal profile—trapezoidal trajectory profiles—in a reliable and low computational-cost algorithm. The simulations and experiments show satisfactory results on typical simple sensor based applications. This method is applicable for higher multidimensional systems.

Chapter 1

Introduction

1.1. Background

Sensor based applications enhance robotic functions. In sensor-based applications, the performed task is subject to external sensed conditions. Being able for sensing, a sensor-based robotic system is expected to perform desirable reactions against the sensed conditions. In recent continuous developments, many types of sensor are being augmented and implemented in robotic system [3, 8, 9, 10, 11] to extend the system capability and intelligence

Amidst numerous types of applicable sensor, the common required reaction of sensed conditions is motion. The desired motion can be, for example, avoiding obstacles or pursuing or preying targets. These applications have been studied for years as they are applicable in many useful scenarios like catching projectile/flying object, search and rescue, hazardous environment handling, or a classic industrial scenario where robots have to efficiently pick and place objects from/to moving conveyor system.

Thus, it is reasonable to consider motion planning as important part of the spatial sensing ability of a robot. With the expectation to perform or anticipate the sensory information, the robot to some extent should be intelligent and able to plan and generate the motion with respect to the sensed information. Therefore, beside the significance of sensory information process, the motion planning remains important in the way to generate the desired actions.

In a typical system, the motion planner lies on the upper control level of a robotic system. It provides calculated data for the lower control level or joint controller. The data become the reference or desired values for the lower control. Figure 1.1 shows a block diagram of the controller of a robotic system. For sensor-based system, the upper control might content the necessary algorithms to handle the sensory interactions including the motion-planning algorithm.

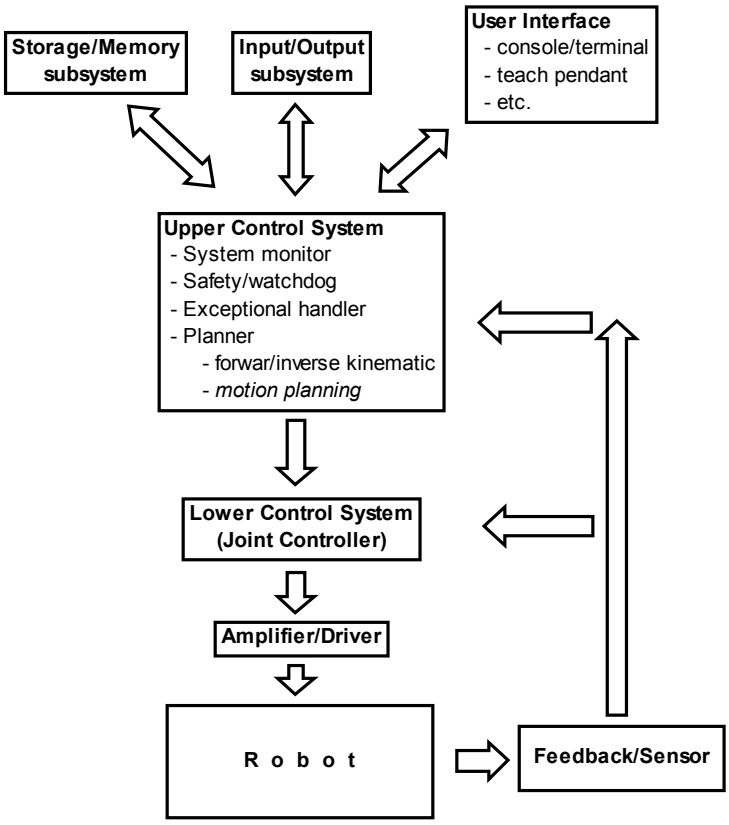

Figure 1.1 Typical components of robot control system

In many non sensor based applications, motion planning roles on pick and place application where the robot should move from designated initial point to a target point in one shot process stop to stop. In such action, the motion planning algorithm will calculate a set of discrete points imposing the desired motion from initial point to target point with zero boundary conditions. In contrast to this “one shot” planning procedure, in a sensor-based application, the target is dynamic and is updated at certain

intervals. Therefore although the final condition remains zero, the motion planning has to be able to accommodate the dynamic and arbitrary initial conditions.

Nevertheless, the motion must be acceptable and if possible it must be optimal. Further, as the information is continuously updated, the motion planning process has to be reliable and fast relative to refresh rate of the sensing process. The study presented here addresses the demand of fast reactive sensor based motion planning.

1.2. Related work

1.2.1. Motion Planning

Robot as it is defined in [12] imposes two subsystems: the mechanism capable to perform motion manipulation and the computer algorithm/controller capable to plan and control the motions. Either mobile or the fix-based manipulator type conforms to this definition.

Trajectory or motion planning as part of the robot's computer algorithm/controller has a basic function. It defines the trajectory connecting the initial and final position. Moreover, it may characterize how efficient and optimal a motion will be. Another formal definition of trajectory/motion planning, as stated in [28], is the algorithm for finding a suitable spatial or physical path without taking into account the dynamics of the system.

In common practices, trajectories are defined in Cartesian space or task space [4]. The controller will map the trajectory to the corresponding joint angles. Although the task space planning is desirable for its direct sensation to the user's view, for certain reasons and applications the joint space planning is also used as it is easier and satisfactorily applicable in many areas.

In contrast to pre-defined linear, circular, and spline path of CNC applications [1, 2], a

trajectory in robotics is defined with respect to the task. When the desired motion is a predefined path, the motion is called path constrained for example in welding, sealing, gluing, or spraying applications. When only initial and final points are considered it is called point to point motion. The study presented in this thesis is also regarding the point to point motion planning.

Although paths or trajectories of robots motion are often computed separately, by joining piecewise trajectories through some knots, it is possible to form curved paths. This method is useful in constructing a collision avoidance path like many works have addressed.

In general, the motion-planning process in robot controller can be described as follows. Given the initial and final point (and intermediate knots if applicable), the trajectory is calculated using certain profiler equations. The result of the calculation is a set of discrete points connecting initial and final points for each controller's sampling time step. Joint controllers will ensure that the actuator achieves this reference position at every time step. If it is desirable, the controller may also refer to the reference velocity information from the controller [34].

The productivity of a robotic working cell would correlate with time-optimal and efficient works. This optimality can be achieved by managing the task such to consume minimum energy input, cost, and time. Thus, the common objective of motion planning is to generate effective and efficient working motions.

Nevertheless, optimal motion should be generated subject to some actuator limitations such as allowable speed, acceleration, and jerk if applicable. Jerk, or torque rates [26], is the derivative of acceleration. For a given actuator limitation, the system is expected to plan a time-optimal motion within this limit. The importance of the limitation is obvious. From the design view, violations of the limit introduce uncertainties to the

performance measurements. Whereas from a practical or maintenance view, the over-limit usages, in long term end, will become unexpected cost and time losses.

1.2.2 Optimality issue

Robotic manipulators have become common in recent automated working cell, and there are always great interests of performance improvements. To achieve this optimality question, the system has to be well programmed. The implementation can be done in different strategy such as energy optimality algorithm, action optimality, etc. However, mostly the common way is through time optimality [27].

Although many problems of robot motion/trajectory planning have been addressed in [35], the subject is still becoming an area of considerable interest and importance. Other authors like [36, 37] also describe novel discussions on motion planning problems. Reducing the movement time within system limitation/capabilities to obtain optimal motion is also still a challenging problem as theoretically there are no single solution for realizing a motion from one point to the target point. Many authors have worked on time optimal motions problems, like [16 – 28, etc.].

Optimal trajectory planning is also challenging because of the complexity due to the fact that typical manipulators are coupled multi-body systems resulting in highly nonlinear dynamic system. This complexity increases exponentially with the number of degrees of freedom. Despite the demand of solid computational resources for finding the solution, this dynamic analysis is desirable because it offers a complete system solution. However, linearization and other simplified model-based approaches have been used to include the dynamics. As a result, it will respectively rely on the accuracy of the model used.

In their works, many researches proposed the dynamic optimization problems using

numerous techniques and systems, for example [17, 18, 21, 34] proposed the optimization of commercial controllers. Most of the proposed methods applied optimization of parameterized trajectory techniques that are earlier introduced by Bobrow [16]. Some authors combined the technique with evolutionary search algorithm, for example [25, 30]. Constantinescu *et al*. [26] focuses the improvement of smoothness of trajectory for motion planner in typical industrial manipulators by ensuring a bounded jerk throughout motions. Bailin *et al*. [22] also proposed the same improvement, however, as a trade off, travel time or movement time is not considered anymore.

Research in optimal trajectory planning mostly falls into two categories. The first type involves optimal trajectory planning along a prescribed path like the one proposed by Shin and McKay [29] and furthered by many others such as [16, 20, 22, 24, 26]. And the second type is to find the optimal trajectory for a common point to point motion like in [19, 21, 30, 34, 38, 39].

The proposed methods mostly use a bang-bang time optimal solution and expect saturation of at least one joint actuator [26]. The solution often becomes problematic due to violations of actuator operational limitations/bounds especially on torque rate or jerk. Therefore it appears that additional works are still required to ensure smoothness.

Those mentioned authors proposed the solution of the problem by concerning the dynamics of the manipulator. Although the solution can be considered as a complete and global solution, it has been found that the dynamic complexity has brought a remarkable computational burden. This computational problem makes the solution applicable only at off-line level. A simplified algorithm involving dynamics, which is proposed by Lin *et al*. [31] using cubic-based path approximation, still brings hefty computation because it needs to keep acceleration continuity within a dynamic

formulation. At the end the method may only applicable at off-line level as well.

In an effort to develop online algorithm involving system dynamics, Miro [34] used industrial controllers for optimal trajectory planning. However, the work only concerns on optimization of tractability to maximize system utility while the kinematic constraints are neglected.

To be more practical, it appears that a simpler approach can be acceptable where the dynamics are not highlighted. As actuators have physical limitations like maximum speed, maximum acceleration, and maximum torque, it will be simpler and more practical if the solution is based on purely the kinematic restrictions. The similar approach will be also applicable in Cartesian space planning, i.e. using corresponding Cartesian kinematic bounds. The solution will be kinematically optimal. This simpler perspective is also preferred in industrial applications [40]. As is proven later, kinematical optimization also offers much faster computation resulting in cheaper systems; which also makes it suitable for sensor-based applications.

1.2.3 Sensor based application

Meanwhile, recent applications such as medical robotic, mobile system, etc., dictate sensor-based systems. Sensors give feedback information for the system. By utilizing the feedback, the system is expected to be more intelligent by allowing reactions against the sensed conditions.

The sensor-based applications open problems for motion planning. Many authors, such as [42, 43], have been interested and working on mobile system motion planning where sensory behaviors in large spatial arena are likely more representing the need of sensory interactions. Most of the works are on the system navigation and finding a safe path through a cluttered environment, harsh terrain, or amid dynamic objects. For fix-

based manipulators, problems of avoiding obstacles have also been researched earlier using techniques like configuration space and search algorithms [44, 45, 46]. Instead of this obstacle avoidance problem, concern has also been addressed for manipulator interception or rendezvous problems [48, 61, 62, 40, 49, 50, 51, 64] using either variant methods of Prediction-Planning-Execution—which is mostly used—or the Navigation Guidance.

A principal consideration in a sensor-based system is computation time. Motion planner algorithms for sensor-based systems have to be fast relative to sensor's refresh rate. The fast algorithm will allow real time responses. It is found in the mentioned works, that fast calculation is mostly achieved by incorporating simple calculation, simplified optimality criteria, and the use of common joint trajectory profiler.

1.2.3.1 A view on common profiles: cubic, quintic, and trapezoidals

There have been many works in the area of smooth trajectory profile generation [16, 22, 26, 58, 59]. Widely known and used profiles are: polynomial types, i.e. cubic, quintic; and blend types, i.e. trapezoidal velocity, trapezoidal acceleration [3, 5]. Chand *et al.* [59] used another polynomial spline to interpolate joint target, however jerk is not considered. Very few works use quartic. Chang *et al.* [60] used a quartic spline to approximate path or path tracking; however, the method requires advance knowledge of the path. Piecewise cubic is used in [16, 22] to obtain a smooth off-line time optimal constrained path trajectory. Cubics have also shown satisfactory results in an application of characterizing a bounded deviation path [52].

For online applications, Tondu use three piecewise cubics to characterize optimal online joint trajectory profiles under several constraints [40]. Although the method allows fast computation, it is still not reactive in the sense that the trajectory is not re-

planned and executed in real-time but rather to wait the previous planned motion completion. The method also permits overshoots or oscillation tendency of polynomials—some call it wandering—and even utilizes it as a constraint parameter. Jerk is also not considered in the proposed method.

Although higher degree polynomials tend to easily oscillate, quintic is still a preferable choice. For online applications, especially for visual control/coordination or interception applications, many have used it despite some underlying considerations. Andersson uses quintic for the impressive experiment of visual coordination in the robotic ping-pong player [61]. The algorithm is based on a predictive method to *a priori* known hit planes, thus adapting tolerances of the final points, and the motion planning practically is a stop to stop quintic. The method thus to some extent could not be considered as real-time reactive motion generation. Buttazzo uses a better strategy to realize real-time reactive action for the robotic mouse buster [62]. The algorithm allows quintic-based trajectories to be re-planned within motions for a continuous sensor-based prediction. Croft *et al.* improved the prediction strategy to obtain optimal and smooth preying motion while implementing the same quintic re-planning method [49, 26, 48, 47]. However, regarding to the predictive algorithm that is used by both authors, the on-line re-planning strategy is only applicable for small and determined target changes. On another development of an online quintic profiler, Macfarlane and Croft improved the smoothness using a bounded jerk point to point planning method [54] but still for small target changes. Earlier, Lin *et al.* [50] also proposed reactive motion planner based on a quintic profiler. But, optimality is not considered in their work.

Quintic appears to have a better smoothness characteristic. Thus it is a preferable choice for certain application such as to minimize the effect of the dynamics of flexible

or elastic components [53]. As another example of application, Guarino *et al.* [57] used quintic to minimize and optimize the curvature variability of the steering curve for a mobile system.

The fast trapezoidal profile is commonly used in industrial robots [14, 17, 18, 21]. As another application example, a force-torque sensor-based excavating system in [63] uses a trapezoidal velocity profiler to get fast excavating trajectories. Wikman *et al.* [46] proposed their collision free reflex control algorithm also by incorporating a trapezoidal velocity profiler to obtain fast reactions. The main weakness of the works is the jerky and non-smooth motions. Nam and Oh used a novel reactive phase resolved trapezoidal profiler algorithm for a visual servoing system [55]. However, the canonical algorithm in their method still requires high computation as a result of complex phase resolutions to obtain a smooth and optimal trajectory.

1.2.3.2 Summary

The mentioned common profilers and the proposed algorithms have proven their essential advantages one over another. It rather becomes trivial to choose the preferred one especially in context with on-line applications. It is desirable to have a clear comparative analysis over several relevant performance measures. Further the demand of low computational cost, fast, and reactive motion planner seems still has not found a satisfactory answer. The identified problems of adapting the large target position change, the tendency of oscillation or wandering of higher order polynomials, the efficient computations, smoothness, and optimality still remain as open problems for a typical reactive real-time sensor-based system.

Earlier development [15] although has proven a satisfactory performance on a visual servoing application, this however, still encountered computational problems. This

work improves the computation/algorithm flow and tries to achieve better accuracy.

1.3 Objectives, Scope, and Methodology

The objective of this work is

- to study motion or trajectory profile characteristics especially in correlation with reactive sensor-based motion planning applications.
- to develop a suitable fast reactive sensor-based motion planning algorithm that is able:
    - to perform tasks of reaching static or dynamic target with zero velocity and zero acceleration
    - to react fast, and smoothly, at any time to a large change of target position
    - to conform to velocity and acceleration bounds, and jerk bound if applicable,
    - to apply in multidimensions, either in joint space or task space applications.

The work covers analysis and synthesis for an optimal motion planning algorithm subject to kinematic constraints, i.e. maximum velocity, maximum acceleration, and maximum jerk. Thus the dynamics of system is not considered. A multi dimensional application involving 6 DOF is implemented at simulation level using graphical user interface.

The algorithm development began with the comparison and analysis of one-dimension trajectory profilers that are commonly used in motion planning. The comparison provides references for a preferable profile. Trapezoidal profiles are found to excel other profiles especially in correlation with reactive sensor based applications. The

developed motion planning algorithms thus are based on trapezoidal profiles. Prior to the experiments on real systems, simulations are done for one and multi dimensional arrangements to verify planner performance and to find out better strategies such as scaling or coordinated axis algorithms. Although actual implementation in a fully articulated sensor-based robotic system is beyond this work, simulations and experiments on other platform show effective results for typical fast reactive and accurate sensor based applications [65].

1.4 Summary of Contribution

The motion planner is designed to be suitable for target tracking application in sensor-based systems that need fast and reactive behavior with good accuracy. The critical analysis provides a clear comparison between polynomial and trapezoidal type profilers. Each has distinguishing advantages over the other as well as disadvantages for on-line sensor based applications.

1.5 Outline of Thesis

The first chapter describes introduction to the work, covering background and related works. Prior to the algorithm development, a critical analysis and comparison of common profiles is presented in Chapter Two. Base on the findings in Chapter Two, the fast reactive sensor based motion planning algorithm is developed and detailed in Chapter Three. Chapter Four and Chapter Five cover the simulation and experimentation of the developed algorithm. Chapter Six summarizes and concludes the work.

Chapter 2

Critical Analysis of Motion Planner Profiles

Prior to the development and analysis of the fast reactive motion planner, an analysis and comparison of motion planner profiles is presented here to study the characteristics of motion profiles especially in correlation with reactive properties. Earlier, Park [56] proposed a comparison and analysis of features. However the interest is on energy efficiency and particularly only addressing repetitive point to point motions.

The profiles that will be discussed in this chapter are those which are commonly used in joint trajectory profiles, i.e. cubic, quintic, trapezoidal velocity, and trapezoidal acceleration. The profiles are analyzed under several performance measures. The objective is to find one which is fast, optimal under certain kinematic measures, having low computation cost, and reliable for a sensor based motion planner algorithm.

The analysis presented here will be restricted to point to point profiles. There are two point to point conditions that will be analyzed: zero to zero condition and non-zero to zero condition. A zero to zero condition conforms to a stop to stop scenario whereas a non-zero to zero reflects the dynamic motion planning where the motion starts from a nonzero initial condition and eventually to a stop position when the target achieved. The second condition imposes a reactive motion planning of sensor based application.

2.1 Point to Point

Point to point motion planning is a procedure of planning a trajectory to move from an initial position at $t = 0$ to a desired final position at $t = T$ by only considering initial and

final state (velocity and acceleration). As the motion eventually stops, the final velocity and acceleration are zero. By associating q as displacement and T as movement time, the position and velocity at initial and final point can be written as:

$$q(t)|_{t=0} = q_0 = 0 \qquad ; q(t)|_{t=T} = q(T) = q_f \tag{2.1}$$

$$\dot{q}(t)\big|_{t=0} = v(t)\,|_{t=0} = v(0) \qquad ; \dot{q}(t)\,|_{t=T} = v(t)\,|_{t=T} = v(T) = 0 \tag{2.2}$$

and then considering the acceleration, it will be

$$\ddot{q}(t)\,|_{t=0} = a(t)\,|_{t=0} = a(0) \qquad ; \ddot{q}(t)\,|_{t=T} = a(t)\,|_{t=T} = a(T) \tag{2.3}$$

Thus, for zero to zero motion, the conditions required are

$$v(0) = 0, \quad v(T) = 0$$

$$a(0) = 0, \quad a(T) = 0$$

and for nonzero to zero the conditions required are

$$v(0) = v_s, \quad v(T) = 0$$

$$a(0) = a_s, \quad a(T) = 0$$

where the s symbol denotes “start”. To fulfill the boundary conditions and obtain a considerable smoothness, higher order polynomial types like cubic and quintic polynomials or a constructed blend type like trapezoidal velocity or trapezoidal acceleration profiles can be used to generate the trajectory profile.

In an objective of optimality and efficiency, trajectories should be generated at a shortest move time T while satisfying the practical limitations of the actuators, i.e. maximum velocity v, maximum torque/force. As torque/force is proportional to acceleration, it can be associated to the maximum acceleration a. In addition, it is an established knowledge that limiting the jerk in manipulator trajectories is important for reducing wear and improving the motion [5, 54, 66]. Although jerk is not a nominal practical limitation of actuators, if applicable, it is preferably bounded to a desirable

maxima $\dddot{q}(t) = j$.

2.2 Measures

The trajectory profiles will be compared using several measures, i.e. movement time, total jerk, total energy/acceleration, velocity characteristics, and computation cost.

- Movement time (T)

Movement time is the needed time to achieve final position.

- Total jerk

Total jerk along a trajectory is defined as

$$\int_0^T | j(t) | dt$$

This integration represents motion smoothness. Motion smoothness practically affects life-time performance of actuators. Yet it is also a problem of accuracy since high jerks at the boundaries will affect tractability or result in undesirable vibrations [22, 47, 48, 28].

- Total energy

Total energy is the amount of energy consumption along the motion. Although exact total energy should be integrated from electrical current drawn by actuators, but considering that

$$E \text{ (energy)} \sim \int |I(t)|\, dt \quad \text{(electrical current)}$$

$$\sim \int \tau(t)\, dt \quad \text{(torque)}$$

$$\sim \int |a(t)|\, dt$$

the total energy also proportional to the total area under the acceleration curve [22]. Hence total energy measure can be represented by

$$\int_0^T | a(t) | dt$$

- Velocity

This measure describes velocity characteristics along the trajectory for each profile type.

- Computation cost (more relevant for reactive motion, i.e., for nonzero to zero condition)

The motion planning algorithm calculates the desired points for every time step. Computation cost may not become a problem for recent digital control system but as the degree of freedom of the system scales up, the higher computation cost may corrupt the overall system performance. This measure will figure how intensive the calculation of each profile algorithm is. The cost is based on the number of summation and multiplication operations in each algorithm. Floating point and integer operations are considered to be similar. Logical expressions are considered as summation. Although square root or rational exponent computation actually requires great numbers of step, for simplification reason it is considered to be equivalent with multiplications.

In correlation with computation cost, reliability (or flexibility) is also observed. Reliability means the ability of the algorithm to maintain trajectories continuity with any initial state without violating the given limitations. Practically only velocity and acceleration continuity are concerned. To be able to track the target at any moment, with a current state, the new trajectory must be immediately re-planned and executed regardless to the previous planned trajectory. The measure of computation cost also includes the steps to ensure this reliability feature.

2.3 Trajectory profiles

The profiles that will be discussed are cubic, trapezoidal velocity, quintic, and trapezoidal acceleration. At first, to know the characteristic of each profile, the

following subsections discuss a **zero to zero** condition.

2.3.1 Cubic

Using cubic or third order polynomial

$$q(t) = c_0 + c_1 t + c_2 t^2 + c_3 t^3$$

where c_0, c_1, c_2, and c_3 are the coefficients and t is the time parameter, one can obtain a smooth trajectory profile connecting the starting point and the final/target point. By considering equations (2.1) and (2.2) under a zero to zero condition, the corresponding motion equations become

$$q(0) = c_0 = 0 \tag{2.4}$$

$$q(T) = c_0 + c_1 T + c_2 T^2 + c_3 T^3 = q_f \tag{2.5}$$

$$\dot{q}(0) = v(0) = c_1 + 2c_2 t + 3c_3 t^2 \Big|_{t=0} = 0 \tag{2.6}$$

$$\dot{q}(T) = v(T) = c_1 + 2c_2 T + 3c_3 T^2 = 0 \tag{2.7}$$

Hence the coefficients c_0, c_1, c_2, and c_3 can be solved, i.e.

$$c_0 = 0, \quad c_1 = 0, \quad c_2 = \frac{3q_f}{T^2}, \quad c_3 = -\frac{2q_f}{T^3}$$

Hence the completed trajectory equations are

$$q(t) = q_f\left(\frac{3}{T^2}t^2 - \frac{2}{T^3}t^3\right) \tag{2.8}$$

$$\dot{q}(t) = v(t) = q_f\left(\frac{6}{T^2}t - \frac{6}{T^3}t^2\right) \tag{2.9}$$

$$\ddot{q}(t) = a(t) = q_f\left(\frac{6}{T^2} - \frac{12}{T^3}t\right) \tag{2.10}$$

Once T is known, the trajectory profile can be computed. A typical cubic profile is shown in Figure 2.1.

For a given kinematic bounds with the maximum velocity v and maximum acceleration a, it is possible to find the move time T. Having symmetrical properties of zero to zero condition, v will be achieved at $t = ½ T$. Substitution of this condition to (2.9) will give

$$T = \frac{3q_f}{2v}$$

On the other hand, as maximum acceleration a may only be achieved at $t = 0$ or $t = T$, substitutions to (2.10) will give

$$T = \sqrt{\frac{6q_f}{a}}$$

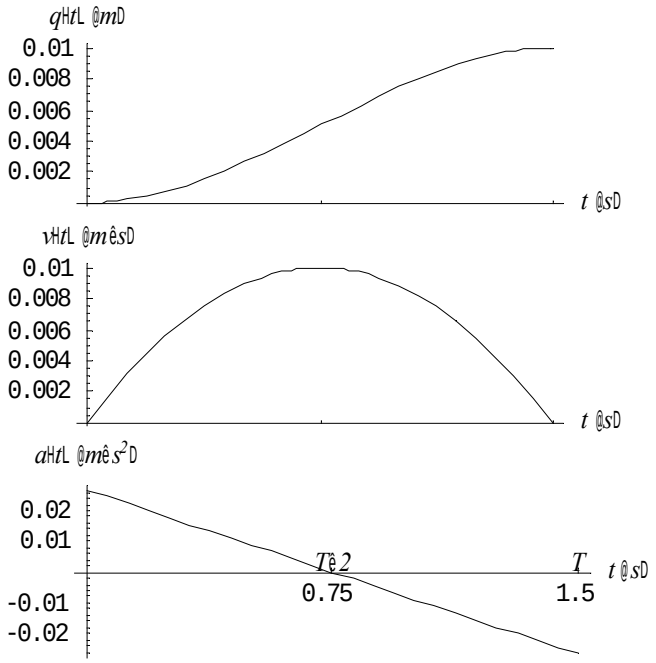

Figure 2.1 Typical zero to zero cubic profile for a distance $q_f = 0.01$ m, kinematic bounds $v = 0.01$ m/s, and $a = 0.2$ m/s^2. In this case the move time $T = 1.5$ s is subject of v.

It is shown that each bound gives a different solution for T. Therefore for given kinematic bounds, the move time T that maintains the limit is the maximum between the two, i.e.

$$T = \max\left(\frac{3q_f}{2v}, \sqrt{\frac{6q_f}{a}}\right) \tag{2.11}$$

Hence, it is also obvious that for a set of given bounds cubic will only satisfy one.

For the jerk analysis of the zero to zero condition, despite a constant acceleration derivative with a value $\dddot{q}(t) = -12\, q_f / T^3$, the jerk value is infinite at the boundaries, i.e. at initial and final points. As it is shown in Figure 2.1, the acceleration at these points is not zero. This condition imposes discontinuity of acceleration profile or infinite jerks, and thus the total jerk for zero to zero condition is indefinite.

$$j(t) = \infty \quad , t = 0 \text{ and } t = T \tag{2.12}$$

The energy measure for the zero to zero condition can be derived from total integration of (2.10) or the total area of acceleration curve, i.e.

$$\int_0^T |a(t)|\, dt = 2 \int_0^{T/2} |a(t)|\, dt = 2v(t)|_{t=T/2} = 2v \tag{2.13}$$

The velocity profile of cubic is a quadratic function. For the symmetrical zero to zero condition, the maximum velocity v will be reached at $t = ½\ T$, i.e. when $a(t) = 0$.

2.3.2 Trapezoidal velocity

This trajectory planner type is also known as linear function with parabolic blends [5]. The parabolic portions correspond to the constant acceleration and deceleration phases, i.e. the first and third phases of three phases of motion. The acceleration and deceleration has the same magnitude but with opposing sign. The typical profile for a distance q_f and movement time T is as shown in Figure 2.2.

With the maximum velocity bound v and the maximum acceleration bound a as shown in Figure 2.2, the trajectory can be divided into three phases:

- at $0 \le t \le t_1$, the constant acceleration phase with

  $v(t) = v_0 + a\, t$

  $q(t) = q_0 + ½\ a\, t^2$

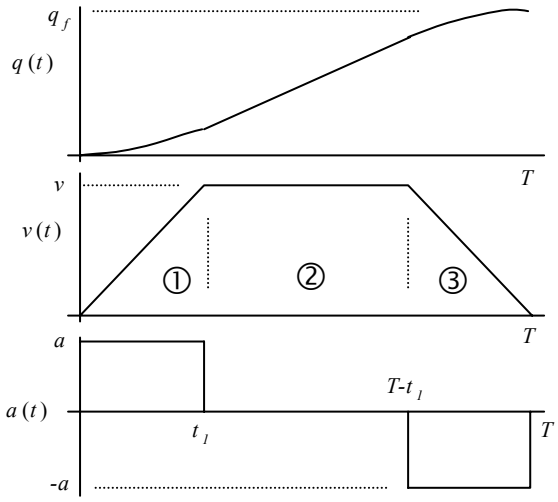

Figure 2.2 Typical trapezoidal velocity profile. The profile can be segmented into three phases, 1, 2, and 3.

By taking $v_0 = 0$ and $q_0 = 0$, the velocity and position equation at $t = t_1$ will give

$$t_1 = \frac{v}{a} \tag{2.14}$$

$$q_1 = ½\, a\, t_1^2 = v^2/2\, a \tag{2.15}$$

- at $t_1 < t \le T–t_1$, the cruising phase or constant velocity phase with

$$v(t) = v$$

$$q(t) = q_1 + v\,(t - t_1)$$

therefore at $t = T–t_1$

$$q_2 = v^2/2\, a + v\,(T–2t_1) \tag{2.16}$$

- at $T–t_1 < t \le T$, the constant deceleration phase with

$$v(t) = v – a\,(t – (T – t_1))$$

$$q(t) = q_2 + v(t – (T–t_1)) – ½\, a\,(t – (T–t_1))^2$$

and therefore at $t = T$ the velocity and position equation will give

$$0 = v – a(T – (T–t_1)) \tag{2.17}$$

$$q_f = q_2 + v^2/2\, a \tag{2.18}$$

Thus, equations (2.15-17) will give

$$T-(T-t_1)=t_1=\frac{v}{a} \tag{2.19}$$

$$(T-2t_1)=\frac{q_f}{v}-\frac{v}{a} \tag{2.20}$$

Hence, movement time T for a typical zero to zero condition is

$$T=t_1+(T-2t_1)+t_1=\frac{q_f}{v}+\frac{v}{a} \tag{2.21}$$

and correspondingly the position is given by

$$q(t)=\begin{cases}\frac{1}{2}a\,t^2 & ;\ 0<t\le t_1 & ;\ (\text{constant accel.},a)\\ \frac{v^2}{2a}+v(t-t_1) & ;\ t_1<t\le T-t_1 & ;\ (\text{constant velocity},v)\\ -\frac{v^2}{2a}+v\,t-\frac{1}{2}a(t-T+t_1)^2 & ;\ T-t_1<t\le T & ;\ (\text{constant decel.},-a)\end{cases}$$

It is shown from (2.21) that both bounds v and a will directly determine T. For this reason, the motion will be realized as fast as possible satisfying both bounds.

However, like cubic, there are acceleration discontinuities at the boundaries and also at $t = t_1$ and $t = T–t_1$. This discontinuity corresponds to indefinite jerk.

$$j(t)\ =\infty \quad ,\ t=0,\ t=t_1,\ t=T-t_1,\ t=T \tag{2.22}$$

The energy measure for zero to zero condition can be obtained from the integration of the acceleration profile

$$\int_0^T|\,a(t)\,|dt=\int_0^{t_1}|\,a(t)\,|\,dt+\int_{t_1}^{T-t_1}|\,a(t)\,|\,dt+\int_{T-t_1}^{T}|\,a(t)\,|\,dt$$

$$=a\,t_1+0+a\,t_1$$

$$=2v \tag{2.23}$$

As another illustration, Figure 2.3. shows a profile for given kinematic bounds $v = 0.01$ m/s, and $a = 0.2$ m/s^2. The acceleration and deceleration phase has linear velocity slope a and $–a$. The maximum velocity v will be achieved at $t = v/a$.

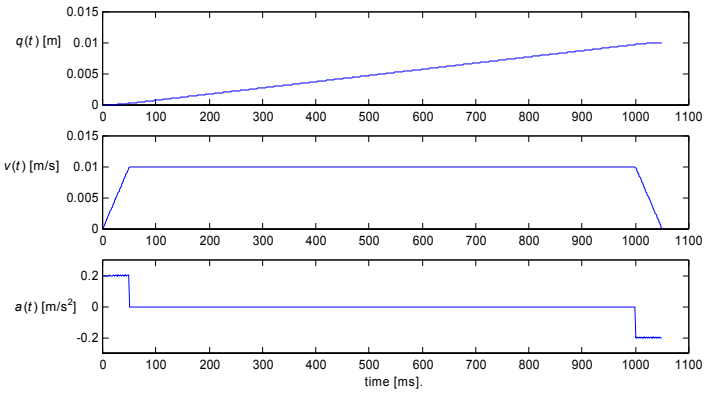

Figure 2.3 Trapezoidal velocity profile for distance q_f = 0.01 m, and kinematic bounds v = 0.01 m/s, a = 0.2 m/s^2. Move time T = 1.05 s.

There is a particular/special condition for further consideration. If q_f is a short distance then the constant velocity phase may be reached, that is when $(T - 2t_1) \leq 0$ or $q_f \leq v^2/a$. Figure 2.4 illustrates the two phase condition with triangle velocity profile. In this short distance condition the analysis of movement time T of the two phase motion becomes as follow.

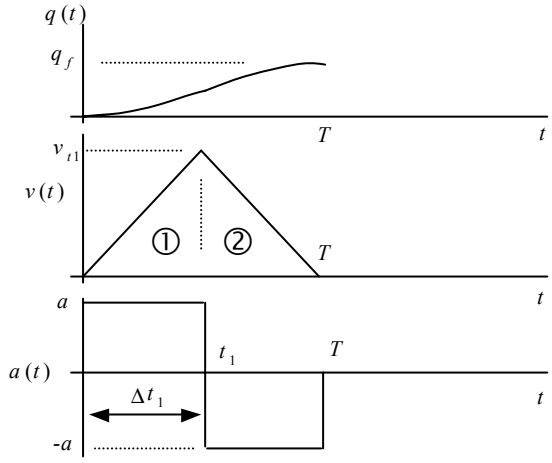

Figure 2.4 Trapezoidal velocity profile for short distance. Two phases, 1 and 2, now compose the motion.

- At $0 \leq t \leq t_1$ it has constant acceleration phase with

$$v(t) = v_0 + a\,t$$

$$q(t) = q_0 + \tfrac{1}{2}\,a\,t^2$$

Taking $v_0 = 0$ and $q_0 = 0$, the velocity and position equation at $t = t_1$ will give

$$t_1 = v_{t1}/a \tag{2.24}$$

$$q_1 = \tfrac{1}{2}\, a\, t_1^2 = (v_{t1})^2/2\, a$$

- At $t_1 < t \le T$ it has constant deceleration phase with

$$v(t) = v_{t1} - a\,(t - t_1)$$

$$q(t) = q_1 + v_{t1}\,(t - t_1) - \tfrac{1}{2}\, a\,(t - t_1)^2$$

and therefore at $t = T$

$$0 = v_{t1} - a(T - t_1) \quad \text{or} \quad T - t_1 = v_{t1}/a = t_1$$

$$q_f = q_1 + (v_{t1})^2/2\, a = (v_{t1})^2/a$$

Hence,

$$T = 2t_1 = 2\, v_{t1}/a \quad \text{or} \quad v_{t1} = \tfrac{1}{2}\, a\, T$$

and

$$q_f = \tfrac{1}{4}\, a\, T^2$$

Thus the motion time T is,

$$T = 2\sqrt{\frac{q_f}{a}} \tag{2.25}$$

and correspondingly the position is given by

$$q(t) = \begin{cases} \frac{1}{2} a\, t^2 & ;\ 0 < t \le t_1 \quad ;\ (\text{constant accel.}, a) \\ -q_f + 2\sqrt{a\, q_f}\ t - \frac{1}{2} a\, t^2 & ;\ t_1 < t \le T \quad ;(\text{constant decel.}, -a) \end{cases}$$

For the total jerk measure, since the acceleration profile remains discontinuous, then it is obvious that the total jerk is infinite as in (2.22). Whereas, the energy measure can be expressed as

$$\int_0^T |\, a(t)\, | dt = 2 \int_0^{t_1} |\, a(t)\, |\, dt \ = 2a\, t_1 \ = \ 2 v_{t1}$$

Hence, principally the last two measures remain similar as in the common/typical profile.

2.3.3 Quintic

Quintic or fifth order polynomial is another polynomial that is commonly used to generate smooth trajectories. The quintic polynomial can be written as

$$q(t) = c_0 + c_1 t + c_2 t^2 + c_3 t^3 + c_4 t^4 + c_5 t^5$$

With a zero to zero condition of (2.1–2.3), and regarding to the following derivatives

$$\dot{q}(t) = v(t) = c_1 + 2c_2 t + 3c_3 t^2 + 4c_4 t^3 + 5c_5 t^4$$

$$\ddot{q}(t) = a(t) = 2c_2 + 6c_3 t + 12c_4 t^2 + 20c_5 t^3$$

$$\dddot{q}(t) = j(t) = 6c_3 t + 24c_4 t + 60c_5 t^2$$

there will be six equations for six unknown coefficients with one parameter (T). With this set of equations and unknowns the coefficients can be solved, e.g..

$$c_0 = c_1 = c_2 = 0 \;;\; c_3 = \frac{10q_f}{T^3} \;;\; c_4 = -\frac{15q_f}{T^4} \text{ ; and } c_5 = \frac{6q_f}{T^5}$$

Hence, for the zero to zero condition, the complete motion equations become

$$q(t) = q_f\left(\frac{10}{T^3}t^3 - \frac{15}{T^4}t^4 + \frac{6}{T^5}t^5\right) \tag{2.26}$$

$$\dot{q}(t) = v(t) = q_f\left(\frac{30}{T^3}t^2 - \frac{60}{T^4}t^3 + \frac{30}{T^5}t^4\right) \tag{2.27}$$

$$\ddot{q}(t) = a(t) = q_f\left(\frac{60}{T^3}t - \frac{180}{T^4}t^2 + \frac{120}{T^5}t^3\right) \tag{2.28}$$

$$\dddot{q}(t) = j(t) = q_f\left(\frac{60}{T^3} - \frac{360}{T^4}t + \frac{360}{T^5}t^2\right) \tag{2.29}$$

Like in cubic analysis, the move time T is required to generate the trajectory. The symmetrical property dictates that the maximum velocity bound v will be reached at $t = ½\ T$. Substitution of this condition to (2.27) gives

$$v = \frac{15q_f}{8T} \qquad \text{or} \qquad T = \frac{15q_f}{8v}$$

On the other hand, the maximum acceleration bound a is reached when jerk expressed

by (2.29) is zero. By solving this zero jerk condition, the time of maximal acceleration can be found, i.e.

$$t = \frac{3T \pm T\sqrt{3}}{6} \tag{2.30}$$

Substitution to (2.28) gives

$$a = \frac{10q_f}{T^2\sqrt{3}} \qquad \text{or} \qquad T = \sqrt{\frac{10q_f}{a\sqrt{3}}}$$

Likewise, it is possible to find T from the quadratic jerk function. The jerk is bounded and maximal at the boundaries, i.e. at $t = 0$ and $t = T$. Substitutions to (2.29) gives

$$T = \sqrt[3]{\frac{60q_f}{j}}$$

where j is the maximum jerk bound. Similar with cubic, each bound in quintic appears to give different solution of T. Therefore for a given kinematic bounds v, a, and j, the move time T shall be the maximum between the three, i.e.

$$T = \max\left(\frac{15q_f}{8v},\ \sqrt{\frac{10q_f}{a\sqrt{3}}},\ \sqrt[3]{\frac{60q_f}{j}}\right) \tag{2.31}$$

It is also obvious that the bounds can not be satisfied simultaneously. Figure 2.5 shows an example of quintic profile satisfying v bound. It would be a desirable to satisfy the bounds simultaneously in one motion planning; at least for velocity and acceleration bounds. In next few sections a proposed profile is discussed to meet this requirement.

By considering the maximum jerk at the boundaries, total jerk measure $\hat{U}|j(t)|dt$ can be computed from the integration of jerk curve, i.e.

$$\int_0^T |j(t)|\,dt = \int_0^{\frac{1}{6}(3T-T\sqrt{3})} |j(t)|\,dt + \int_{\frac{1}{6}(3T-T\sqrt{3})}^{\frac{1}{6}(3T+T\sqrt{3})} |j(t)|\,dt + \int_{\frac{1}{6}(3T+T\sqrt{3})}^{T} |j(t)|\,dt = 4a \tag{2.32}$$

On the other hand, the total acceleration measure for zero to zero condition can be derived from integration of (2.28), i.e.

$$\int_0^T |a(t)|\,dt = 2\int_0^{T/2} |a(t)|\,dt = 2\,v(t)\big|_{t=T/2} = 2v \qquad (2.33)$$

Velocity curve now is a quartic or fourth order polynomial and it will be smoother than cubic's. For zero to zero condition v will be reached at $t = ½\ T$, the time when $a(t) = 0$.

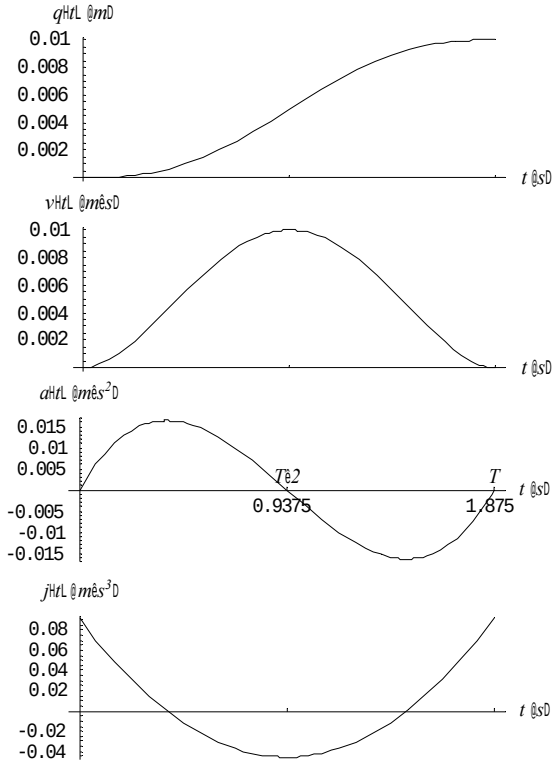

Figure 2.5 Typical quintic profile for distance $q_f = 0.01$ m, and kinematic bounds $v = 0.01$ m/s, and $a = 0.2$ m/s^2, and $j = 10$ m/s^3. In this case the move time $T = 1.875$ s is obtained using v criterion.

2.3.4 Trapezoidal acceleration

Another common jerk limited profile is the trapezoidal acceleration profile. By limiting the jerk of the trapezoidal velocity, it is possible to generate a smoother trajectory. As a result, the profile has seven segments, i.e. with additional four constant jerk phases. The typical motion profile is shown in Figure 2.6 and the following, similar approaches are applied to analyze phase segments.

- At $0 \le t \le t_1$ it has a constant jerk phase with $j(t) = +j$, therefore at $t = t_1$

$$t_1 = \frac{a - a_0}{j} = \frac{a}{j}$$

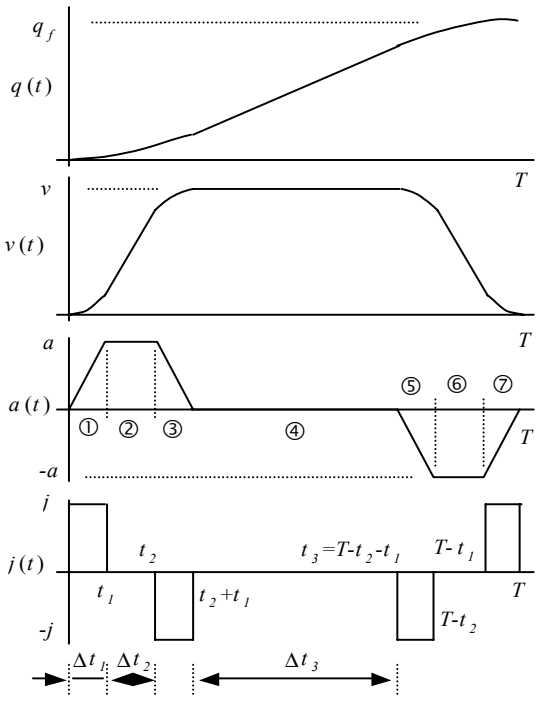

Figure 2.6 Typical trapezoidal acceleration profile. The profile can be segmented into seven phases, 1–7.

$$v_1 = v_0 + a_0 t_1 + {}^1\!/_2 j t_1^2 = {}^1\!/_2 j t_1^2 = a^2/2j$$

$$q_1 = q_0 + v_0 t_1 + {}^1\!/_2 a_0 t_1^2 + {}^1\!/_6 j t_1^3 = {}^1\!/_6 j t_1^3$$

$$= a^3/6j^2$$

- At $t_1 < t \le t_2$ it has a constant acceleration phase with

$$a(t) = a$$

$$v(t) = v_1 + a(t - t_1)$$

$$q(t) = q_1 + v_1 (t - t_1) + {}^1\!/_2 a(t - t_1)^2$$

and at $t = t_2$

$$v_2 = a^2/2j + a(t_2 - t_1) \tag{2.34}$$

$$q_2 = a^3/6j^2 + a^2(t_2 - t_1)/2j + {}^1\!/_2 a (t_2 - t_1)^2 \tag{2.35}$$

- At $t_2 < t \le t_2 + t_1$ it has a constant jerk phase with

$$j(t) = -j$$

$$a(t) = a - j(t - t_2)$$

$$v(t) = v_2 + a(t - t_2) - {}^1\!/_2 j(t - t_2)^2 \tag{2.36}$$

$$q(t) = q_2 + v_2(t - t_2) + {}^1/_2\, a(t - t_2)^2 - {}^1/_6\, j(t - t_2)^3 \tag{2.37}$$

and at $t = t_2 + t_1$

$$a(t) = a - j\, t_1 = 0; \quad \text{hence again } t_1 = a/j \tag{2.38}$$

$$v(t) = v_2 + a\, t_1 - {}^1/_2\, j\, t_1^2 = v \tag{2.39}$$

Substitution of (2.34) and (2.38) to (2.39) gives

$$(t_2 - t_1) = \frac{v}{a} - \frac{a}{j} \tag{2.40}$$

and accordingly v_2 and q_2 are

$$v_2 = v - a^2/2\, j \tag{2.41}$$

$$q_2 = \frac{v^2}{2a} - \frac{a\ v}{j} + \frac{a^3}{6j^2} \tag{2.42}$$

and then substitution of (2.40), (2.41), and (2.42) to (2.37) gives

$$q(t) = q_{21} = \frac{v^2}{2a} + \frac{a\ v}{2j} \tag{2.43}$$

- At $t_2 + t_1 < t \le t_3$ (note: $t_3 = T - t_2 - t_1$ due to its similarities/symmetrical with the first three phases) it has a constant velocity phase with

  $v(t) = v$

  $q(t) = q_{21} + v(t - t_2 - t_1)$

  and at $t = t_3$

  $q(t) = q_{21} + v\,(t_3 - t_2 - t_1)$

- Finally, since at $t_3 < t \le T$ the velocity and acceleration profile are symmetric with that of $0 < t \le t_2 + t_1$ then it is possible to express q_f as

  $q(T) = q_f = q_{21} + v\,(t_3 - t_2 - t_1) + q_{21}$

  Substitution of (2.43) will give

$$(t_3 - t_2 - t_1) = \frac{q_f}{v} - \frac{v}{a} - \frac{a}{j} \tag{2.44}$$

Hence for zero to zero condition the move time T is

$$T = [t_1 + (t_2 - t_1) + t_1] + (t_3 - t_2 - t_1) + [t_1 + (t_2 - t_1) + t_1] = \frac{q_f}{v} + \frac{v}{a} + \frac{a}{j} \qquad (2.45)$$

And correspondingly the seven phases of position $q(t)$ can be written as

$$q(t) = \begin{cases} \frac{1}{6} j t^3 & ; 0 < t < t_1 \\ & \text{(constant jerk, } + j) \\ \frac{a^3}{6j^2} + \frac{a^2}{2j}(t - t_1) + \frac{1}{2} a (t - t_1)^2 & ; t_1 < t < t_2 \\ & \text{(constant acc., } + a) \\ \left(\frac{v^2}{2a} - \frac{av}{2j} + \frac{a^3}{6j^2}\right) + \left(v - \frac{a^2}{2j}\right)(t - t_2) + & ; t_2 < t < t_2 + t_1 \\ \quad \frac{1}{2} a (t - t_2)^2 - \frac{1}{6} j (t - t_2)^3 & \text{(constant jerk, } - j) \\ \left(\frac{v^2}{2a} + \frac{av}{2j}\right) + v(t - t_1 - t_2) & ; t_2 + t_1 < t < T - (t_2 + t_1) \\ & \text{(constant vel., } + v) \\ \left(vT - \frac{3av}{2j} + \frac{3v^2}{2a}\right) + v(t - T + t_1 + t_2) - & ; T - (t_2 + t_1) < t < T - t_2 \\ \quad \frac{1}{6} j (t - T + t_1 + t_2)^3 & \text{(constant jerk, } - j) \\ \left(vT - \frac{av}{2j} - \frac{3v^2}{2a} - \frac{a^3}{6j^2}\right) + \left(v - \frac{a^2}{2j}\right)(t - T + t_2) - & ; T - t_2 < t < T - t_1 \\ \quad \frac{1}{2} a (t - T + t_2)^2 & \text{(constant dec., } - a) \\ \left(vT - \frac{a^2 v - 2jv^2 - av}{2aj} - \frac{4a^3 + 3a^2}{6j^2}\right) + & ; T - t_1 < t < T \\ \quad \frac{a^2}{2j}(t - T + t_1) - \frac{a}{2}(t - T + t_1)^2 + \frac{j}{6}(t - T + t_1)^3 & \text{(constant jerk, } + j) \end{cases} \quad \ldots$$

…..(2.46)

Similar with trapezoidal velocity, (2.45) shows that the kinematic bounds v, a, and j determine T value; and this indicates that the motion will be performed as fast as

possible satisfying all bounds. Obviously, the movement time T will be slightly longer than trapezoidal velocity as a trade-off for the sloped acceleration phases.

The jerk now is bounded, $\pm j$. The total jerk, i.e. integration of jerk curve area along the trajectory is

$$\int_0^T |\, j(t)\,|\, dt = 4\int_0^{t_1} |\, j(t)\,|\, dt = 4a \tag{2.47}$$

which is equal to quintic's total jerk in (2.32). The bounded jerk preserves a better motion smoothness.

The acceleration curve now has sloped phases before and after reaching constant phases. The total integration of this curve gives the acceleration (energy) measure

$$\int_0^T |\, a(t)\,|\, dt \;=\; 4\int_0^{t_1} |\, a(t)\,|\, dt + 2\int_{t_1}^{t_2} |\, a(t)\,|\, dt = \; 2v \tag{2.48}$$

The velocity curve is no longer trapezoidal. It is now smoother than trapezoidal velocity's as result of the bounded jerk. The maximum velocity bound v will be achieved at t = t_1+t_2 = v/a + a/j. As an example, Figure 2.7 shows a profile for given kinematic bounds v = 0.01 m/s, a = 0.2 m/s^2, and j = 10 m/s^2.

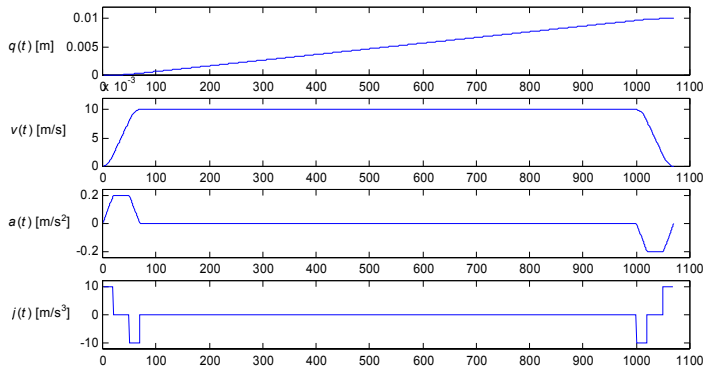

Figure 2.7 Trapezoidal acceleration profile for distance q_f = 0.01 m, and kinematic bounds v = 0.01 m/s, a = 0.2 m/s^2, and j = 10 m/s^3. Move time T = 1.07 s.

There are also particular/special conditions for further consideration. If the distance is relatively short then the phase composition may become different and so does the

movement time *T*. The possible conditions are the *six phases* and the *four phases* depicted in Figure 2.8 (a) and (b). The movement time analysis is discussed below.

– *Six phases*

When the distance is relatively short such that the maximum velocity bound *v* is not reached—refer to condition of the following (2.55)—, the constant velocity phase does not exist. Thus the motion is composed by six phases instead of typically seven phases. Refer to Figure 2.8(a), the analysis of movement time *T* for this six-phases motion becomes as follow.

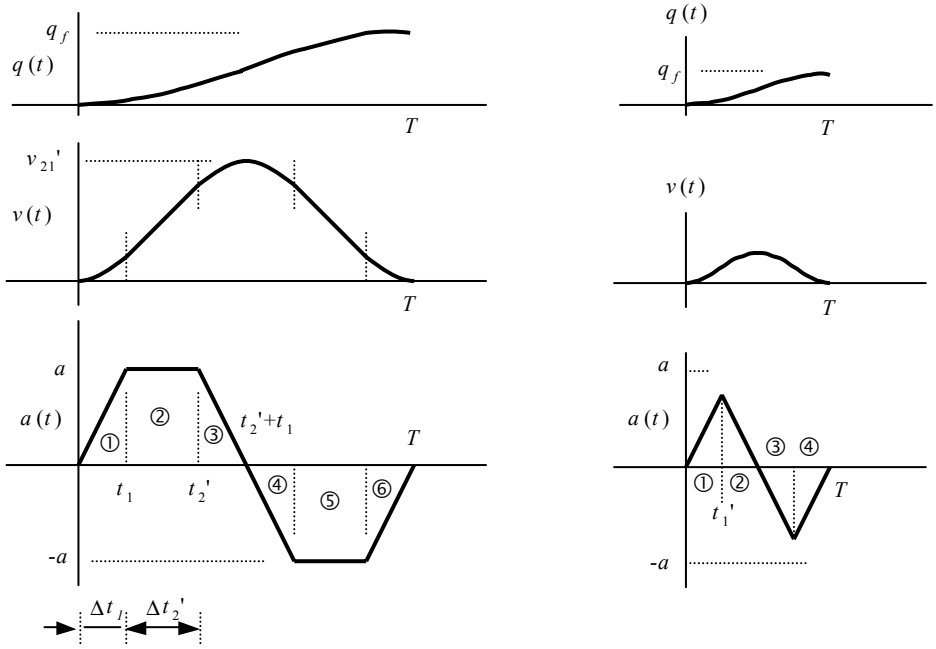

Figure 2.8 Special conditions of trapezoidal acceleration profile for short distance. Six phases motion (a), and four phases motion (b).

- At $0 \le t \le t_1$ similarly it has constant jerk phase $j(t) = +j$ and at $t = t_1$

  $a(t) = a = j\, t_1$, hence $t_1 = a/j$

  $v(t) = v_1 = a^2/2\, j$

  $q(t) = q_1 = a^3/6\, j^2$

- At $t_1 < t \le t_2$' it has constant acceleration phase, and at $t = t_2$'

  $$v(t) = v_2' = a^2/2\, j + a(t_2' - t_1) \qquad (2.49)$$

$$q(t) = q_2' = a^3/6\,j^2 + a^2(t_2' - t_1)/2\,j + {}^1/_2\,a\,(t_2' - t_1)^2 \tag{2.50}$$

- At $t_2' < t \le t_2' + t_1$ it has constant negative jerk $j(t) = -j$ and at $t = t_2' + t_1$

$$v(t) = v_{21}' = v_2' + a\,t_1 - {}^1/_2\,j\,t_1^2 \quad \text{or}$$

$$v_{21}' = a(t_2' - t_1) + \frac{a^2}{j} \tag{2.51}$$

and

$$q(t) = q_{21}' = q_2' + v_2\,t_1 + {}^1/_2\,a\,t_1^2 - {}^1/_6\,j\,t_1^3 \quad \text{or}$$

$$q_{21}' = \frac{3\,a^2}{2j}(t_2' - t_1) + \frac{a}{2}(t_2' - t_1)^2 + \frac{a^3}{j^2} \tag{2.52}$$

Due to the symmetrical property, the distance can be expressed as

$$q_f = 2\,q_{21}'$$

and it is a quadratic function of $(t_2' - t_1)$. The root of this quadratic function will be

$$(t_2' - t_1) = \frac{-3a^{3/2} \pm \sqrt{a^3 + 4j^2 q_f}}{2j\sqrt{a}} \tag{2.53}$$

from which T can be computed, i.e.

$$T = 2\,[t_1 + (t_2' - t_1) + t_1] = 2\left(\frac{a}{j} + \frac{-a^{3/2} + \sqrt{a^3 + 4j^2 q_f}}{2j\sqrt{a}}\right) \tag{2.54}$$

Equation (2.54) shows that the maximum velocity bound v is no longer determining the movement time T. Recalling (2.44) and (2.53), as the constant velocity phase does not exist and since there should be a constant acceleration phase, i.e. $(t_2' - t_1) \ge 0$, then the distance q_f should be

$$\frac{2a^3}{j^2} \;\le\; q_f < \;\; \frac{v^2}{a} + \frac{a\;\; v}{j} \tag{2.55}$$

The jerk is still bounded and the total jerk would be similar with (2.47). Whereas, the energy measure is

$$\int_0^T |a(t)|\,dt = 4\int_0^{t_1} |a(t)|\,dt + 2\int_{t_1}^{t_2} |a(t)|\,dt = 2v_{21}' \qquad (2.48)$$

– Four phases

When the distance is even shorter—as in (2.59)—, the constant acceleration phase may even be reached. Thus the motion is sufficiently realized in four phases. Referring to Figure 2.8(b), the analysis of movement time T for this four phases motion becomes as follows.

- At $0 \le t \le t_1$' similarly it has constant jerk phase $j(t) = +j$ and at $t = t_1$

  $a(t) = a_1' = j\,t_1'$, hence $t_1' = a_1'/j$

  $v(t) = v_1' = (a_1')^2/2j$

  $q(t) = q_1' = (a_1')^3/6j^2$

- At $t_1' < t \le 2t_1'$ it has constant negative jerk $j(t) = -j$ and at $t = 2t_1'$

  $a(t) = 0 = a_1' - j\,t_1'$, hence again $t_1' = a_1'/j$

  $v(t) = v_{21}' = v_1' + a_1'\,t_1' - {}^1/_2\, j(t_1')^2 = (a_1')^2/j$

  $q(t) = q_{21}' = q_1' + v_1'\,t_1' + {}^1/_2\, a_1'(t_1')^2 - {}^1/_6\, j(t_1')^3 = (a_1')^3/j^2$

Due to the symmetrical property, the distance can be expressed as

$$q_f = 2\,q_{21}' = 2(a_1')^3/j^2 \qquad (2.56)$$

and movement time T can be expressed as

$$T = 4\,t_1 = 4(a_1')/j \qquad (2.57)$$

From these last two equations, the relation between T and q_f under a given kinematic bounds is

$$T = \sqrt[3]{4\,j\,q_f} \qquad (2.58)$$

Further, as the constant acceleration phase no longer exist, i.e. $a_1' < a$, and recalling (2.56) it is easy to find the condition for q_f, i.e.

$$0 \le q_f < \frac{2a^3}{j^2}$$

The jerk is still bounded and the total jerk would be

$$\int_0^T |\, j(t)\,|\, dt = 4\int_0^{t_1'} |\, j(t)\,|\, dt = 4a_1'$$

Whereas, the energy measure is

$$\int_0^T |\, a(t)\,|\, dt \;=\; 4\int_0^{t_1} |\, a(t)\,|\, dt = \; 2v_1'$$

Hence the two measures for both special conditions are relatively similar with those of typical profile.

2.3.5 Summary of typical profiles for zero to zero condition

Table 2.1 below summarizes the analysis of four common motion planner profiles: cubic, trapezoidal velocity, quintic, and trapezoidal acceleration.

Measure	Cubic polynomial	Trapezoidal velocity	Quintic polynomial	Trapezoidal acceleration
Movement time (T)	$T = \max\left(\frac{3q_f}{2v}, \sqrt{\frac{6q_f}{a}}\right)$	$T = \frac{q_f}{v} + \frac{v}{a}$	$T = \max\left(\frac{15q_f}{8v}, \sqrt{\frac{10q_f}{a\sqrt{3}}}, \sqrt[3]{\frac{60q_f}{j}}\right)$	$T = \frac{q_f}{v} + \frac{v}{a} + \frac{a}{j}$
Total jerk	indefinite	indefinite	4 a	4 a
Energy	2 v	2 v	2 v	2 v
Computation cost	6 A, 37 M	22 A, 14 M	12 A, 93M	75 A, 128 M

Table 2.1 Comparison of performance of the four typical profiles with zero boundary conditions. 'A' represents equivalent addition/subtraction and 'M' represents equivalent multiplication operations.

From the table it is shown that the energy measure is the same for the four profiles. The jerk is infinite for cubic polynomial and the trapezoidal velocity profile, and 4a for the other two planners. Although there are different phase compositions for short distance trapezoidals, it has been shown that the main characteristics remain similar. Obviously the movement duration is larger for the trapezoidal acceleration than for the

trapezoidal velocity, and generally under the same maximum velocity criteria, larger for the fifth order polynomial than for the third order. It is important to note that the trapezoidal profiles are minimal time for the given kinematic bounds. The trapezoidal velocity profile requires less movement time than the cubic polynomial and the trapezoidal acceleration less than the quintic polynomial since both two trapezoidal planners are able to immediately reach the limit. For this reason, the trapezoidal type is kinematically time optimal. Next, the following section analyzes the remaining question about the reactive properties of the motion profiles.

2.4 Reactive motion

Reactive motion/response is a typical motion of a sensor-based system. Using sensory information the system ought to immediately react or perform desirable motion. Regardless of the previously planned motion, the system has to be able to plan and execute a new motion if required, provided with smooth transition. As a consequence, the new motion typically will begin from a non zero initial condition.

To preserve smooth transitions, the motion profiles have to maintain continuity. The continuity and smooth transition of position can be achieved by maintaining, at least, velocity continuity. Continuity of higher derivative order will preserve better smoothness accordingly [34].

In realizing this feature, the profile computation may not be as simple as in zero to zero condition. Typically the symmetrical property will no longer exist. This difference may lead to a more intensive and even to a very hefty computation.

2.4.1 Cubic

For nonzero initial condition with initial velocity $v_s = \dot{q}(0) \neq 0$, the velocity equation (2.6) will be

$$v(0) = v_s = c_1 + 2c_2 t + 3c_3 t^2 \tag{2.59}$$

and together with (2.4), (2.5), and (2.7), it will form a set of four equations with four unknown coefficients c_0, c_1, c_2, c_3, and one parameter T. The solutions for the coefficients are

$$c_0 = 0, \quad c_1 = v_s, \quad c_2 = \frac{3q_f - 2T\ vs}{T^2}, \quad \text{and} \quad c_3 = -\frac{2q_f + T\ vs}{T^3}$$

and thus

$$q(t) = v_s\ t + \frac{3q_f - 2T\ v_s}{T^2} t^2 + \frac{-2q_f + T\ v_s}{T^3} t^3 \tag{2.60}$$

$$v(t) = v_s + \frac{6q_f - 4T\ v_s}{T^2} t + \frac{-6q_f + 3T\ v_s}{T^3} t^2 \tag{2.61}$$

$$a(t) = \frac{6q_f - 4T\ v_s}{T^2} + \frac{-12q_f + 6T\ v_s}{T^3} t \tag{2.62}$$

As the profile is no longer symmetric, the maximum velocity bound v will not be reached at $t = ½T$. It will be achieved when $a(t) = 0$. Substitution of this condition to (2.62) gives the moment of maximum velocity achievement, i.e. at

$$t_1 = \frac{T(-3q_f + 2T\ v_s)}{-6q_f + 3T\ v_s} \tag{2.63}$$

Consecutively, substitution of t_1 to (2.60) will give the velocity bound v value

$$v\ = -\frac{(3q_f - 2T\ v_s)^2}{3T(-2q_f + T\ v_s)} \tag{2.64}$$

and then the positive T solution for $v_s \neq 0$ is

$$T = T_v = \frac{3q_f\left(v - \sqrt{v}\sqrt{v - v_s} + v_s\right)}{v_s(3v + v_s)} \tag{2.65}$$

Similarly if the maximum acceleration bound a is used to obtain T and by noting that

the maximum acceleration bound a may only be achieved at $t = 0$ and $t = T$, substitutions of these conditions to (2.62) give two possibilities

$$a = \frac{6q_f - 4T\, v_s}{T^2} \tag{2.66}$$

$$a = -\frac{2(-3q_f + T\, v_s)}{T^2} \tag{2.67}$$

from where each solution for positive T is obtained, i.e.

$$T = T_{a1} = \frac{-2v_s + \sqrt{6a\, q_f + 4\, v_s^{\,2}}}{a} \tag{2.68}$$

$$T = T_{a2} = \frac{-v_s + \sqrt{6a\, q_f + v_s^{\,2}}}{a} \tag{2.69}$$

Hence, for the nonzero initial condition the move time T depends on v_s. For a given maximum velocity bound v and maximum acceleration bound a, the T value that maintains the limits is the maximum value among the three, i.e. $T = \max(T_v\,, T_{a1}\,, T_{a2})$, and only one bound will be satisfied. Figure 2.9 shows an example of a nonzero initial condition with velocity bound v as the criterion to get a maximum move time T.

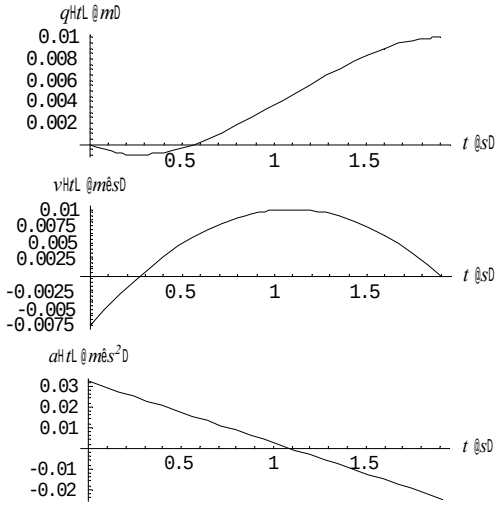

Figure 2.9 Cubic profile with nonzero initial condition, q_f = 0.01 m, v_s = –0.0075 m/s, and the maximum velocity bound v = 0.01 m/s.

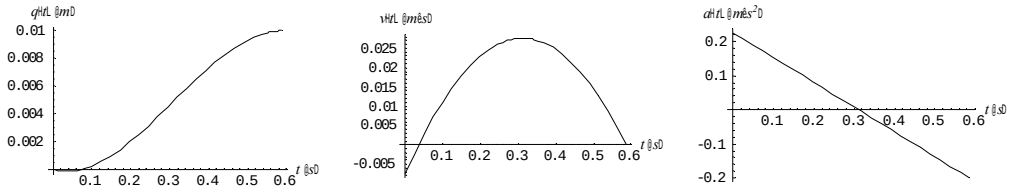

Figure 2.10 Cubic profile with nonzero initial condition and bounded final acceleration. Initial acceleration violates the given maximum acceleration bound $a = 0.2$ m/s^2.

Unlike T_v, both T_{a1} and T_{a2} are trivial. As both are obtained from different linear cases, T_{a1} or T_{a2} needs further analysis to confirm the validity. For example, if T_{a2} of (2.67) and (2.69) is applied to control final acceleration, then (2.66) has to be used to check the initial acceleration. Fig 2.10 shows an example inapplicable solution where a correctly bounded final acceleration meet violated initial acceleration bound.

In such consecutive point to point reactive motions the acceleration profiles in general will be discontinuous. As motion smoothness must be maintained—i.e. velocity continuity—position and velocity equations are actually sufficient to find the motion parameters.

For the total jerk measure, despite a definite derivative value $\dddot{q}(t) = -(12q_f - 6T v_s)/T^3$ of (2.62), since the acceleration is discontinuous at the boundaries then the jerk is indefinite accordingly.

$$j(t) = \infty \qquad , t = 0, t = T \tag{2.70}$$

On the other hand, the total acceleration (energy) measure for nonzero initial condition will include the initial velocity v_s, i.e.

$$\int_0^T |\, a(t)\,|\, dt = \int_0^{t_1} |\, a(t)\,|\, dt + \int_{t_1}^T |\, a(t)\,|\, dt = v_s - \frac{2(3q_f - 2T\, v_s)^2}{3T(-2q_f + T\, v_s)}$$

and referring to (2.64), it can be expressed as

$$\int_0^T |\, a(t)\,|\, dt \;=\; 2v + \left[v_s - \frac{3T^2 v_s^{\,2}}{3T(-2q_f + T\, v_s)} \right] \tag{2.71}$$

In comparison to (2.13), the expression within the rectangular bracket denotes the initial velocity contribution.

The velocity curve remains quadratic. It is no longer symmetric with the maximum moment at $t = t_1$ as described in (2.63).

To find out the reactive feature, the author has tried to implement and realized a reactive motion planner algorithm using cubic polynomial. Chapter 4 will shortly cover the algorithm. Cubic has a relatively light computation cost with 27 multiplications and 5 additions in trajectory generation. An additional 18 multiplications and 8 additions are needed at the turning point, i.e. when target point is changed, due to the computations of new parameters for the new trajectory.

However there remain several considerations for the reactive cubic motion planning algorithm. It can only ensure velocity continuity. Acceleration and jerk continuity are not controllable including the infinite jerks at the boundaries. For the computation, the maximum velocity criterion is preferable whereas the maximum acceleration criterion remains trivial. However, the light computation cost can be useful in multidimensional applications.

2.4.2 Trapezoidal velocity

For nonzero initial condition with $v_s \neq 0$ there may be additional fraction of time to be compensated. The typical profile for non zero initial condition is shown in Figure 2.11 and the analysis will be as follow.

- At $0 \leq t \leq t_1$' it has constant acceleration phase $a(t) = a$ and at $t = t_1$'

$$t_1' = (v - v_s)/a \tag{2.72}$$

$$q(t) = q_1' = v_s\, t_1' + \tfrac{1}{2}\, a\, (t_1')^2 = (v^2 - v_s^2)/2\, a$$

- At $t_1' < t \leq T - t_1$ it has constant velocity phase and at $t = T - t_1$

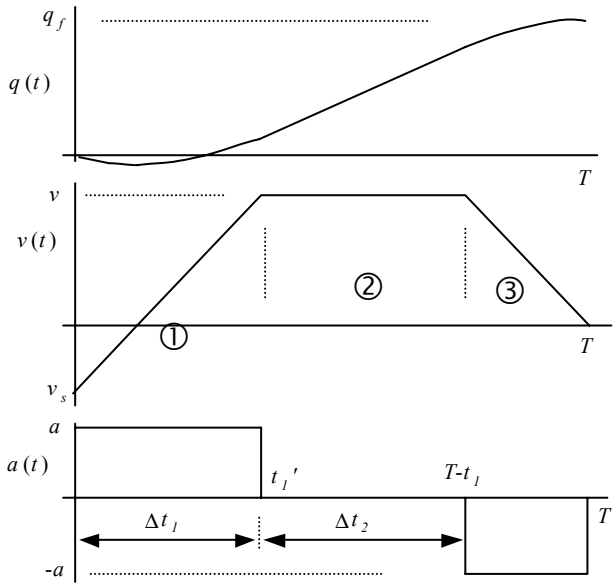

Figure 2.11 Typical nonzero to zero trapezoidal velocity profile.

$$q(t) = q_2 = (v^2 - v_s^2)/2\,a + v\,(T - t_1 - t_1') \tag{2.77}$$

- At $T - t_1 < t \le T$ it has constant deceleration phase $a(t) = -a$ and the profile is similar with the third phase of the zero to zero condition. Recalling (2.14) and (2.15), at $t = T$ the velocity and position expression will be

$$v(T) = 0 = v - a(T - (T - t_1)) \tag{2.78}$$

$$q(T) = q_f = q_2 + v^2/2\,a = (v^2 - v_s^2)/2\,a + v\,(T - t_1 - t_1') + v^2/2\,a \tag{2.79}$$

and thus

$$T - (T - t_1) = t_1 = \frac{v}{a} \tag{2.80}$$

$$(T - t_1 - t_1') = \frac{q_f}{v} - \frac{v}{a} + \frac{v_s^2}{2av} \tag{2.81}$$

Hence, move time T for this typical nonzero to zero condition is

$$T = t_1' + (T - t_1 - t_1') + t_1 = \frac{q_f}{v} + \frac{v}{a} + \left[\frac{v_s^2}{2\,a\,v} - \frac{v_s}{a}\right] \tag{2.82}$$

and correspondingly the position is given by

$$q(t)=\begin{cases} v_s t+\frac{1}{2}a\,t^2 & ;\ 0<t\le t_1' \\ & (\text{const. accel.},a) \\ \dfrac{v^2}{2a}+vt-\dfrac{(v-v_s)^2+v^2}{2a} & ;\ t_1'<t\le T-t_1 \\ & (\text{const. vel.},v) \\ -\dfrac{v^2}{2a}+v\,t+\frac{1}{2}a(t-T+t_1)^2-\dfrac{(v-v_s)^2+v^2}{2a} & ;\ T-t_1<t\le T \\ & (\text{const. decel.},-a) \end{cases} \tag{2.83}$$

For the total jerk measure, since the acceleration will be discontinuous, the total jerk also remains infinite as in (2.22). On the other hand, the energy measure for nonzero initial condition can be derived as

$$\int_0^T |\,a(t)\,|\,dt=\int_0^{t_1'}|\,a(t)\,|\,dt+\int_{t_1'}^{T-t_1}|\,a(t)\,|\,dt+\int_{T-t_1}^{T}|\,a(t)\,|\,dt$$

$$=2v+|vs| \tag{2.84}$$

To find out the flexibility and the computation cost, the author has developed reactive motion planning algorithm able to generate trapezoidal velocity profile. It is possible to use the derived formulas but it appears that the acceleration can always be set to eventually construct the desired velocity profile. The detail of the algorithm will be discussed in Chapter 3. The algorithm has low computation cost, i.e. 16 multiplications and 40 additions operations; hence it would be suitable for a fast real time trajectory generation. However considering the mentioned drawbacks, the system is likely applicable for/in relatively slow motions where jerk limitations are not highlighted..

There are particular/special conditions that require further considerations as for the zero to zero condition. When the distance to the target is relatively short, the phase compositions might be different and so the motion formulas. However, from the typical profile analysis, it is shown that the main characteristics would remain similar.

2.4.3 Quintic

For non zero initial condition, similar with the previous approach, the move time *T* is

going to be analyzed first to be able to generate the profile. The condition for six equations with six unknown coefficients and a parameter T is as follow

$$q(t)|_{t=0} = q_0 = 0 \quad ; \quad q(t)|_{t=T} = q_f$$

$$\dot{q}(t)|_{t=0} = v(0) = v_s \quad ; \quad \dot{q}(t)|_{t=T} = v(T) = 0$$

$$\ddot{q}(t)|_{t=0} = a(0) = a_s \quad ; \quad \ddot{q}(t)|_{t=T} = a(T) = 0$$

and the solutions for the coefficients are

$$c_0 = 0, \quad c_1 = v_s, \quad c_2 = \frac{v_s}{2}, \quad c_3 = -\frac{-20q_f + 3a_s T^2 + 12T v_s}{2T^3},$$

$$c_4 = -\frac{30q_f - 3a_s T^2 - 16T v_s}{2T^4}, \quad c_5 = -\frac{-12q_f + 3a_s T^2 + 6T v_s}{2T^5}$$

Hence the position, velocity, acceleration, and jerk equations are

$$q(t) = v_s t + \frac{a_s}{2}t^2 - \frac{3a_s T^2 + 12T v_s - 20q_f}{2T^3}t^3 - \frac{-3a_s T^2 - 16T v_s + 30q_f}{2T^4}t^4 - \frac{a_s T^2 + 6T v_s - 12q_f}{2T^5}t^5 \tag{2.85}$$

$$\dot{q}(t) = v(t) = v_s + a_s t - \frac{3(3a_s T^2 + 12T v_s - 20q_f)}{2T^3}t^2 - \frac{2(-3a_s T^2 - 16T v_s + 30q_f)}{T^4}t^3 - \frac{5(a_s T^2 + 6T v_s - 12q_f)}{2T^5}t^4 \tag{2.86}$$

$$\ddot{q}(t) = a(t) = a_s - \frac{3(3a_s T^2 + 12T v_s - 20q_f)}{T^3}t - \frac{6(-3a_s T^2 - 16T v_s + 30q_f)}{T^4}t^2 - \frac{10(a_s T^2 + 6T v_s - 12q_f)}{T^5}t^3 \tag{2.87}$$

$$\dddot{q}(t) = j(t) = -\frac{3(3a_s T^2 + 12T v_s - 20q_f)}{T^3} - \frac{12(-3a_s T^2 - 16T v_s + 30q_f)}{T^4}t - \frac{30(a_s T^2 + 6T v_s - 12q_f)}{T^5}t^2 \tag{2.88}$$

Similarly, to generate the profile, the movement time T has to be solved. Maximum velocity v is reached when $\ddot{q}(t) = a(t) = 0$ and from (2.87) the possible root is

$$t_{1,2} = \frac{-15q_f\ T + 2a_s\ T^3 + 9T^2 v_s}{-60q_f + 5a_s\ T^2 + 15T\ v_s}$$

$$\pm \frac{\sqrt{(60q_f - 8a_s T^2 - 36v_s T)^2 + 2a_s T^4 (60q_f - 5a_s T^2 - 30v_s T)}}{-120q_f + 10a_s T^2 + 60v_s T} \qquad (2.89)$$

However, substitution of this result may lead to a complex high order rational function. Substitution to $\dot{q}(t) = v(t) = v$ leads to an equation in T of an order of fourteen! Equation (A.1) in Appendix shows the details. Pioneered previously by Ruffini, Abel proved that there is no closed form roots in radicals beyond quartics or fourth order equations [6, 7]. The theorem is emphasized by Galois's group theory [7]. There is a closed form solution to a fifth order polynomial but it is necessary to go beyond the extraction of roots and to use modular elliptic and hyper-geometric functions [7]. Therefore, practically, numerical method will be a preferable tool to find the solution of T. However, the numerical solutions for given q_f, v_s, a_s, and v as observed using MATHEMATICA^{TM} [32], so far remain restricted to a few positive roots beside many failed cases resulting in complex, negative roots, or extreme oscillation/wandering [40]. Figure 2.12 shows an example of oscillation as a result of an undesirable choice of root. In addition, even a possible positive T solution may still result in a violation of the velocity bound v itself. Figure 2.13 shows an example of such a violation case. For this reason, the solution based on maximum velocity criterion may not always exist.

Therefore, although it preserves velocity and acceleration continuity, the maximum velocity criterion is trivial and undesirable. The problem of formulating particular conditions for a feasible solution in this maximum velocity criterion is beyond the scope of this work.

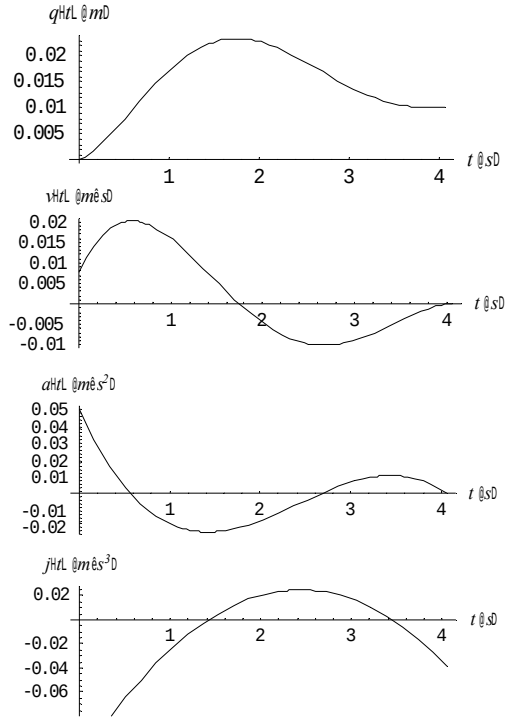

Figure 2.12 Nonzero to zero quintic profile with undesirable choice of root of the maximum velocity criterion, resulting in oscillation (wandering) effect of position. Motion parameters are $q_f = 0.01$ m, $v_s = 0.0075$ m/s, $a_s = 0.05$ m/s^2, $v = 0.01$ m/s. The selected root from the numerical computation is $T = 4.05$ s

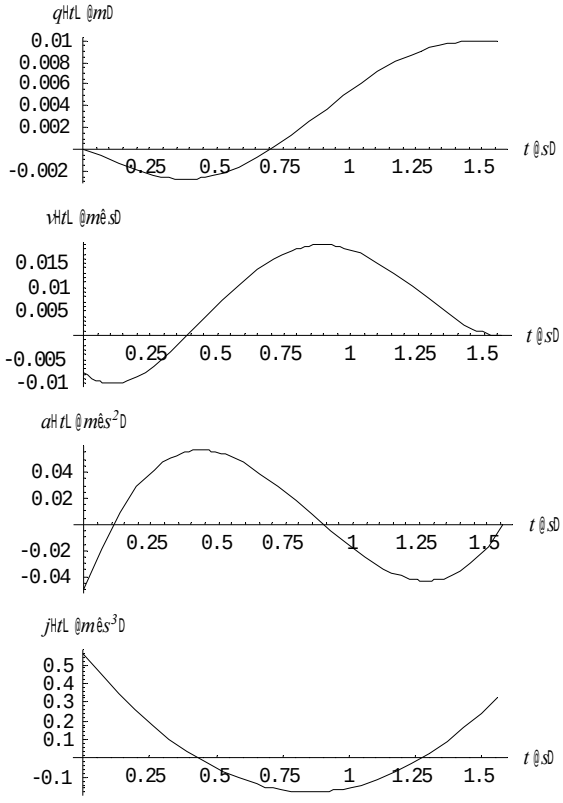

Figure 2.13 Example of unsafe profile under v criterion with solution $T = 1.56$ s for a given $q_f = 0.01$ m, $v_s = -0.0075$ m/s, $a_s = -0.05$ m/s^2, and $v = 0.01$ m/s. Velocity bound v is maintained at $t = 0.11$ s but violated at $t = 0.85$ s

On the other hand, by using the maximum acceleration criterion it is also possible to find the move time T. Similar with previous analysis, the maximum acceleration is achieved when the jerk $j(t)$ in (2.88) is zero. From this quadratic expression, the zero jerk condition will give

$$t_{1,2} = \frac{-30q_f\ T + 3a_s\ T^3 + 16T^2 v_s}{-600q_f + 5a_s\ T^2 + 30T\ v_s}$$

$$\pm \frac{T\sqrt{2}\sqrt{600{q_f}^2 - 80a_s q_f T^2 + 3{a_s}^2 T^4 - 600q_f v_s T + 42a_s v_s T^3 - 152{v_s}^2 T^2}}{-120q_f + 10a_s T^2 + 60v_s T}$$

….. (2.90)

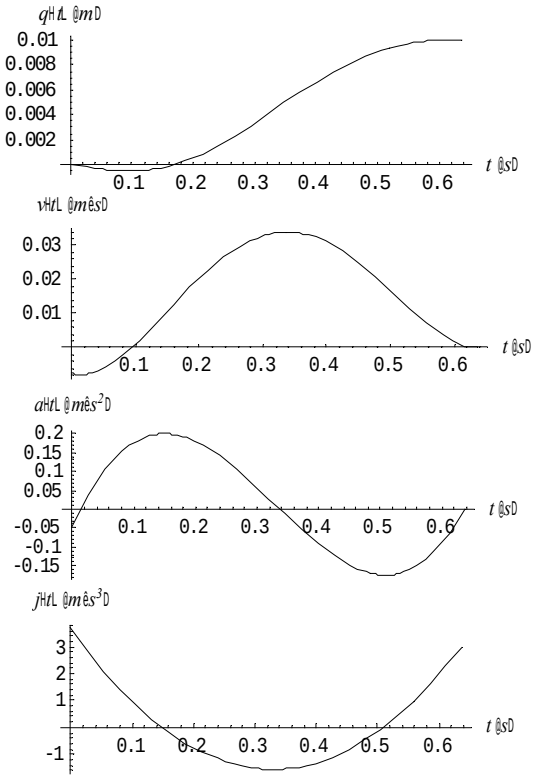

Figure 2.14 Safely planned quintic profile under maximum acceleration criterion with $T = 0.636575$ s for $q_f = 0.01$ m, $v_s = -0.0075$ m/s, $a_s = -0.05$ m/s^2, and $a = 0.2$ m/s^2.

and substitutions to $\ddot{q}(t) = a(t) = a$ leads to an equation in T of the order of eight. Equation (A.2) in Appendix shows the detail. Once again numerical method will be a preferable way to find T. The numerical solution for given q_f, v_s, a_s, and a, as observed

using MATHEMATICA™, although remains trivial and restricted to few possible positive roots, offers better possibilities for a desirable non-oscillatory displacement. Figure 2.14 shows an example of a profile obtained using the maximum acceleration criterion for the same initial condition with those in Figure 2.13. In addition, the solution is more reliable in maintaining the kinematic limit. However, as it only controls acceleration, the velocity extrema is no longer controlled.

Meanwhile, from the discontinuous jerk profile it is also possible to find the T solution. The jerk is bounded at the boundaries and at the extrema. Thus substitution of $t = 0$ or $t = T$ condition to the jerk equation (2.88) will give

$$\dddot{q}(0) = j(0) = j = -\frac{9a_s T^2 + 36T v_s - 60q_f}{T^3} \tag{2.91}$$

$$\dddot{q}(T) = j(T) = j = -\frac{3a_s T^2 + 24T v_s - 60q_f}{T^3} \tag{2.92}$$

The other solution comes from the extrema of the parabolic jerk curve. Solving this extrema, i.e $\overset{iv}{q}(t) = 0$, will give

$$t = \frac{T(-30q_f + 3a_s T^2 + 16Tv_s)}{-60q_f + 5a_s T^2 + 30Tv_s}$$

Substitution to (2.88) gives one more maximum jerk equation

$$\dddot{q}(t) = j = -\frac{1800{q_f}^2 - 120q_f T(2a_s T + 15v_s)}{5T^3(-12q_f + a_s T^2 + 6v_s T)}$$

$$+\frac{3T^2(3{a_s}^2T^2 + 42a_s T v_s + 152{v_s}^2)}{5T^3(-12q_f + a_s T^2 + 6v_s T)} \tag{2.93}$$

Hence there would be three possibilities for the T solution under the maximum jerk criterion. Equation (A.3) in the Appendix shows the detail. The first two equations can give a straightforward closed form third order function, whereas the third needs a numerical solution to find the roots of the fifth order function of T. However among

the three possibilities, as also observed using MATHEMATICA^{TM}, the solution is trivial and may only be valid for the one of (2.93). The other two often give negative or complex numbers. Unfortunately, the solution of (2.93) is also undesirable as it may result in a violation of the jerk bound itself; a similar situation with the maximum velocity criterion. As an example, the negative $j(0)$ in Figure 2.15 illustrates a limiting condition of the applicable solution. The problem of finding a closed form formulation of the applicable conditions for this jerk bound criterion is beyond the scope of this work.

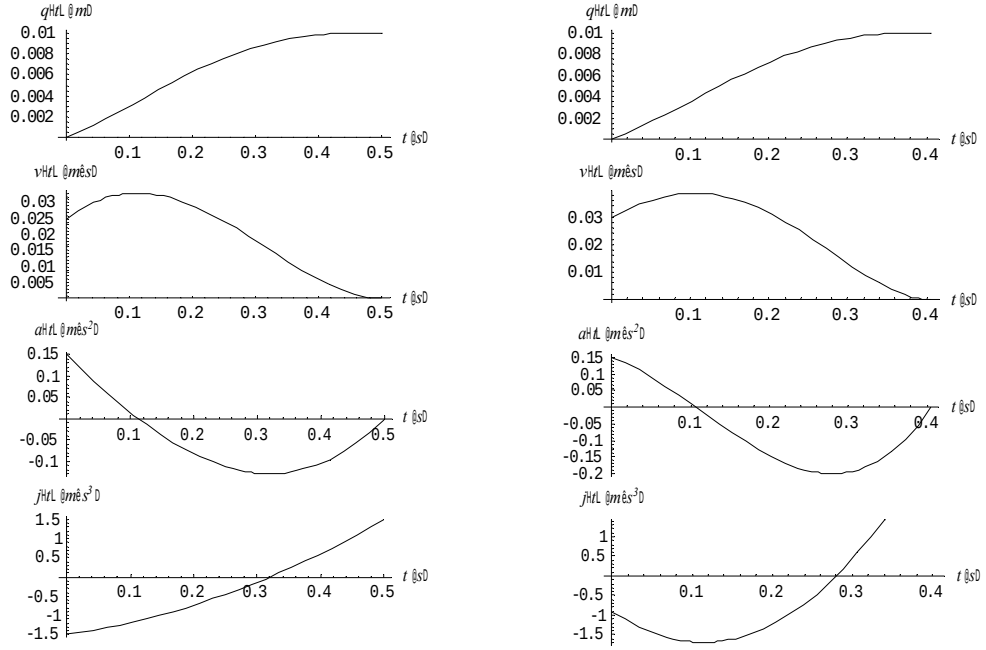

Figure 2.15 Nonzero to zero quintic under maximum jerk criterion with jerk root $t_1 < 0$. Given $q_f = 0.01$ m, $v_s = 0.025$ m/s, $a_s = 0.15$ m/s^2, and maximum jerk $j = 1.5$ m/s^3 the resulting move time is $T = 0.5$ s as in left figure. Setting jerk bound below 1.5 m/s^3 will cause jerk bound violation as jerk minima at $t = 0$ becomes smaller than -1.5 m/s^3 as in right figure.

Hence it appears that the desirable solution may only come from the maximum acceleration criterion.

Using $t_{1,2}$ of (2.90), the total jerk for nonzero initial condition can be computed as

$$\int_0^T |\, j(t)\,|\, dt = \int_0^{t_1} |\, j(t)\,|\, dt + \int_{t_1}^{t_2} |\, j(t)\,|\, dt + \int_{t_2}^{T} |\, j(t)\,|\, dt \quad \text{for } t_1 \geq 0 \text{ and } t_2 > 0 \qquad (2.94.a)$$

$$= \int_0^{t_2} |\, j(t)\,|\, dt + \int_{t_2}^{T} |\, j(t)\,|\, dt \quad \text{for } t_1 \le 0 \text{ and } t_2 > 0 \tag{2.94.b}$$

$$= f(q_f, a_s, v_s, T)$$

which are functions in q_f, a_s, v_s, and T. Equation (A.4) in the Appendix shows the details. Figure 2.16 shows an example of the condition with negative t_1. Hence, the integration will depend on the parameter values. However, by investigating the evolution of acceleration curve, the jerk can be expressed as

$$\int_0^{T} |\, j(t)\,|\, dt = a_s + 2a + 2c \qquad ;\ c < a \tag{2.92}$$

Using quintic, it is possible to maintain acceleration and velocity continuity. The jerk at every turning point in reactive planning will be bounded.

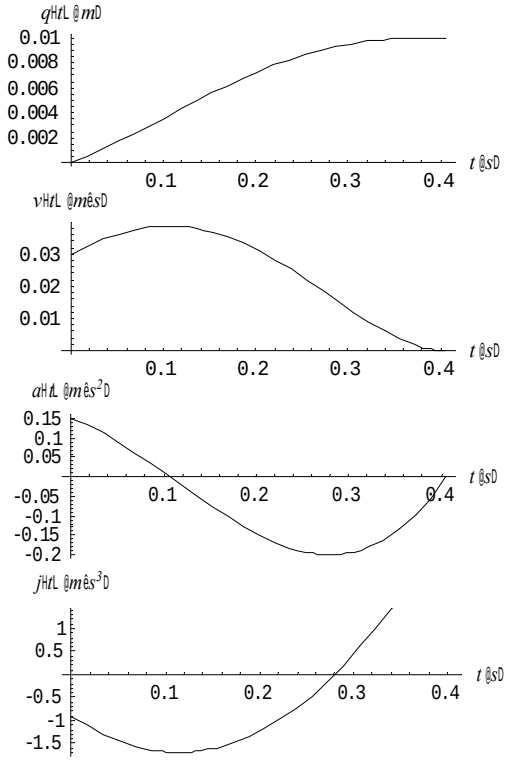

Figure 2.16 Nonzero to zero quintic under maximum acceleration criterion with negative jerk root $t_1 < 0$. Motion parameters $q_f = 0.01$ m, $v_s = 0.03$ m/s, $a_s = 0.15$ m/s2, and $a = 0.2$ m/s^2 give jerk root $t_1 = -0.0523197$ s, $t_2 = 0.280129$ s, and later the movement time is found as $T = 0.405448$ s.

For the energy measure analysis with the t of (2.90), integration of the segments of acceleration profile gives a function of q_f, a_s, v_s, and T.

$$\int_0^T |a(t)|\,dt = \int_0^{t_1} |a(t)|\,dt + \int_{t_1}^{t_2} |a(t)|\,dt + \int_{t_2}^{T} |a(t)|\,dt \quad \text{for } t_1 \geq 0 \text{ and } t_2 > 0 \qquad (2.95.a)$$

$$= \int_0^{t_2} |a(t)|\,dt + \int_{t_2}^{T} |a(t)|\,dt \quad \text{for } t_1 \leq 0 \text{ and } t_2 > 0 \qquad (2.95.b)$$

$$= f(q_f, a_s, v_s, T) \quad \cong \quad 2v + |v_s|$$

Equation (A.5) in the Appendix shows the details. Note that the approximation value $2v + |v_s|$ is observed numerically as T is also obtained numerically.

The velocity curve will be continuous and smoother than cubic's as a result of acceleration continuity. The maximum velocity v will be reached at $t = t_1$ or $t = t_2$ as described in (2.89).

In realizing a reactive motion planner, the author has developed and simulated the reactive quintic motion planning algorithm using the maximum acceleration criterion. It is noted that the computation cost is 220 multiplications and 46 additions excluding numerical method calculations. The numerical Eigenvalue Method root solver [33] is noted to cost up to 5.5 trillion additions and 2.2 trillion multiplications. Authors like [26, 47, 48, 49, 54, 61, 62] proved the possibility to realize and implement on-line sensor based quintic motion planner complete with the trivial and numerical method for the roots. However it is applied for predicted and relatively small target change. It is also unclear whether the resulting profiles are as expected or not. Under this hefty computation process and trivial procedure, a real-time, fast/optimal, and reactive multidimensional application may need some further investigations and considerations. A set of proper motion parameters needs to be carefully selected in addition to the numerical procedure to avoid undesirable oscillation and/or bound violation.

2.4.4 Trapezoidal acceleration

For nonzero initial condition with $v_s \neq 0$ and $a_s \neq 0$, there may be an additional fractions of time to be compensated. Typically the profile with nonzero initial condition will be as shown in Figure 2.17 and the analysis becomes as follows.

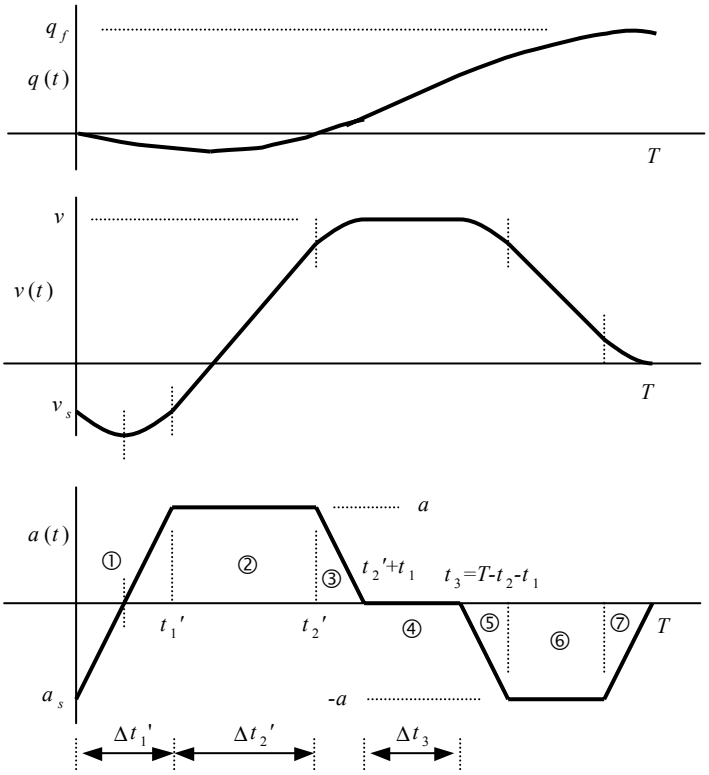

Figure 2.17 Typical nonzero to zero trapezoidal acceleration profile.

- At $0 \le t \le t_1$' it has constant jerk phase $j(t) = +j$ therefore at $t = t_1$'

$$t_1' = \frac{a - a_s}{j} = \frac{a}{j} + \left(-\frac{a_s}{j} \right) \tag{2.96}$$

$$v(t) = v_1' = v_s + a_s\, t_1' + \tfrac{1}{2} j\, (t_1')^2 = v_s + (a^2 - a_s^2)/2j \tag{2.97}$$

$$q(t) = q_1' = v_s\, t_1' + {}^1\!/_2\, a_s\, (t_1')^2 + {}^1\!/_6 j\, (t_1')^3$$

$$= v_s \frac{(a - a_s)}{j} + \frac{(a + 2a_s)(a - a_s)^2}{6j^2} \tag{2.98}$$

- At $t_1' < t \le t_2$' it has constant acceleration phase $a(t) = a$ and at $t = t_2$'

$$v(t) = v_2' = v_1' + a(t_2' - t_1') \tag{2.99}$$

$$q(t) = q_2' = q_1' + v_1'(t_2' - t_1') + {}^1\!/_2\, a\, (t_2' - t_1')^2 \tag{2.100}$$

- At $t_2' < t \le t_2' + t_1$ it has constant negative jerk phase $j(t) = -j$. Note that t_1 can be simply recalled from zero to zero condition, e.g. equation (2.38), because it is similar. Hence at $t = t_2' + t_1$

$$a(t) = 0 = a - j\,((t_2' + t_1) - t_2'); \quad \text{hence } t_1 = a/j \tag{2.101}$$

$$v(t) = v = v_2' + a\,((t_2' + t_1) - t_2') - {}^1\!/_2\, j\,((t_2' + t_1) - t_2')^2$$

$$\left(v_s + \frac{a^2 - a_s^2}{2j} + \right) + a(t_2' - t_1') + \frac{a^2}{2j} \tag{2.102}$$

$$q(t) = q_2' + v_2'((t_2' + t_1) - t_2') + {}^1\!/_2\, a((t_2' + t_1) - t_2')^2 - {}^1\!/_6\, j((t_2' + t_1) - t_2')^2 \tag{2.103}$$

Substitution of (2.96-100) to (2.102) gives

$$(t_2' - t_1') = \frac{v - v_s}{a} - \frac{2a^2 - a_s^2}{2\,a\,j} = \frac{v}{a} - \frac{a}{j} + \left[\frac{a_s^2}{2\,a\,j} - \frac{v_s}{a} \right] \tag{2.104}$$

and accordingly substitution of (2.103) to (2.99) and (2.100) give v_2' and q_2'

$$v_2' = v - a^2/2j \tag{2.105}$$

$$q_2' = -\frac{a_s^4}{8\,a\,j^2} + \frac{2a^3 - 3a_s{}^2 a + 4a_s{}^2}{12j^2} + \frac{a_s{}^2 v_s}{2\,a\,j} - \frac{a\,(v - v_s) + 2a_s v_s}{2j} + \frac{v^2 - v_s^2}{2a} \tag{2.106}$$

and then substitution of (2.104–106) to (2.103) gives

$$q(t) = q_{21}' = -\frac{a_s^4}{8\,a\,j^2} + \frac{a_s{}^2(4a_s - 3a)}{12j^2} + \frac{a_s{}^2 v_s}{2\,a\,j} + \frac{a\,(v + v_s) - 2a_s v_s}{2j} + \frac{v^2 - v_s^2}{2a} \tag{2.107}$$

- At $t_2' + t_1 < t \le t_3$ where $t_3 = T - t_2 - t_1$ and t_1 and t_2 are recalled back from (2.38) and (2.40) due to its similarities, it has a constant velocity phase $v(t) = v$. Therefore and at $t = t_3$

$$q(t) = q_{21}' + v\,(t_3 - (t_2' - t_1))$$

- Finally at $t_3 < t \le T$ the velocity and acceleration profile are similar with those of zero to zero condition. By recalling (2.43), at $t = T$ it is possible to express the distance to target q_f as

$$q(T) = q_f = q_{21}' + v\,(t_3 - (t_2' - t_1)) + v^2/2a + a\,v/2j$$

and accordingly $(t_3 - (t_2' - t_1))$ can be derived, i.e.

$$(t_3 - (t_2' - t_1)) = \frac{q_f - q_{21}'}{v} - \frac{v}{2a} - \frac{a}{2j} = \frac{q_f}{v} - \frac{v}{a} - \frac{a}{j} + \left[-\frac{q_{21}'}{v} + \frac{v}{2a} + \frac{a}{2j} \right] \quad (2.108)$$

Hence for nonzero to zero condition the move time T is

$$\begin{aligned} T &= [t_1' + (t_2' - t_1') + t_1] + (t_3 - (t_2' - t_1)) + [t_1 + (t_2 - t_1) + t_1] \\ &= \frac{q_f}{v} + \frac{v}{a} + \frac{a}{j} + \left[\frac{a - 2a_s}{2j} + \frac{v - 2v_s}{2a} + \frac{a_s^2}{2\,a\,j} - \frac{(q_{21}')^2}{v} \right] \end{aligned} \quad (2.109)$$

And correspondingly the seven phases of position $q(t)$ can be written as

$$q(t) = \begin{cases} v_s t + \frac{1}{2} a_s t^2 + \frac{1}{6} j t^3 & ; 0 < t < t_1' \\ & \text{(const. jerk, } + j) \\ q_1' + v_1'(t - t_1') + \frac{1}{2} a (t - t_1')^2 & ; t_1' < t < t_2' \\ & \text{(const. acc., } + a) \\ q_2' + v_2'(t - t_2') + \frac{1}{2} a (t - t_2')^2 - \frac{1}{6} j (t - t_2')^3 & ; t_2' < t < t_2' + t_1 \\ & \text{(const. jerk, } - j) \\ q_{21}' + v(t - (t_2' + t_1)) & ; t_2' + t_1 < t < T - (t_2 + t_1) \\ & \text{(const. vel., } + v) \\ q_{21}' + v(T - (t_2 + t_1) - (t_2' + t_1)) + & ; T - (t_2 + t_1) < t < T - t_2 \\ v(t - (T - t_2 - t_1)) - \frac{1}{6} j (t - (T - t_2 - t_1))^3 & \text{(constant jerk, } - j) \\ q_{21}' + v(T - (t_2 + t_1) - (t_2' + t_1)) + v t_1 - \frac{1}{6} j t_1^3 + & ; T - t_2 < t < T - t_1 \\ \left(v - \frac{a^2}{2j} \right)(t - (T - t_2)) - \frac{1}{2} a (t - (T - t_2))^2 & \text{(constant dec., } - a) \\ q_{21}' + v(T - (t_2 + t_1) - (t_2' + t_1)) + v t_1 - \frac{1}{6} j t_1^3 + & ; T - t_1 < t < T \\ \left(v - \frac{a^2}{2j} \right)(t_2 - t_1) - \frac{1}{2} a (t_2 - t_1)^2 + & \text{(constant jerk, } + j) \\ \frac{a^2}{2j}(t - (T - t_1)) - \frac{a}{2}(t - (T - t_1))^2 + \frac{j}{6}(t - (T - t_1))^3 & \end{cases}$$

……..(2.110)

The jerk is still a step function bounded at ±*j*. and the total jerk, i.e. the integration of jerk profile along the trajectory is

$$\int_0^T |\, j(t)\,|\, dt = \int_0^{t_1'} |\, j(t)\,|\, dt + 3\int_0^{t_1} |\, j(t)\,|\, dt = (a_s + a) + 3a = 4a + a_s \qquad (2.111)$$

The bounded jerk will give better trajectory smoothness than trapezoidal velocity's.

When integrating the acceleration profile to find the energy measure, it is possible to compare and obtain the difference with zero to zero. Note that the two conditions will differ at the first and second phase. By recalling (2.38), (2.96), (2.40), and (2.104) it is possible to express the difference respectively as Δt_I and Δt_{II} where

$$\Delta t_I = t_1' - t_1 = -\frac{a_s}{j} \quad \text{(at the constant jerk)} \qquad (2.112)$$

$$\Delta t_{II} = t_2' - t_2 = \frac{a_s^2}{2\,a\,j} - \frac{v_s}{a} \quad \text{(at the constant acceleration)} \qquad (2.113)$$

and it helps in simplifying the integration of acceleration curve. Hence the total integration results in that for zero to zero condition plus two additional areas: i) a triangle area with height $|a_s|$, width Δt_I; ii) rectangular area with height a and width Δt_{II}

$$\int_0^T |\, a(t)\,|\, dt = 2v + \left[\tfrac{1}{2}\left(-\frac{a_s}{j} \right) |a_s| + a\left(\frac{a_s^2}{2\,a\,j} - \frac{v_s}{a} \right) \right] \qquad (2.114)$$

Similar with the trapezoidal velocity, yet there remain particular/special conditions that might need further considerations. A relatively short target distance combined with the nonzero initial velocity condition might yield into numerous combinations of phases and correspondingly into different motion formulas. However, section 2.3.4 shows that the main characteristics of such conditions would be similar.

In realizing a reactive motion planning algorithm, the author has also developed an algorithm that is able to generate equivalent trapezoidal acceleration profile. It is possible to use the derived formulas, but it appears that the jerk can always be set to

eventually construct the desired acceleration and the rest of profiles. The details of the algorithm will be discussed in Chapter 3. The developed algorithm has been cascaded into 141 multiplication and 125 addition operations. This is more complex than trapezoidal velocity algorithm, however, in comparison to quintic, this planner is able to satisfy the bounds, including jerk bound, without the need of numerical solver routine. Therefore it is relatively optimal, fast, and having low computation cost.

2.4.5 A view on modified quintic planner for zero to zero condition

Previous discussions on quintic motion show that for zero to zero condition quintic will only satisfy one bound. For nonzero initial conditions, the trivial procedure restricts the quintic to be practically applicable only under maximum acceleration criterion. It will be desirable if it is possible to satisfy kinematic bounds simultaneously, at least acceleration and velocity bounds.

This section discusses the proposed modified quintic to meet the requirement. The proposed method, however, needs a free boundary parameter. As the final velocity is zero to bring the system to stop, the only available parameter is the acceleration.

For a zero to zero condition, the freed boundary condition of the acceleration will allow the profile to fit the bound. The acceleration profile will be stretchable to reach the bound. Thus by introducing nonzero boundary acceleration a_s and $-a_s$, the profile is able to reach the acceleration and velocity bounds simultaneously.

Hence, for the zero to zero condition, the corresponding equation set of position, velocity, and acceleration will be

$$q(t)|_{t=0} = q_0 = 0 \quad ; \quad q(t)|_{t=T} = q_f$$

$$\dot{q}(t)|_{t=0} = v(0) = 0 \quad ; \quad \dot{q}(t)|_{t=T} = v(T) = 0$$

$$\ddot{q}(t)|_{t=0} = a(0) = a_s \quad ; \quad \ddot{q}(t)|_{t=T} = a(T) = -a_s$$

The solutions to the coefficients are

$$c_0 = 0, \qquad c_1 = 0, \qquad c_2 = \frac{v_s}{2}, \qquad c_3 = -\frac{-20q_f + 4a_s T^2}{2T^3},$$

$$c_4 = -\frac{30q_f - 5a_s T^2}{2T^4}, \qquad c_5 = -\frac{-12q_f + 2a_s T^2}{2T^5}$$

and then the rest of motion equation can be completed.

Using previous approach, the symmetrical property dictates that the maximum velocity bound v will be reached at $t = ½ T$. Substitution to the velocity equation will give

$$v = \frac{15q_f}{8T} - \frac{a_s T}{16} \tag{2.115}$$

On the other hand, the maximum acceleration bound a is reached when jerk $\dddot{q}(t) = j(t) = 0$, and correspondingly, by solving this condition from the jerk equation, the moment for the maxima can be derived,

$$t_{1,2} = \frac{-T(-30q_f + 5a_s T^2) \pm T\sqrt{5}\sqrt{60q_f{}^2 - 16a_s q_f T^2 + a_s{}^2 T^4}}{2(30q_f - 5a_s T^2)} \tag{2.116}$$

Substitution to acceleration equation will give

$$a = \frac{(-10q_f + a_s T^2)\sqrt{60q_f{}^2 - 16a_s q_f T^2 + a_s{}^2 T^4}}{T^2(a_s T^2 - 6q_f)\sqrt{5}} \tag{2.117}$$

Equation (2.115) and (2.117) denote two equations with two unknowns, T and a_s. Due to the complexities, numerical method is used to find the solutions. The appropriate solutions are those with real a_s and real positive T. Figure 2.18 shows the example of the profile. In comparison to v-bounded normal zero to zero quintic in Figure 2.5, with the same kinematic bounds, the move time T in this modified quintic is remarkably improved.

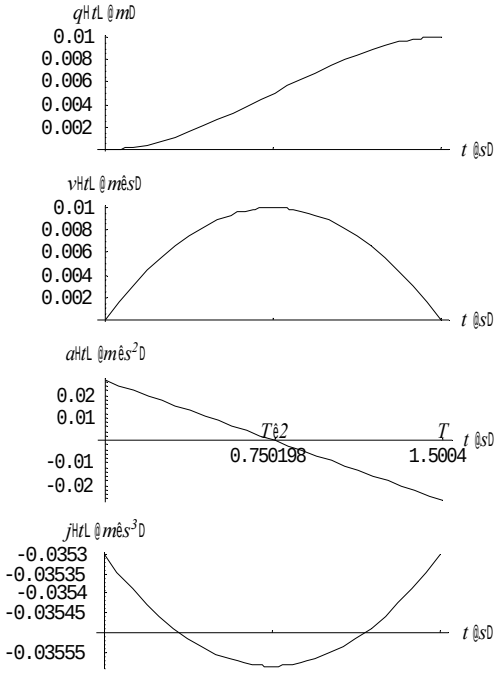

Figure 2.18 Modified quintic profile. Note the initial and final acceleration $\pm a_s$. The profile is for $q_f = 0.01$ m, $v = 0.01$ m/s, $a = 0.2$ m/s^2 the calculated initial-final acceleration $a_s = \pm 0.0266$ m/s^2, and $T = 1.5$ s. Although the maximum acceleration a is not actually reached, the curve extension to both sides will satisfy it.

For nonzero condition with known v_s and a_s, the condition will be

$$q(t)|_{t=0} = q_0 = 0 \qquad ; \qquad q(T) = qf$$

$$\dot{q}(t)|_{t=0} = v(0) = v_s \qquad ; \qquad \dot{q}(t)|_{t=T} = v(T) = 0$$

$$\ddot{q}(t)|_{t=0} = a(0) = a_s \qquad ; \qquad \ddot{q}(t)|_{t=T} = a(T) = a_f$$

Note that since q_f, v_s, a_s, v, and a are known, it appears that the curve is already determined and there is no possibilities to allow the dual bound achievement. The following discussion will discuss the possibilities by freeing up the final acceleration a_f.

The equation set gives the coefficients solution,

$$c_0 = 0, \quad c_1 = v_s, \quad c_2 = \frac{v_s}{2}, \quad c_3 = -\frac{-20q_f - a_f T^2 + 3a_s T^2 + 12v_s T}{2T^3},$$

$$c_4 = -\frac{30q_f + 2a_f T^2 - 3a_s T^2 - 16v_s T}{2T^4}, c_5 = -\frac{-12q_f - a_f T^2 + a_s T^2 + 6v_s T}{2T^5}$$

The corresponding position, velocity, acceleration, and jerk equations can be completed afterward.

Using similar approach, the time of maximal velocity and maximal acceleration can be obtained by solving the zero condition of the corresponding derivatives equations. As results, complex rational forms of t_v, $t_{a1,}$ and t_{a2} respectively for the achievement time of maximum velocity and maximum acceleration are obtained with q_f, v_s, a_s, a_f, and T as parameters. The maximum velocity and maximum acceleration expression thus can be completed. Equation (A.6) in the Appendix shows the detail of the two equations.

Since q_f, v_s, a_s, v, and a are given parameters, then the unknown are a_f and T, and the solutions can be expected from the two equations. However, as it is shown in (A.6), the equation forms are complex that so far the author has not been able to find any possible solution either in closed form or numeric. For then, no further analysis will be given for this nonzero initial condition of modified quintic profile.

Hence, for one shot zero to zero condition, the modified quintic method is able to satisfy v and a bounds simultaneously. However the nonzero initial and final acceleration introduces infinite jerk at the boundaries. Therefore, for zero to zero condition the acceleration will be discontinuous and the total jerk is indefinite.

$$j(t) = \infty \quad , t = 0, t = T \tag{2.118}$$

As acceleration curve is symmetric for zero to zero condition, the energy measure can computed as twice of the half acceleration profile integration,

$$\int_0^T | a(t) | dt = 2 \int_0^{T/2} | a(t) | dt \cong 2\, v \tag{2.119}$$

Note that the $2v$ value is approximated numerically as T is also obtained numerically.

Further analysis shows some restrictions for this zero to zero profile. The applicable acceleration is

$$\frac{128\,v^2}{45\,q_f\sqrt{3}} \le a \le \frac{256\,v^2}{125\,q_f} \tag{2.120}$$

At the minimum value the profile is the normal zero to zero quintic. Below that, a_s will be negative and consequently it will result into opposing velocity slopes and thus undesirable oscillations of the position. Whereas, a larger value than the range is not recommended as the maximum acceleration will never be realized literally in the motion. Figure 2.18 also shows an example of such condition where the maximum acceleration is not realized in the motion.

The velocity bound now is achievable as well as the acceleration bound. The symmetrical property dictates that the velocity bound v is achieved at $t = ½\ T$.

Computation cost for this zero to zero algorithm is noted with 128 multiplication and 27 addition operations, excluding the numerical routine. Therefore it suggests further considerations for multidimensional real time sensor based implementations.

Overall, the modified quintic profile so far is applicable and solvable for one shot zero to zero condition only. Despite the infinite jerk at the boundaries, this modified quintic is able to satisfy both acceleration and velocity bound thus offers optimality.

2.4.6 Summary for reactive motions

It appears that trapezoidal types have shorter move time T than polynomial's. It has been discussed that move time T of polynomials are typically trivial and very restricted whereas trapezoidal conforms and are directly determined by the kinematic bounds.

With the lacks, polynomials becomes relatively time consuming. In addition polynomials can only satisfy one bound at a time. Cubic is easier to implement using maximum velocity criterion than maximum acceleration. Whereas, quintic may only be applicable using maximum acceleration criterion. Other bound criteria are

undesirable since the method may result in oscillation or bound violations. It is possible to satisfy both acceleration and velocity bound in quintic using the proposed modified profile. However it is not suitable for reactive motion planning and implies infinite jerk at the boundaries.

On the other hand, trapezoidal easily accommodates kinematic bounds. With this ability, it will give a fast motion satisfying the kinematic bounds. It is important to note that due to this characteristic, the trapezoidal profiles are kinematically optimal for all cases.

Although it is difficult to compare of total jerk, energy, and velocity measures of the four profiles, there are some main characteristics that can be pointed out. Similar with trapezoidal velocity, cubic has infinite jerk as a result of acceleration discontinuity. Thus both lack on smoothness and might be suitable only for slow movement applications. Quintic can maintain acceleration continuity and excel the smoothness over other planner types. This finding supports many previous works in this particular objective [26, 27, 47, 48, 49, 54]. Effort to simultaneously satisfy kinematic bounds using quintic will acquire acceleration discontinuity and consequently disrupt the smoothness.

Measure	Cubic polynomial	Trapezoidal velocity	Quintic polynomial	Trapezoidal acceleration
Computation cost	10 A, 45 M	22 A, 14 M	Numerical	75 A, 128 M

Table 2.2 Comparison of the number of operations required by the four planner profiles in one-dimensional with non-zero initial conditions. 'A' represents equivalent addition/subtraction and 'M' represents equivalent multiplication operations.

Another important measure is the computation cost. For the simplicity and the availability of the analytical solutions, it may appear that cubic becomes the simplest choice to generate smooth motion profiles with arbitrary change. As long as the proper solution of T is found, the rest of coefficients and motion profiles can be obtained.

However, the procedure to solve T might become problematic, trivial, and time consuming. Therefore it also appears to have practical disadvantages for reactive planning with arbitrary large changes of target position.

Although cubic is comparable to trapezoidal velocity on several measures, however, from the table it can be seen that the trapezoidal velocity still excels cubic in computation cost with lesser multiplication and also in optimality. For applications with relatively slow motion trapezoidal velocity appears to be the most suitable choice. On the other hand, when jerk becomes important, trapezoidal acceleration also require much lesser computation cost over quintic, and is more optimal. Although quintic excels on smoothness, the simple bounded jerk of trapezoidal acceleration may considerably be sufficient for many fast reactive applications.

2.5 Summary of profile analysis

The results of reactive motion analysis of the profiles emphasize those summarized on zero-to zero condition discussed in section 2.3.5. Trapezoidal types appear to have preferable characteristics over polynomial. Among the important measures, trapezoidal types are kinematically optimal and having low computation cost. Due to these facts, it appears that trapezoidal planners offer more practical advantages for fast reactive sensor based applications. It is possible to use polynomials for the same purpose particularly since polynomial also offers better motion smoothness. However, there will be some considerations that have to be taken into account, i.e. the optimality, the trivial determination of motion parameters, and the computation cost. For multidimensional real time reactive application this limitation may become problematic.

Chapter 3

Sensor Based Motion Planning

3.1. Introduction

It has been shown in previous chapters that one of the critical characteristics of a reactive motion planner is the computation time against the reliability to accommodate target position changes. The computation, in minimal time, has to ensure a desirable trajectory without obscurities of profile such as extreme overshoots or oscillations. Further, the planner has to be kinematically optimal to obtain a fast motion/reaction, and smooth if applicable.

It has been discussed that trapezoidal velocity and trapezoidal acceleration algorithm are able to meet the requirements. The reactive sensor based motion planners developed here are based on these trapezoidal types.

The developed motion planning algorithms are able to give equivalent profile of the trapezoidal velocity or trapezoidal acceleration profile. It is possible to realize reactive trapezoidal motion planners analytically using the derived equations in the previous chapter. However the last development reveal that determining the current phase to which next motion should refer to is problematic. The resulting numerical errors sometimes lead to instability [13]. To circumvent these problems, the algorithm that selects the action corresponding to the detected current state has been developed. Based on the detected state the algorithm selects the correct motion parameters; which in turn equivalently constructs trapezoidal motion planning profile.

This work has completed two reactive motion planning algorithms, equivalent to the

trapezoidal velocity profile (Figure 2.4), and trapezoidal acceleration profile (Figure 2.6). The development is done on simulation level using MATLAB^{TM} [67] prior to a lower level programming environment and real system implementation. The following sections will discuss each algorithm.

The discussion will begin from one dimension reactive motion planner algorithm. The description of the algorithm steps describes how it selects the desired and correct motion parameters to anticipate target position changes. Target position is presumably given by the sensors. Once the algorithms perform well in one dimension, the work is furthered into multidimensional motion planning coordination.

3.2. Trapezoidal velocity algorithm

The analytical equations—(2.83), (2.110), and the corresponding zero to zero equations—describe the trapezoidal velocity motion planning profile. The profile consists of constant acceleration phase, cruising or constant velocity phase, and the braking or constant deceleration phase. The cruising or constant velocity phase actually corresponds to zero acceleration. Therefore, the entire phases actually can be characterized by controlling the acceleration.

The developed algorithm of trapezoidal velocity profile here, rather than utilizing mentioned novel analytical equations, uses a controlled acceleration to equivalently construct a trapezoidal velocity profile. The algorithm, through series of conditionals, selectively chose the acceleration value to achieve the target position. The selected acceleration value corresponds to current condition and the objective, i.e. the target. The series of conditions control this selection process for a proper acceleration value until the target is reached.

3.2.1 Algorithm for reactive trapezoidal velocity

This algorithm works as a continuous discrete time loop until a certain stopping condition is achieved. The discrete trajectory and the corresponding profiles are generated for each time step dt. Letting $a(k+1)$, $v(k+1)$, $q(k+1)$, $a(k)$, $v(k)$, $q(k)$ represent acceleration, velocity, and position at the next and current time steps, with k as the loop index, the algorithm can be describes in steps as follows:

Step 1: Asking whether the remaining distance $|q_f - q(k)|$ to the target is smaller than a small limiting distance ε?

If the answer is yes, then

Step 1.1: Stop, there is no need to move further. The target is presumably achieved.

If the answer is no, then

Step 1.2: Compute the braking distance d_{brk} using a method to be discussed later

Step 1.3: Asking whether the remaining distance is smaller than braking distance d_{brk}

If the answer is yes, then

Step 1.3.1: Start to brake.

Corresponds to the polarity or the direction, select the appropriate deceleration value $a(k+1) = \pm a$.

If the answer is no, then

Step 1.3.2: Asking whether the current speed $v(k)$ is much higher than maximum velocity v

If the answer is yes, $v(k) > v$, then

Step 1.3.2.1: Start to brake/slow down the motion.

Corresponds to the polarity or the direction, select the appropriate deceleration value $a(k+1) = \pm a$

If the answer is no, $v(k) \leq v$, then

Step 1.3.2.2: Asking whether the current speed $v(k)$ is equal to maximum velocity v

If the answer is yes, , $v(k) = v$ then

Step 1.3.2.2.1 Set the acceleration to be zero $a(k+1) = 0$, maintain the constant maximum speed v.

If the answer is no, $v(k) \neq v$, then

Step 1.3.2.2.2: Accelerate

Corresponds to the polarity or the direction, select the appropriate acceleration value $a(k+1) = \pm a$

Step 2: Integrate the corresponding velocity and position state

$v(k+1) = v(k) + a(k+1)\, dt$

$q(k+1) = \mathrm{q}(k) + \mathrm{v}(k+1)\, dt + ½\, \mathrm{a}(k+1)\, dt^2$

Step 3: Increment the loop index $k = k + 1$

Step 4: Repeat the loop from *Step 1* for the next time step.

The flowchart shown in Figure 3.1 summarizes the mentioned steps flow.

The limiting distance ε value is a small empirical stopping value. The value has to ensure a smallest or shortest oscillation period at the end of motion.

The braking distance d_{brk} is the required distance to bring the motion to stop from the current condition. Thus braking distance is computed in real-time with respect to the current state. The braking distance can be computed by considering a sloped deceleration phase of the corresponding motion profile expressed in d as

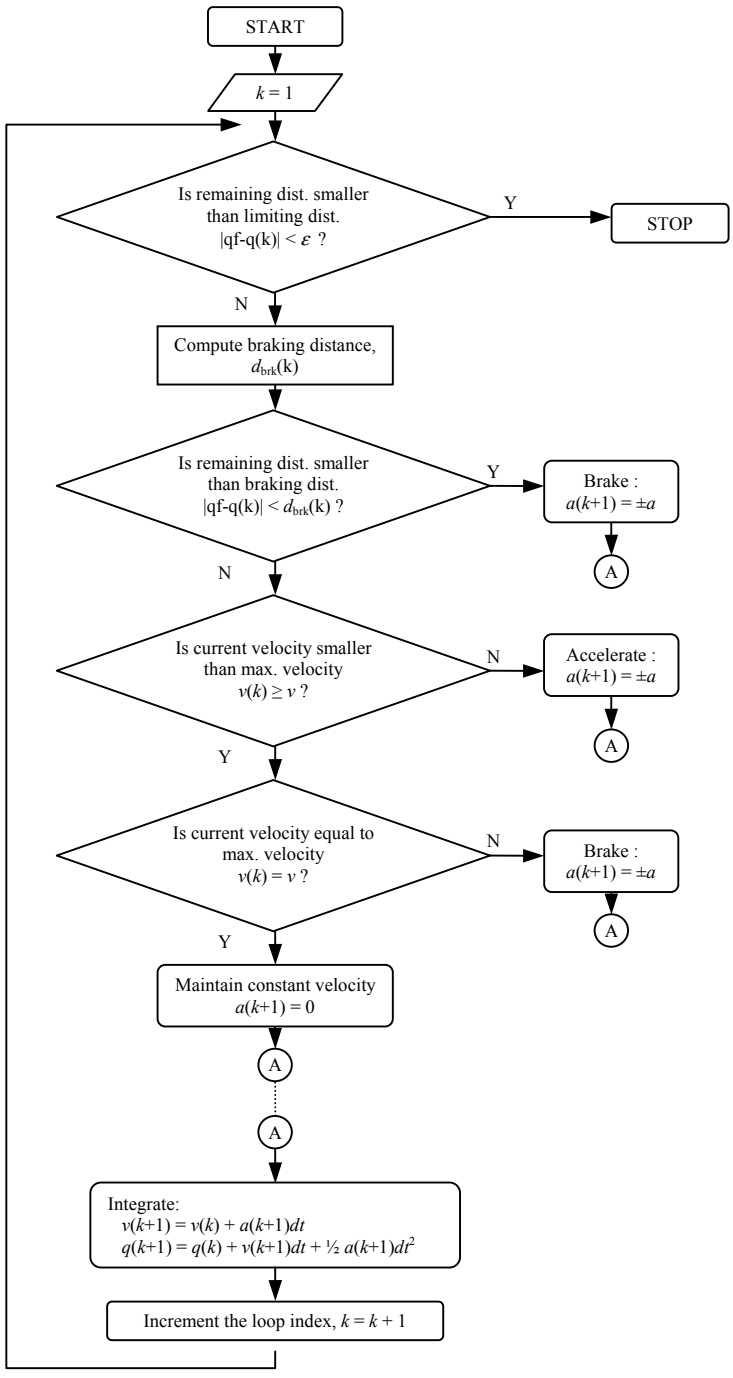

Figure 3.1 The flowchart of trapezoidal velocity motion planning algorithm.

$$d(t) = d_0 + v_0\, t - \tfrac{1}{2}\, a\, t^2$$

$$= v_0\, t - \tfrac{1}{2}\, a\, t^2 \qquad (3.1)$$

with d_0 can be considered zero. Meanwhile, the corresponding velocity equation is

$$v(t) = v_0 - a\, t$$

and at the final condition $v(t) = 0$, thus

$$t = v_0 / a$$

and substitution to (3.1) gives

$$d(t) = \frac{v_0^{\,2}}{2\,a} = d_{\text{brk}}$$

Referring back to discrete time, the braking distance for a corresponding time step k is

$$d_{\text{brk}}(k) = \frac{v^2(k)}{2\,a(k)} \tag{3.2}$$

3.2.2 Typical result

As discussed, this algorithm is simple and straightforward. The algorithm can easily alternate acceleration value to a desirable one. Those conditional evaluations are done real time; thus it is possible to accommodate target changes coming from sensory information in very minimum time and performed continuously up until the target is achieved. Being constructed in this way, the planner allows optimal motion achieving dynamic target by satisfying acceleration and velocity bounds.

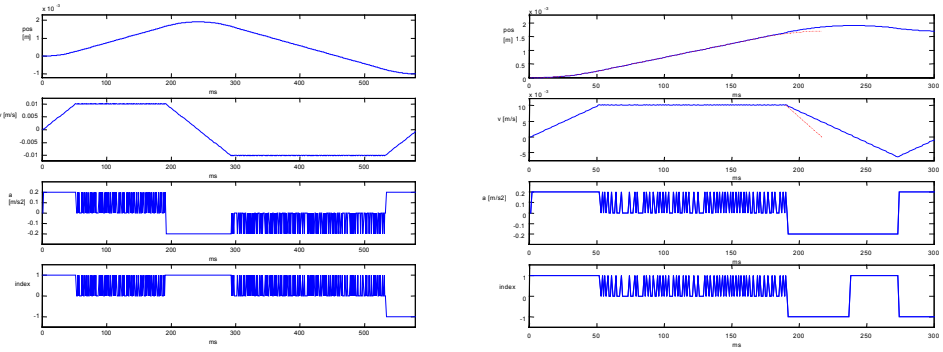

(a) (b)

Figure 3.2 One dimensional trapezoidal velocity algorithm pursuing target changes (a). The algorithm generates necessary overshoot for a close target change (b).

A simple one dimensional result of the algorithm pursuing target changes is shown in Figure 3.2. The figure shows that the algorithm can anticipate the target changes regardless of how far the distance is. Even if the target suddenly is too close, the

algorithm can easily generate the necessary overshoot. Figure 3.2b shows an example of overshoot motion.

3.2.3 Identified problem

There are identified problems in the algorithm. Due to numerical error the final velocity likely will not be zero. This velocity discrepancy even though only has a small magnitude at moments just before stop, however, it may result in undesirable effects.

Further, as it shown in the typical result, the acceleration experiences a chattering effect at constant velocity phase. Although it is bounded within permissible acceleration value, it might result in undesirable effects to the system. Similar with the native infinite jerk at boundaries, this chattering acceleration may also result to tracking problems as well as physical vibration of system affecting accuracy and device's lifetime. It is important to know the impact of this behavior to the system and it will be discussed in next chapter.

3.3 Trapezoidal acceleration algorithm

To prevent infinite jerk during fast motion one can use higher order polynomial i.e. quintic or bounded jerk profile, i.e. trapezoidal acceleration profile. However, as trapezoidal acceleration offers more practical advantages, it becomes more desirable.

Like trapezoidal velocity profile, it is possible to develop motion planning algorithm using analytical equations such as (2.110) in previous chapter. However, this analytical method is problematic and in addition, as it is shown from the derived equations in Chapter Two, it is also found to be time consuming [13, 14, 15].

Rather than utilizing analytical method, the developed algorithm also uses conditionals to control the motion. The algorithm is able to equivalently construct trapezoidal

acceleration profile. The algorithm, with respect to current conditions, selectively chooses the jerk through series of conditionals and generate the motion trajectory until the target is reached.

3.3.1 Algorithm for reactive trapezoidal acceleration

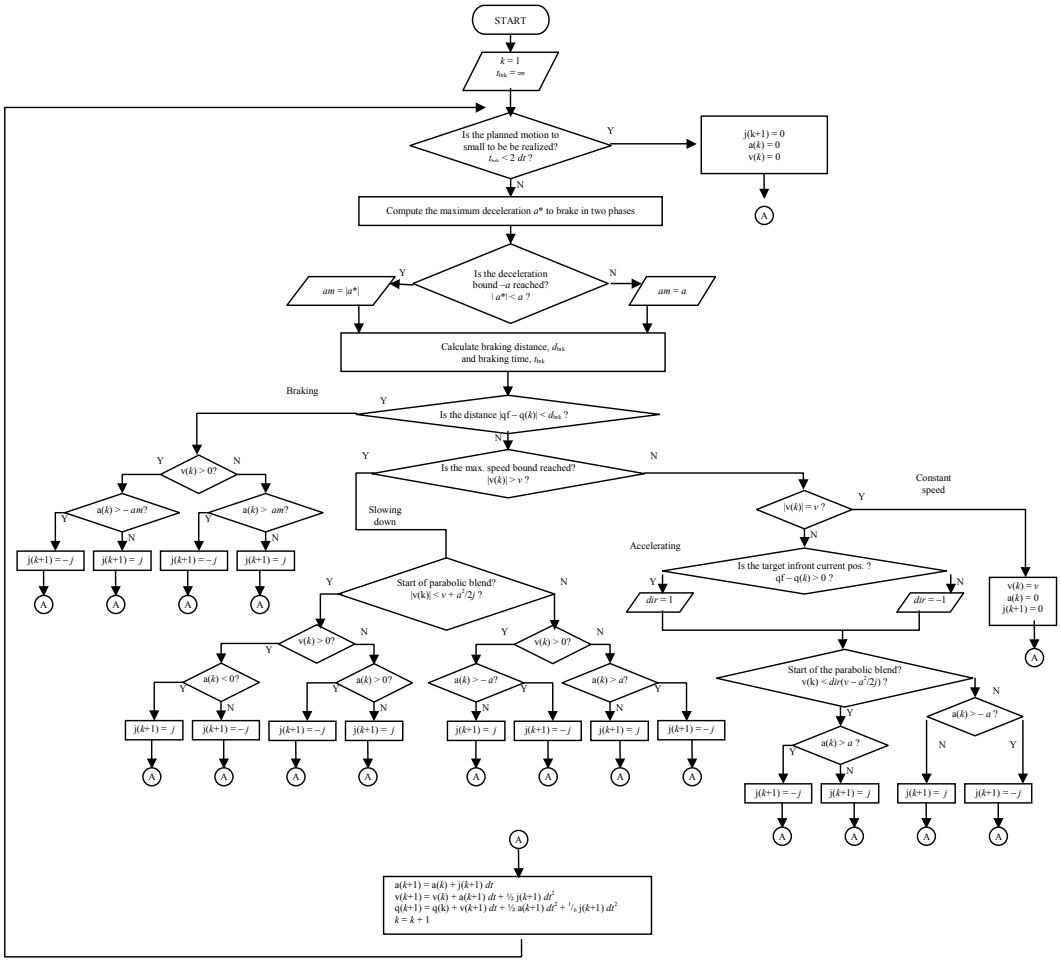

Figure 3.3 Flowchart of trapezoidal acceleration motion planning algorithm

Similarly, the algorithm works as a continuous discrete time loop with sampling time *dt* as illustrated in Figure 3.3.

The target position is determined from the sensor. Based on a known braking time t_{brk} the algorithm decides whether the motion is feasible or not under the sampling time *dt*. At start time with zero state, the braking time t_{brk} is simply initialized to a large number. If $t_{\text{brk}} < 2dt$ then the motion is not feasible thus the trajectory generation is terminated, otherwise the algorithm computes the braking distance d_{brk} and braking

time t_{brk} for current state. There are two braking cases. Figure 3.4 shows the two cases for the computation of braking time which will be discussed in the next section. If the remaining distance to target $|q_f - q(k)|$ is smaller than braking distance then it brakes using appropriate jerk value, otherwise it continues to compare the current velocity with the maximum velocity. If the current velocity is bigger than the maximum velocity, then it brakes, otherwise it accelerates. In either case the appropriate value of jerk (0, $+j$, $-j$) is selected.

The algorithm then calculates the position, velocity, and acceleration at the next time step using the selected jerk value.

$$a(k+1) = a(k) + \mathrm{j}(k+1)$$

$$v(\mathrm{k}+1) = v(\mathrm{k}) + a(\mathrm{k}+1)\, dt + \tfrac{1}{2}\, j(\mathrm{k}+1)\, dt^2$$

$$q(k+1) = q(k) + v(k+1)\, dt + \tfrac{1}{2}\, a(k+1)\, dt^2 + {}^1\!/_6\, j(k+1)\, dt^3 \qquad (3.3)$$

Note that this motion planner does not stop and eventually continue to oscillate around the target, but these oscillations will become so small such that the system will practically not move. The jerk is also set as 0 when the braking time $t_{brk} < 2\, dt$. As the movement results from the integration of the jerk as in (3.3) it is expected that the error in reaching a target will be proportional to the third order of the time step dt^3.

In brief, the flowchart can be described in steps as follows

Step 1. Check whether braking time t_{brk} is smaller than 2 dt

If the answer is yes then no further motion is realizable under sampling time dt. Set the next time step jerk $j(k+1) = 0$ zero; and so does for current acceleration $a(k) = 0$ and current velocity $v(k) = 0$.

If the answer is no then it shall continue to go.

Step 2. Calculate braking distance d_{brk} (and braking time t_{brk}) with respect to the current condition.

Step 3. Compare target distance with braking distance.

If the target distance is closer than braking distance then

Step 3.1. Brake

Step 3.2. Ask the current speed $v(k)$ sign

Step 3.3. Ask current acceleration $a(k)$ corresponding to current speed sign.

Step 3.4. Select appropriate next step jerk value $j(k+1)$.

Otherwise it shall continue to go

Step 3.5 Compare current speed with the limit $v(k) = v$?

If it is above then decrease the speed

Step 3.5.1. Consider the blend when decreasing the speed.

Step 3.5.2. Select appropriate next step jerk value $j(k+1)$.

Otherwise, ask whether current speed is equal with the limit.

If it is equal to the limit then maintain the speed

Step 3.5.3. Zero next step jerk value $j(k+1)$ and zero a pseudo current acceleration $a(k)$

Otherwise accelerate

Step 3.5.4. Consider the blend when accelerate the speed.

Step 3.5.5. Select appropriate next step jerk value $j(k+1)$.

Step 4: Integrate :

$$a(\mathrm{k}+1) = a(\mathrm{k}) + j(k+1)$$

$$v(k+1) = v(k) + a(k+1)\, dt + \tfrac{1}{2}\, j(k+1)\, dt^2$$

$$q(k+1) = q(k) + v(k+1)\, dt + \tfrac{1}{2}\, a(k+1)\, dt^2 + {}^{1}/_{6}\, j(k+1)\, dt^3 \qquad (3.3)$$

Step 5: Increment loop index, $k = k+1$

Step 6: Repeat the loop from *Step 1* to *Step 5* until motion is no longer able to be realized.

3.3.2 Computation of braking time

The previous discussion mentions the two braking cases for the computation of the braking distance and braking time. Figure 3.4 shows the two cases. In case A (Figure 3.4.a) the minimum deceleration $-a$ is not reached and a new lower bound $a = -a^*$ has to be computed, while in the "normal" case, case B (Figure 3.4.b), the deceleration reaches the lower bounds $-a$. Case A typically occurs at moments close to the target, while case B mostly occurs at the other parts.

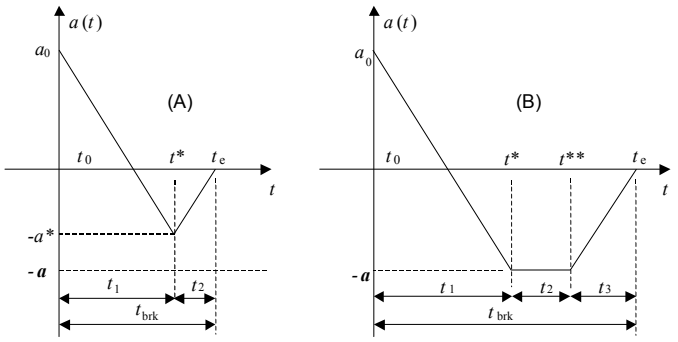

Figure 3.4 Computation of time to brake , (A) close to the target, braking in two phases; (B) normal brake, braking in three phases.

3.3.2.1 Case A, two phases braking

With respect to Figure 3.4.a, for case A, the braking distance is computed as

$$d_{brk} = \int_{t_0}^{t^*} v(t)dt + \int_{t^*}^{t_e} v(t)dt \tag{3.4}$$

and the braking time t_{brk} is derived as follow.

Figure 3.4.a shows that at $t_0 < t < t^*$ the acceleration and velocity are:

$$a(t) = a_0 - j\,(t - t_0) \tag{3.5}$$

$$v(t) = v_0 + a_0\,(t - t_0) - \tfrac{1}{2} j\,(t - t_0)^2 \tag{3.6}$$

To solve t_1, substitution of $a(t^*) = -a^*$ to equation (3.5) gives

$$t_1 = (t^* - t_0) = \frac{a_0 + a^*}{j}$$

and substitution of t_1 to (3.6) gives

$$v^* = v_0 + a_0 \frac{a_0 + a^*}{j} - \tfrac{1}{2} j \left(\frac{a_0 + a^*}{j} \right)^2$$
$$= v_0 + \frac{{a_0}^2 - (a^*)^2}{2j}$$

At $t^* < t < t_e$ the acceleration and velocity are

$$a(t) = -a^* + j\,(t - t^*) \tag{3.7}$$

$$v(t) = v^* - a^*\,(t - t^*) + \tfrac{1}{2} j\,(t - t^*)^2 \tag{3.8}$$

To solve t_2, substitution of $a(t_e) = 0$ to equation (3.7) gives $(t_e - t^*) = t_2 = \frac{a^*}{j}$ and substitution of t_2 to (3.8) gives

$$v_e = v^* - a^* \frac{a^*}{j} + \tfrac{1}{2} j \left(\frac{a^*}{j} \right)^2 = \left(v_0 + \frac{{a_0}^2 - (a^*)^2}{2j} \right) - \frac{(a^*)^2}{2j}$$

hence, the new acceleration bound is

$$a^* = \sqrt{(v_0 - v_e) j + \frac{{a_0}^2}{2}} \tag{3.9}$$

where v_e = final velocity. The braking time can be written as

$$t_{brk} = t_1 + t_2$$

$$= \frac{a_0 + a^*}{j} + \frac{a^*}{j} = \frac{a_0}{j} + \frac{2\,a^*}{j} \tag{3.10}$$

$$= \frac{a_0}{j} + \frac{2}{j} \sqrt{(v_0 - v_e) j + \frac{{a_0}^2}{2}}$$

or like in [13],

$$t_{brk} \equiv t_e - t_0 = \frac{a_0}{j} + \sqrt{\frac{4(v_0 - v_e)}{j} + \frac{2\,{a_0}^2}{j^2}} \tag{3.11}$$

correspondingly, using (3.10), it is possible to rewrite t_1 and t_2

$$t_1 = t^* - t_0 = \frac{1}{2}\left(t_{brk} + \frac{a_0}{j}\right)$$

$$t_2 = t_e - t^* = \frac{1}{2}\left(t_{brk} - \frac{a_0}{j}\right)$$

Hence, (3.4) can also be expressed as

$$d_{\text{brk}} = v_0\, t_1 + \tfrac{1}{2}\, a_0\, t_1^2 - {}^1\!/_6\, j\, t_1^3 + v^*\, t_2 - \tfrac{1}{2}\, a^*\, t_2^2 + {}^1\!/_6\, j\, t_2^3 \qquad (3.12)$$

3.3.2.2 Case B, normal three phases braking

Secondly, on the "normal" case B in Figure 3.4b, the braking distance is

$$d_{brk} = \int_{t_0}^{t^*} v(t)dt + \int_{t^*}^{t^{**}} v(t)dt + \int_{t^{**}}^{t_e} v(t)dt \qquad (3.13)$$

and the braking time t_{brk} is derived as follow.

Figure 3.4b shows that at $t_0 < t < t^*$ the acceleration and velocity are:

$$a(t) = a_0 - j\,(t - t_0) \qquad (3.14)$$

$$v(t) = v_0 + a_0\,(t - t_0) - \tfrac{1}{2}\, j\,(t - t_0)^2 \qquad (3.15)$$

Similarly, to solve t_1, substitution of $a(t^*) = -a$ to equation (3.14) gives

$$t_1 = (t^* - t_0) = \frac{a_0 + a}{j}$$

and substitution of t_1 to (3.15) gives

$$v^* = v_0 + a_0 \frac{a_0 + a}{j} - \tfrac{1}{2}\, j\left(\frac{a_0 + a}{j}\right)^2$$

$$= v_0 + \frac{a_0^{\,2} - a^2}{2j}$$

At $t^* < t < t^{**}$ the acceleration and velocity are

$$a(t) = -a \qquad (3.16)$$

$$v(t) = v^* - a\,(t - t^*)$$

$$= v_0 + \frac{a_0{}^2 - a^2}{2j} - a\, t_2 \tag{3.17}$$

Meanwhile at $t^{**} < t < t_e$ the velocity and acceleration are

$$a(t) = -a + j\,(t - t^{**}) \tag{3.18}$$

$$v(t) = \left(v_0 + \frac{a_0{}^2 - a^2}{2j} - a\, t_2 \right) - a\,(t - t^{**}) + \tfrac{1}{2} j\,(t - t^{**})^2 \tag{3.19}$$

yet, at $t = t_e$ the acceleration is zero, $a(t) = 0$; thus substituting these value to (3.18) gives

$$(t_e - t^{**}) = t_3 = \frac{a}{j}$$

Accordingly, substitution of t_3 to (3.18) will give

$$v_e = v(t_e) = \left(v_0 + \frac{a_0{}^2 - a^2}{2j} - a\, t_2 \right) - a\left(\frac{a}{j}\right) + \frac{j}{2}\left(\frac{a}{j}\right)^2$$

from which t_2 and v^{**} can be obtained, i.e.

$$t_2 = t^{**} - t^* = \frac{v_0 - v_e}{a} + \frac{a_0{}^2 - 2\,a^2}{2\,j\,a}$$

$$v^{**} = v(t^{**}) = v_0 + \frac{a_0{}^2 - a^2}{2j} - a\left(\frac{v_0 - v_e}{a} + \frac{a_0{}^2 - 2\,a^2}{2\,j\,a} \right) \quad = \quad \frac{a^2}{2j} \tag{3.20}$$

Hence, the braking time is

$$t_{brk} = t_1 + t_2 + t_3 \quad = \left(\frac{a_0 + a}{j} \right) + \left(\frac{v_0 - v_e}{a} + \frac{a_0{}^2 - 2\,a^2}{2\,j\,a} \right) + \left(\frac{a}{j} \right)$$

or

$$t_{brk} = t_e - t_0 = \frac{v_0 - v_e}{a} + \frac{a_0{}^2 + 2\,a_0 a}{2\,j\,a} + \frac{a}{j} \tag{3.21}$$

Braking distance equation (3.13) thus can also be expressed as

$$d_{\text{brk}} = (v_0 t_1 + \tfrac{1}{2}\, a_0 t_1{}^2 - {}^1\!/_6\, j\, t_1{}^3) + (v^* - \tfrac{1}{2}\, a\, t_2) + (v^{**}\, t_3 - \tfrac{1}{2}\, a\, t_3{}^2 + {}^1\!/_6\, j\, t_3{}^3) \tag{3.23}$$

3.3.3 Typical result

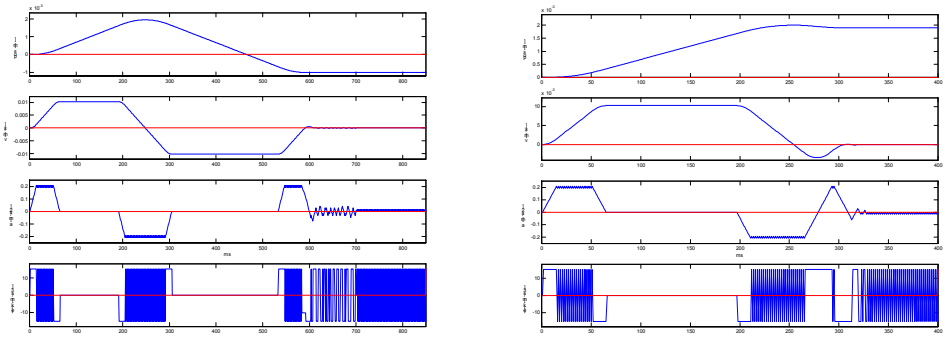

(a) (b)

Figure 3.5 One dimensional trapezoidal acceleration algorithm pursuing target changes. The algorithm generates necessary overshoot for a close target change (b).

The algorithm can easily alternate the jerk value as required. Meanwhile, like trapezoidal velocity, the conditionals can be done in very minimum time. The algorithm is possible to accommodate target changes coming from sensory information while maintain smoothness and optimality by satisfying kinematic bounds.

A typical result of the algorithm pursuing two changes of target position like in trapezoidal velocity example is shown in Figure 3.5. The figure also shows the necessary overshoot when the target becomes too close (Figure 3.5b)

3.3.4 Oscillation

Figure 3.5 also shows the typical oscillation at moments close to target. More apparent oscillation can be seen in the acceleration profile. This considerable small magnitude oscillation occurs due to the necessary overshoots in approaching the target. Numerical errors of the discretization also lead to the discrepancies causing this oscillation.

As the algorithm only controls jerk value—a third order derivative of position—it can be understood that the integrations will have longer response delay than trapezoidal

velocity. The jerk value will affect the oscillation convergence. Higher jerk bound will result in faster convergence of the oscillation, the lower the slower.

Jerk is an empirical value. Commercial actuators never suggest any recommended values. The jerk bound will depend on the type of application and the physical structure of the applied system. To select appropriate bound value users shall refer to the experiences and empirical results, i.e. compromising the desirable motion smoothness and response characteristics, with applicable speed and motion reliability.

In this algorithm, the allowable highest jerk value can be determined from the sampling time *dt*

$$j \leq \frac{a}{dt}$$

A highest jerk setting $j = a/dt$ will allow the acceleration to jump to/from maximum value within one sampling time period *dt* and thus it allows an alternating acceleration like in trapezoidal velocity.

Whereas, the lowest value appears to be unrestricted; however it is important to minimize the oscillations especially at moments close to target. To determine the lowest value it is possible to use a practical approximation as follows. A low jerk value may eliminate constant acceleration phases and let the maximum velocity be achieved in only two consecutive opposing constant jerk phases. i.e. first and third phases or the fifth and seventh phases of the typical trapezoidal acceleration profile. The corresponding acceleration and velocity equations of these two phases will be

$a(t) = j\,t$ and $a(t) = 0 = a - j\,t$

$v(t) = \frac{1}{2}\,j\,t^2$ and $v(t) = v = v_0 + a_0 t - \frac{1}{2}\,j\,t^2$.

Solving the equations for the given bounds *v* and *a* will give

$$j \geq \frac{a^2}{v}$$

Hence for this algorithm, the suggested jerk value is a range of

$$\frac{a^2}{v} \le j \le \frac{a}{dt} \tag{3.24}$$

3.4 Multidimensional reactive motion planner

Multidimensional motion planning will be desirable as manipulators commonly resemble multilink body driven by multi joint actuators, In task space, position and orientation planning also impose a multidimensional planning, i.e. 6 degrees-of-freedom. It is now desirable to develop multidimensional planner using the one dimension algorithm.

3.4.1 Motion planner with independent axis

A simple possibility to construct a multidimensional reactive motion planner consists of using *N* copies of one-dimensional planner working independently for *N*-dimension system. Each dimension (i.e. each axis if planned in joint space) will move as fast as possible relative to the specified kinematic bounds.

Typical result of the planner working independently for each axis is given in Figure 3.6.a. As expected, the resulting trajectories generally do not reach to target simultaneously or from straight line direction, , but tend to approach at different angles corresponding to the velocity bounds. For example, the trajectories make 45^o or 135^o angles if all dimensions have the same velocity bound like in Figure 3.6.a.

This typical result is similar with CNC's rapid feed trajectories generation [1]. As long as motion coordination among axis is not the main consideration, this simple implementation will sufficiently fulfill the need for fast reactive motion planning.

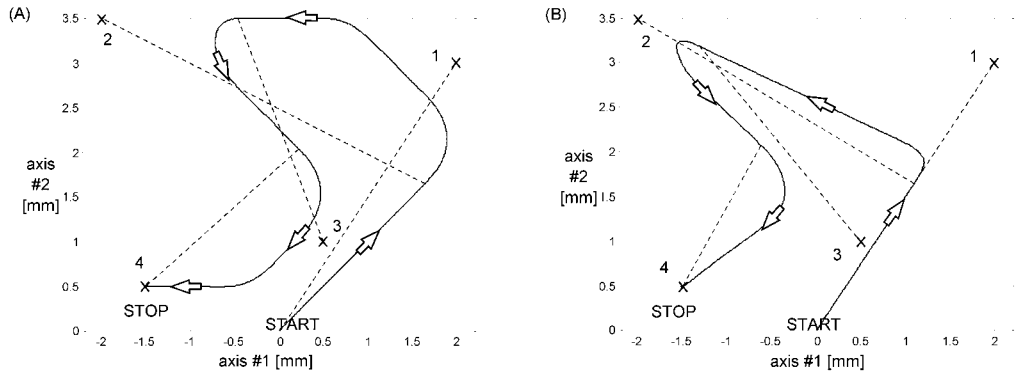

Figure 3.6 Movement of a 2-dimensional motion planner formed of (A) independent, and (B) coordinated one-dimensional reactive trapezoidal velocity planners pursuing changing targets. The dotted line connect point in motion to the new target. The targets 1, 2, 3, and 4 are: (0.002, 0.003) m at t = 0 s, (-0.002, 0.0035) at t = 190 ms, (0.0005, 0.001) m at t = 500 ms, (-0.0015, 0.0005) m at t = 670 ms. The kinematic bounds are v = (0.01; 0.01) m/s and a = (0,2; 0.2) m/s^2.

3.4.2 Motion planner with coordinated axis

Coordinating the trajectories to move straightly to target might become desirable and useful in many applications (such as interception) [26, 48, 49, 61]. In recent application of sensor guided robotic surgery; the motion coordination also will generate motions straightly to the pointing/guiding device and helps to give better sensations. This section describes a simple scaling method for generating coordinated motion among axis.

To bring the trajectory move straightly to target each dimension should coordinate the motion planning. Each axis planner should then be able to adjust motion parameters with respect to other axis. The method discussed here will bring the velocity vector in the direction of the target by modifying the vector of velocity bounds $\mathbf{v} = (v_1, v_2, \ldots v_i, \ldots v_N)$. The velocity bounds vector $\mathbf{v}_{\text{new}}$ is modified to let it point to the target direction. Thus it imposes that $\mathbf{v}_{\text{new}}$ becomes proportional to the vector $\mathbf{c} = (c_1, c_2, \ldots c_i, \ldots c_N)$ between the current position and the target, i.e.

$$\mathbf{v}_{\text{new}} = s\,\mathbf{c} \tag{3.25}$$

where s is the scaling factor to be determined. The scaling factor s has to make the new velocity bound $v_{i\,(new)}$ smaller or equal to the real bound v_i in every dimension i=1…N, i.e.

$v_{i\,(new)} = s\, c_i \leq v_i$, or in other words

$$s \leq \left(\frac{v_i}{c_i} \right) \quad \text{for all } i. \tag{3.26}$$

The maximum s value such that satisfies (3.26) hence is

$$s = \min_i \left(\frac{v_i}{c_i} \right) \quad \text{for all } i. \tag{3.27}$$

According to (3.25) thus the velocity bound is changed in every time step as

$$\mathbf{v}_{\text{new}} = \min_i \left(\frac{v_i}{c_i} \right) \mathbf{c} \tag{3.28}$$

Figure 3.7 illustrates how the velocity bound vector is determined for two different target points. In Figure 3.7a, v_1 is scaled down with a ratio of v_2/c_2 while in Fig. 5B v_2 is scaled down with a ratio of v_1/c_1.

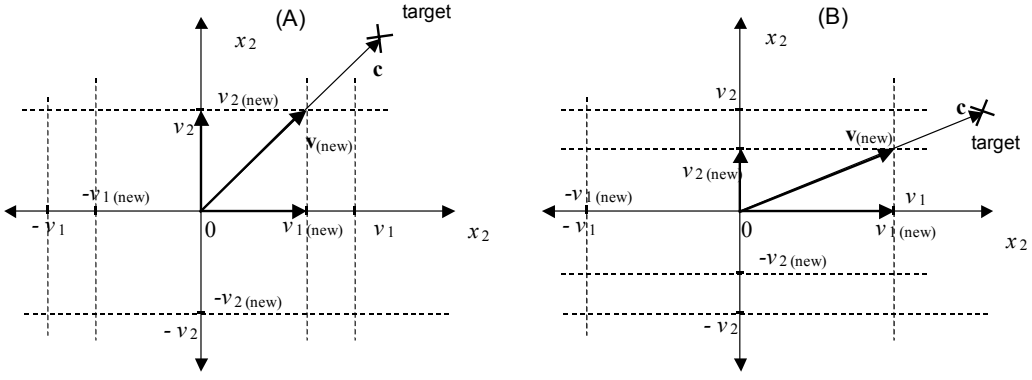

Figure 3.7 Scaling the velocity bounds to reach the target straight for two different cases.

When only the velocity is scaled, it may occur that at the initial phase of the movement (i.e. until the maximal speed is reached) the generated trajectory is not perfectly straight. To avoid this, the acceleration bound vector $\mathbf{a} = (a_1, a_2, \ldots a_i, \ldots a_N)$ also has

to be scaled, i.e. similarly using

$$\mathbf{a}_{\text{new}} = \min_i \left(\frac{a_i}{c_i} \right) \mathbf{c} \tag{3.29}$$

and for the motion planner with trapezoidal acceleration also the jerk bound vector $\mathbf{j} = (j_1, j_2, \ldots j_i, \ldots j_N)$ using

$$\mathbf{j}_{\text{new}} = \min_i \left(\frac{j_i}{c_i} \right) \mathbf{c} \tag{3.30}$$

Typical result of a coordinated motion planning for two axis can be seen in Figure 3.6b. The motion turns towards every new target as fast as possible and then drives straight to it, also providing smooth transitions.

3.5 Prevention of Collisions

As the trajectory is modified along the way and obstacles position can continuously change, it is necessary to check at every time step whether a collision may occur or not. This section describes a simple collision prevention algorithm based on the braking distance d_{brk} under assumption that the distance to the obstacles is provided at every time. This assumption imposes that typical sensor (e.g. laser range finder, ultrasonic sensor, lidar) is measuring and providing information of direction and distance to the closest point on the obstacle in real-time.

The algorithm compares the braking distance with the free distance, defined as the intersection of the normal to the obstacle with a straight line in the forward direction (Figure 3.8). If the free distance is smaller than a safe distance then the robot starts immediately to brake. The safe distance is defined as braking distance with an offset δ, that is safe distance = $(1 + \delta)\, d_{\text{brk}}$. The offset α corresponds to a distance achieved in a period Δt as follows

$\delta = v\,\Delta t + \frac{1}{2}\,a\,\Delta t^2$ for the trapezoidal velocity profile and

$\delta = v\,\Delta t + \frac{1}{2}\,a\,\Delta t^2 + \frac{1}{6}\,j\,\Delta t^3$ for the trapezoidal acceleration.

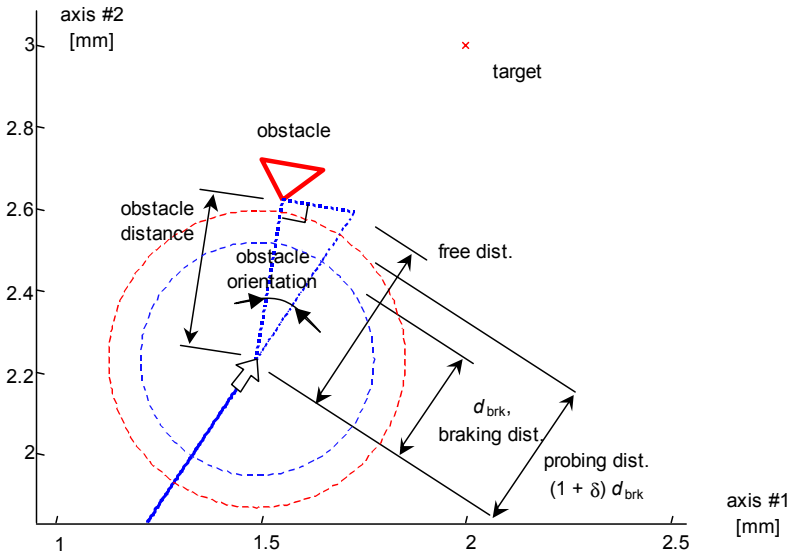

Figure 3.8 Distance diagram for prevention of collisions realized with the motion planner algorithm. The robot might need to brakes to see the free way.

In general $\Delta t = 4\,dt$ will give satisfactory results at any motion direction. Note that $\Delta t = dt$ would be sufficient when the motion is straight, but not when it is turning. During a straight braking motion, the direction is maintained using appropriately scaled deceleration and jerk bounds as previously described. On the other hand, in turning condition the algorithm is turning as fast as possible for each axis. As a consequence, should there be a need to brake due to obstacles; it needs larger free distance offset.

Chapter 4

Simulations and Experiments

To verify the algorithm performance, a series of simulations was done using MATLAB [67]. The simulations focus on the coordinated axis motion planning. As the algorithms directly compute the discrete position using the integration over selected motion parameter rather than pre-calculating the whole trajectory, it becomes desirable to know the planning accuracy. It is also desirable to observe how a modeled system behaves under such reactive action using the algorithms.

4.1 Two dimension reactive motion planning with coordinated axis

A simulation of the algorithms doing two dimensional planning realized in MATLAB is presented in Figure 4.1 and 4.2 respectively for trapezoidal velocity and for trapezoidal acceleration motion planning algorithm. Nine 'jumping' targets are given consecutively without waiting for each target to be reached, except for the last target. The dotted lines indicate the target changes, i.e. connecting a point in motion to the new target. The nine targets, the corresponding changing times, and the kinematic bounds are as described in of the figure captions.

The results show that the motion turns towards every new target as fast as possible and then drives straight to it, and the transitions are always smooth. Note that the imposed kinematic bounds are never exceeded. The trapezoidal acceleration algorithm (Figure 4.2) is smoother than the trapezoidal velocity algorithm (Figure 4.1), but obviously will turn slightly slower towards the targets.

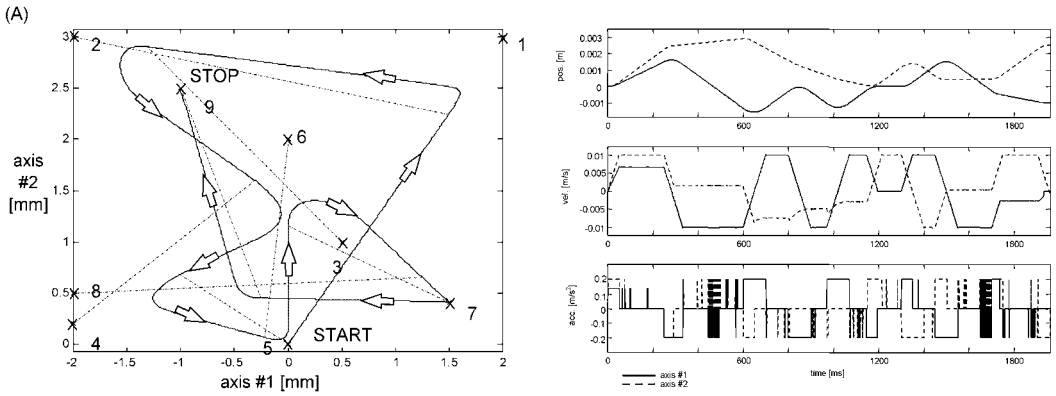

Figure 4.1 Simulation of the motion planner with trapezoidal velocity profile tracking a "jumping target". The bounds are as in Figure 3.6. The targets 1 to 9 are: (0.002, 0.003) m at t = 0 s, (-0.002, 0.0035) at t = 250 ms, (0.0005, 0.001) m at t = 600 ms, (-0.002, 0.0002) m at t = 800 ms, (0,0) at t = 970 ms, (0, 0.002) m at t = 1150 ms, (0.0015, 0.0004) at t = 1300 ms, (-0.002, 0.0005) m at t = 1450 ms, (-0.001, 0.0025) at t = 1700 ms

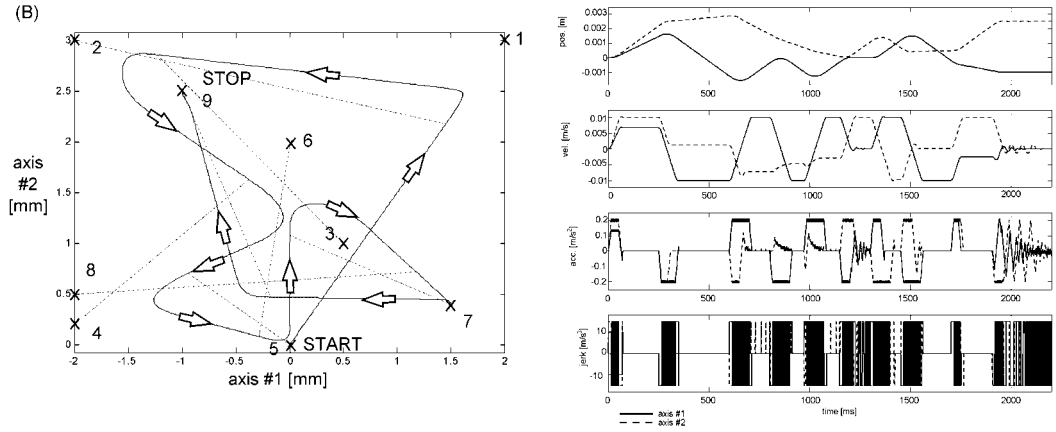

Figure 4.2 The same sensor-guided movement as in Figure 4.1 realized with the motion planner with trapezoidal acceleration. The jerk bounds are j = (15;15) m/s^3.

4.2 Oscillation of trapezoidal acceleration algorithm

The suggested jerk bound value for trapezoidal acceleration motion planning algorithm is given in (3.24). Figure 4.3 below shows a typical final oscillation of trapezoidal acceleration algorithm using two different jerk bounds. The low jerk bound may result into longer oscillation thus takes longer time to settle. The higher the faster. Noting that velocity and acceleration bounds respectively are 0.01 m/s and 0.2 m/s^2, the jerk bound j = 3.5 m/s^3 in Figure 4.3a is lower than the suggested range. On the other hand, a reasonable value of j = 15 m/s^3 in Figure 4.3b gives satisfactory result

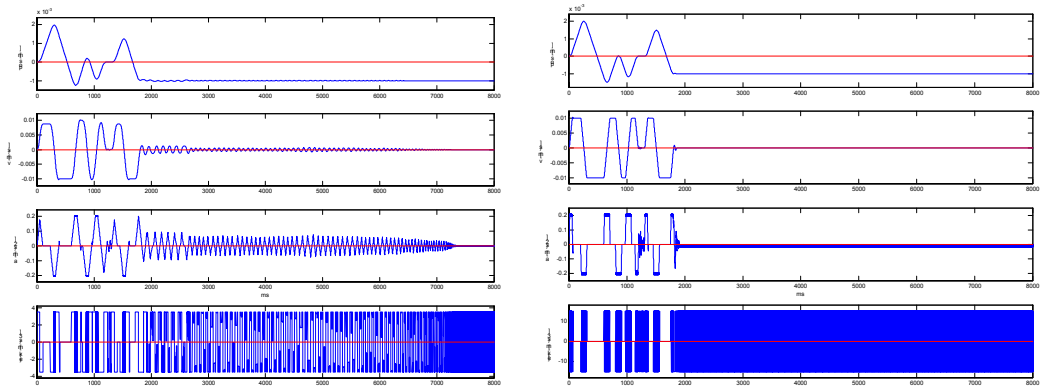

Figure 4.3 Two different jerk bound for same motion sequence. On the left figure j = 3.5 m/s^3 while the right figure is higher, j = 15 m/s^3.

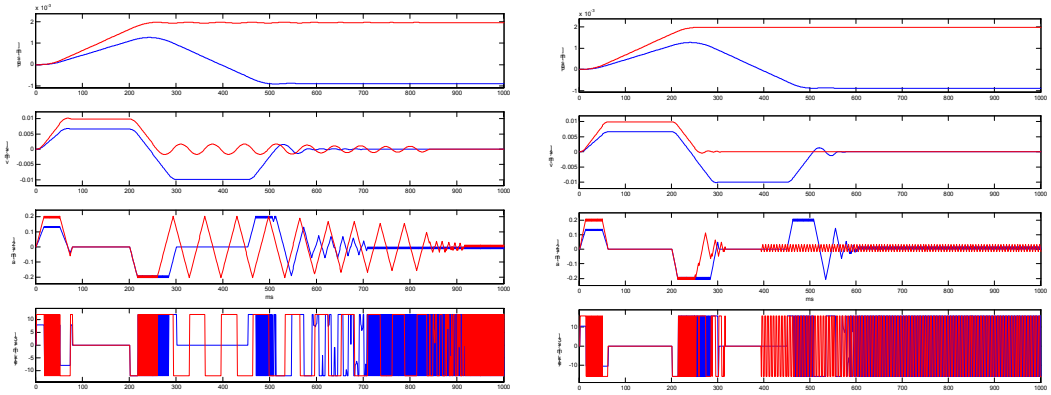

Figure 4.4 Two different jerk bound for same motion sequence. On the left figure j = 12 m/s^3 (3 times of the minimum of the range) while the right figure is higher, j = 16 m/s^3 (4 times of the minimum of the range).

However, the multidimensional implementation might need further considerations. In a multidimensional implementation the coordinated axis method will adjust the bounds to generate straight motion to the target. Therefore the velocity bound will be adjusted correspondingly and according to (3.24) the minimum limit of the range will also be adjusted to a higher number. The assigned jerk bound might not cover the adjustment. Figure 4.4 gives an example of such situation in two dimension application where one axis experienced oscillation as a result of the adjusted kinematic bounds. Hence, it is necessary to select a safe jerk bound value to obtain satisfactory motions in all directions without erratic oscillations. It is observed that in general taking j in range of

$10\frac{a^2}{v} \le j \le \frac{a}{dt}$; with $dt \le v / 10a$ ought to be able to give satisfactory result in all motion directions.

4.3 Reactive position and orientation planning

In addition to the two dimensional reactive planning, the implementation is also done in position and orientation planning. The simulation imposes six degree of freedom motion planning in task space creating a 3D visualization of the reactive motion using the algorithms.

The simulation uses Roll-Pitch-Yaw or any similar three angles representation of orientation. The translation and rotation are planned simultaneously using six-dimensional reactive motion planner with coordinated axes as described previously. The orientation **R** is represented as

$$\mathbf{R} = \mathbf{R}_3\, \mathbf{R}_2\, \mathbf{R}_1 \qquad (4.1)$$

where

$$\mathbf{R}_i = \mathrm{Rot}(\mathbf{x}_i, \alpha_i) \quad ; i = 1,2,3$$

are the three simultaneous rotations with angles α_1; α_2; α_3 about three corresponding perpendicular axes of the reference frame namely $\mathbf{x}_1$; $\mathbf{x}_2$; $\mathbf{x}_3$. By using this representation and resolving α_i such as in [3], it becomes simple to code the remaining orientation distance vector $\boldsymbol{\alpha} = (\alpha_1; \alpha_2; \alpha_3)^T$ to the target as

$$\boldsymbol{\alpha} = \boldsymbol{\alpha}_f - \boldsymbol{\alpha}_c \qquad (4.2)$$

where $\boldsymbol{\alpha}_f = (\alpha_{f1}; \alpha_{f2}; \alpha_{f3})^T$ describes the final orientation vector and $\boldsymbol{\alpha}_c = (\alpha_{c1}; \alpha_{c2}; \alpha_{c3})^T$ the current one. Correspondingly the remaining position $\mathbf{x} = (x_1; x_2; x_3)^T$ can be written as

$$\mathbf{x} = \mathbf{x}_f - \mathbf{x}_c \qquad (4.3)$$

with $\mathbf{x}_f = (x_{f1}; x_{f2}; x_{f3})^T$ and $\mathbf{x}_c = (x_{c1}; x_{c2}; x_{c3})^T$ denotes the final and current position vectors respectively. Hence the planner uses the three orientation parameters (α_1; α_2; α_3) and three Cartesian parameters (x_1; x_2; x_3) for the six dimensional position and orientation planning. Note that when this representation is used for robots with a "wrist" mechanism corresponding to RPY angles, the true motor limitations can be used as orientation kinematic bounds.

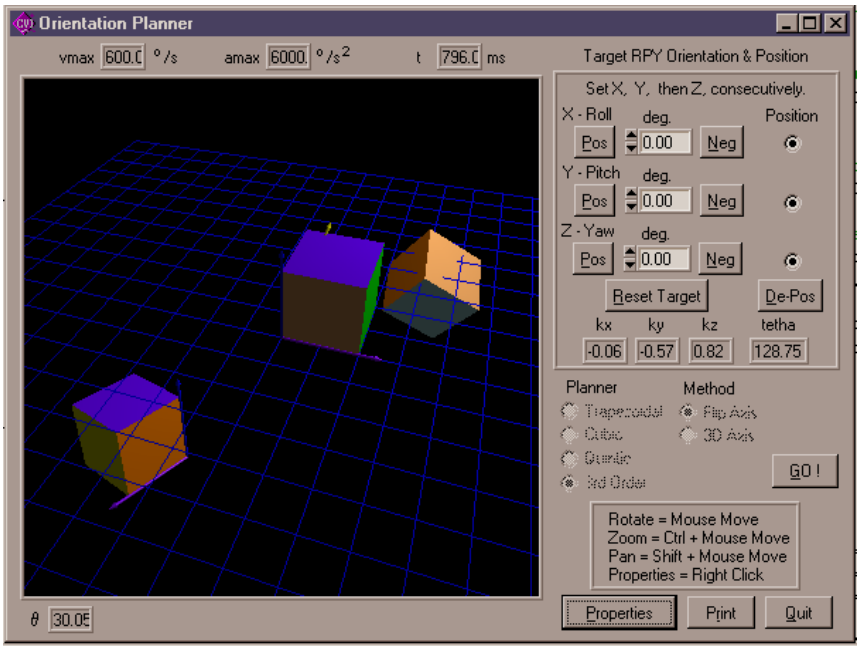

Figure 4.5 3D trajectory and orientation planner simulation program

The visualization is done using the OpenGL graphic library [68] under LabWindows™ development environment [69]. The above algorithms realize coordinated motion of all axes, meaning that all axes will move until the end of the movement. Figure 4.5 shows a screen capture of the simulation program and doing three targets reactive motion. As can be seen in Figure 4.6 the kinematic bounds are satisfied, provided with the smooth transitions. The kinematic bounds are as given in the figure caption. The program gives intuitive 3D trajectory transitions of position and orientation throughout dynamic target changes. However, as rotations are non commutative, the orientation in general

will not be straight on the sphere space. It drives straight in the space of the three orientation parameters.

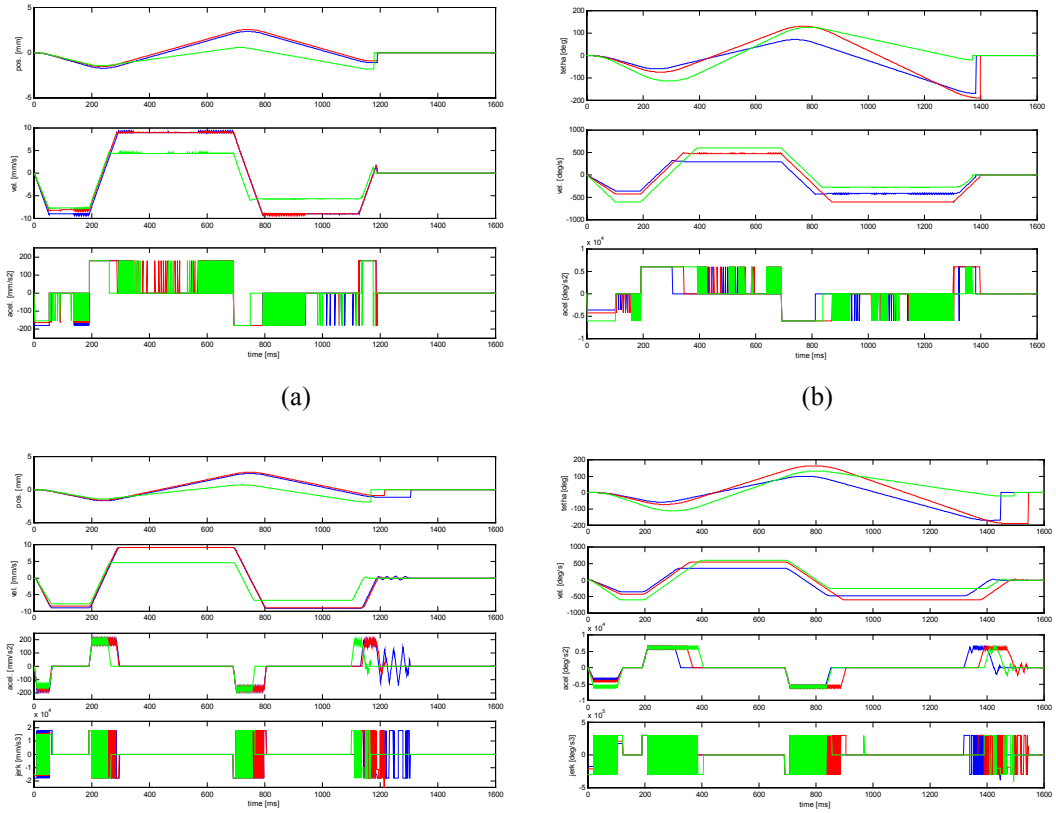

Figure 4.6 Position and orientation graphs using trapezoidal velocity (a) and (b), and using trapezoidal acceleration (c) and (d). The kinematic bounds are $v = 9$ m/s, $a = 180$ m/s^2, $j = 18000$ m/s^3 for position, and $\dot{\theta} = 600$ °/s, $\ddot{\theta} = 6000$ °/s^2, $\dddot{\theta} = 300000$ °/s^2 for orientation.

In addition, the program is also designed to perform polynomial based motion planning, i.e. using cubic and quintic profile. The algorithms use maximum velocity criterion for cubic and maximum acceleration criterion for quintic.

Figure 4.7 shows a typical result for the same three targets reactive motion using polynomials. For a given kinematic bounds, the results show that despite velocity continuities in cubic, the acceleration is not controlled. On the other hand, maintaining acceleration continuity in quintic results in uncontrolled velocity limit. Likely the result seems to be faster than trapezoidals. However this is not necessarily true as the

velocity maxima are higher than trapezoidal's. The trapezoidal algorithms shows its reliability and optimality over the polynomials.

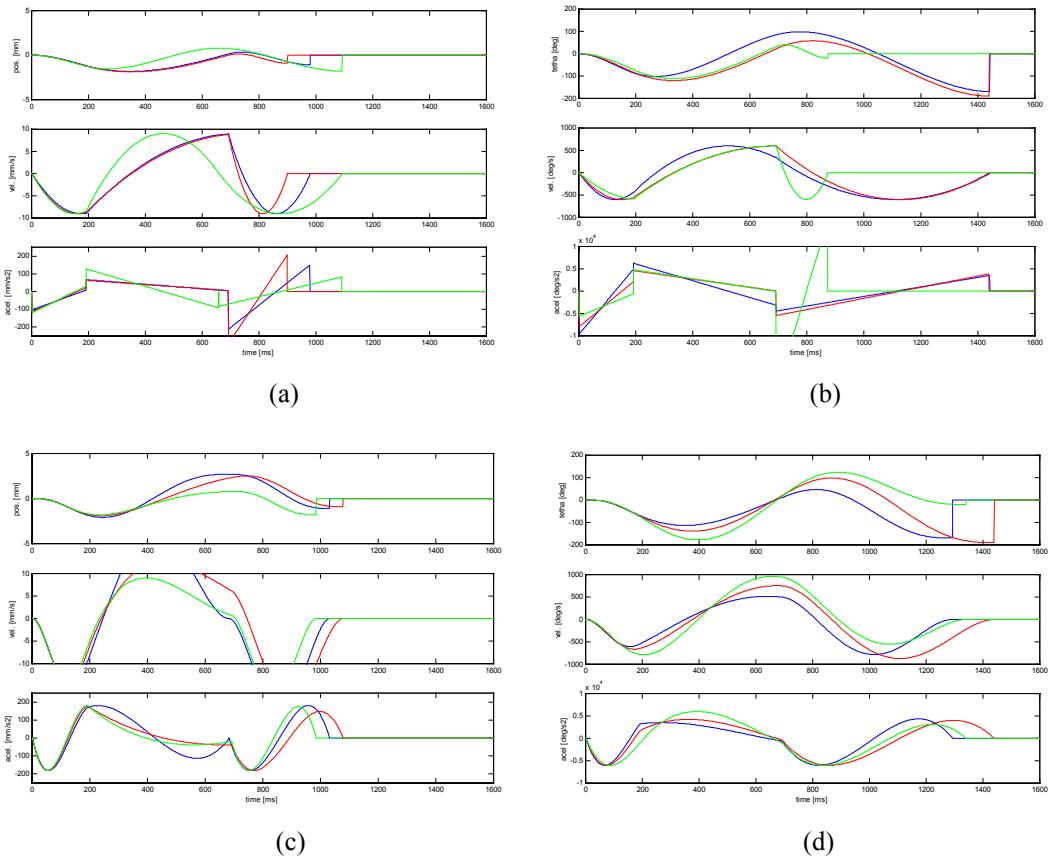

Figure 4.7 Position and orientation graphs of motion planning using cubic (a) and (b) under v criterion, and quintic (c) and (d) under a criterion. The kinematic bounds are $v = 9$ m/s, $a = 180$ m/s^2 for position and $\dot{\theta} = 600$ º/s, $\ddot{\theta} = 6000$ º/s^2 for orientation.

4.4 Optimality of coordinated axis motion planning

The planner algorithm with coordinated axes will make the motion turn as fast as possible to move towards the target straightly and then reach this target as soon as possible. In average this method is faster than the version using copies of N-independent one-dimensional motion planner.

Series of one hundred "random double-target" simulations show the time advantage of coordinated axis motion planning over the uncoordinated method. In these simulations the target position is modified randomly during the motion to the first target, as shown

in Figure 4.8a. The distribution of the difference between the total movement time with the coordinated axes algorithm and the algorithm with uncoordinated axes is shown in Figure 4.8b. Figure 4.8b shows that in 63% of the cases the axes coordination algorithm results in faster motions, and the time saved is about 50 ms in mean. This is due to the fact that the motion planner with coordinated axes is moving in a direction statistically closer to potential second targets than the planner with independent axis.

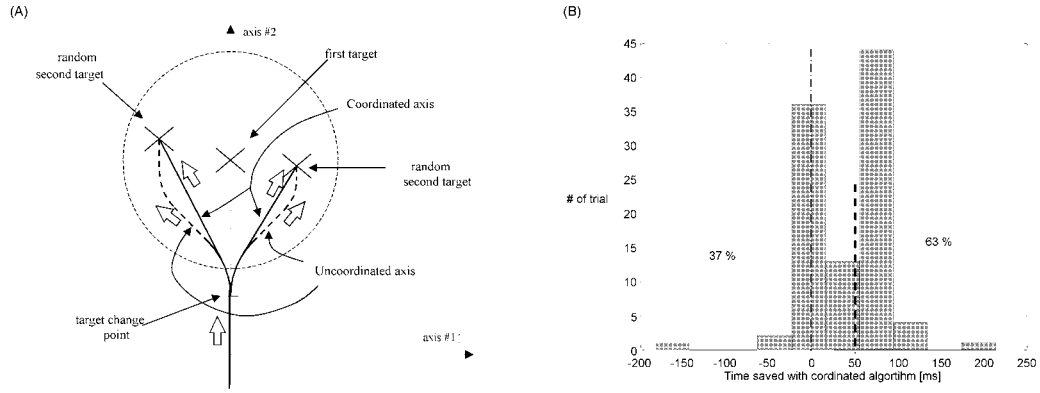

Figure 4.8 (A) Motion planning with independent versus coordinated axes in double-target trials with random second targets. (B) The distribution of the time difference between the coordinated axes and uncoordinated axes algorithm.

4.5 Accuracy

In contrast to common motion planners which do a completely pre-calculated trajectory prior to motion execution such as in polynomial-based motion planner, the algorithms do not calculate and prescribe the trajectory connecting the starting point to the target. The algorithms at every time step directly generate and integrate the next time step position using selected motion parameter. This direct computation is done until the terminating condition is achieved. It is thus becomes desirable to know how close the target can be achieved or how accurate the planning algorithm is.

Series of simulations under MATLAB show the typical position error to the target under given kinematic bounds. It is observed that the trapezoidal velocity motion planning algorithm has an overall error about 10 μm (Figure 4.9) under given

kinematic bounds $a = 0.2$ m/s^2 and $v = 0.01$ m/s. The motion planning algorithm with trapezoidal acceleration results in higher accuracy. The algorithm will slightly oscillate around the target and approach it as close as possible. For example for $j = 15$ m/s^3, $a = 0.2$ m/s^2, $v = 0.01$ m/s the error to the target is only 10 nm (Figure 4.10), i.e. 1000 times smaller than with the trapezoidal velocity.

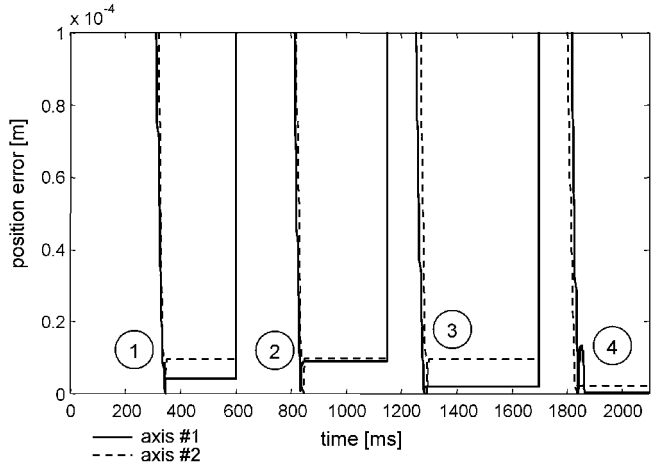

Figure 4.9 Accuracy at which the target is reached using trapezoidal velocity motion planner. The figure shows four consecutive targets (1, 2, 3, 4). Kinematic bounds $a = 0.2$ m/s^2 and $v = 0.01$ m/s.

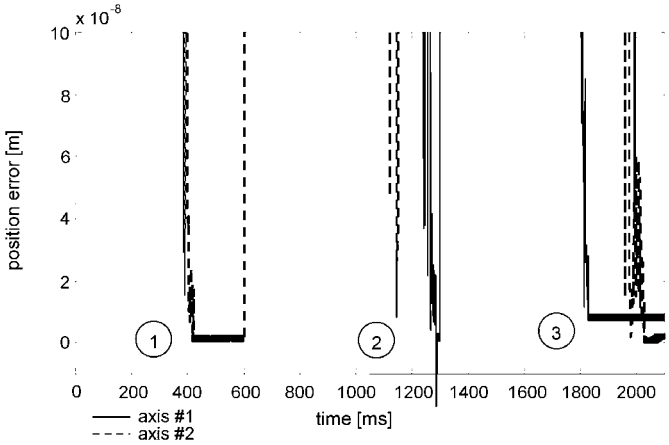

Figure 4.10 Accuracy at which the target is reached using trapezoidal acceleration motion planner. The figure shows three consecutive targets (1, 2, 3). Kinematic bounds: $j = 15$ m/s^3, $a = 0.2$ m/s^2, and v = 0.01 m/s.

4.6 Control simulations

Control simulations provide typical outcomes of a modeled system under reactive motions using the developed algorithms. The chattering acceleration of trapezoidal

velocity algorithm and typical oscillations of the trapezoidal acceleration algorithm may affect the motion and thus it is desirable to observe the results.

The control simulation is done on a modeled mini double pendulum or two link planar arms. The model is based on a microsurgical assisting arms to which this motion planning development is initially purposed for. The mini model is arranged as two link planar arms having mass concentrated at each ends $M_1 = 0.99$ kg, $M_2 = 0.125$ kg, of the length $L_1 = 0.075$ m, $L_2 = 0.095$ m.

Dynamic of the system can be presented as

$$M(q)\ddot{q} + H(q,\dot{q}) = \tau \tag{4.4}$$

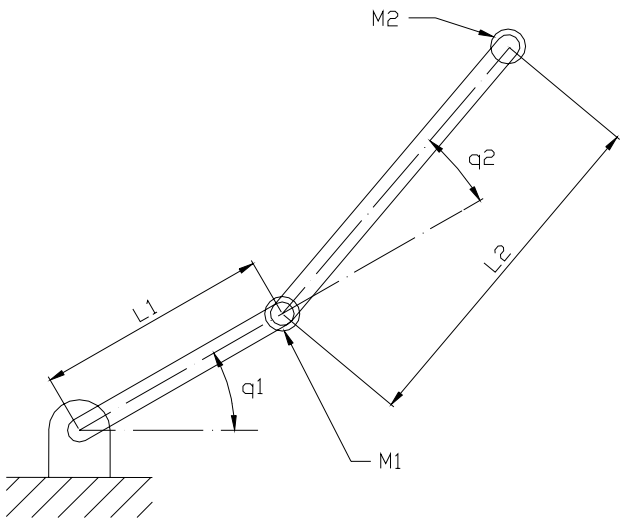

Figure 4.11 Mini two link planar model.

where $M(q)$ is mass matrix and H is components consisting Corriolis $V(q,\ \dot{q})\dot{q}$. The gravity component is zero for planar case. By choosing input-output error as

$$e = q_r - q$$

$$\dot{e} = \dot{q}_r - \dot{q}$$

where q_r and $\dot{q}_r$ is reference position and velocity, q and $\dot{q}$ as actual position and velocity, and by selecting simple path tracking PD controller

$$\tau_i = P_i e_i + D_i \dot{e}_i \quad ;\ i = 1, 2 \tag{4.5}$$

it is expected that through careful selection of control parameters, the system will be able to track the desired motion satisfactorily.

By choosing PD controller constants as **P** = diag(10, 10) Nm/rad and **D** = diag(0.3,0.15) Nm s/rad with corresponding *cut-off* and *corner frequency* approximately 60 rad/sec (3.18 Hz) and 300 rad/sec (47.75 Hz)—far below the sampling rate 1000 Hz—a filtered result can be expected. Figure 4.13 shows the result of the simulations. The figure shows that the chattering effect can be filtered.

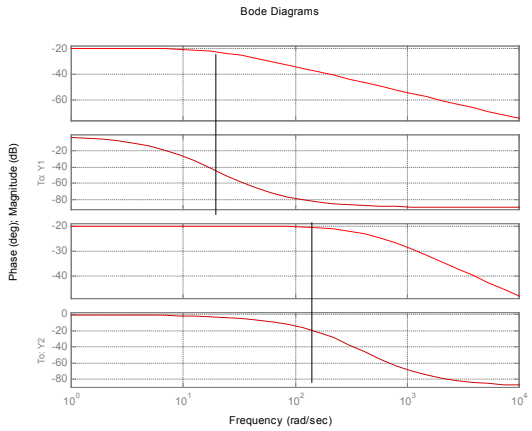

Figure 4.12 PD controller frequency response. Vertical lines marks the corner frequency

The trapezoidal acceleration motion planning algorithm clearly shows that although the chattering acceleration still exists, however the magnitude has been suppressed significantly. Under the same PD controller, overall, it yields smaller tracking error (Figure 4.14); note the smaller standard deviation. The bounded jerk also suppresses acceleration overshoots. In addition the results also show better accuracy at about 100 times of trapezoidal velocity result.

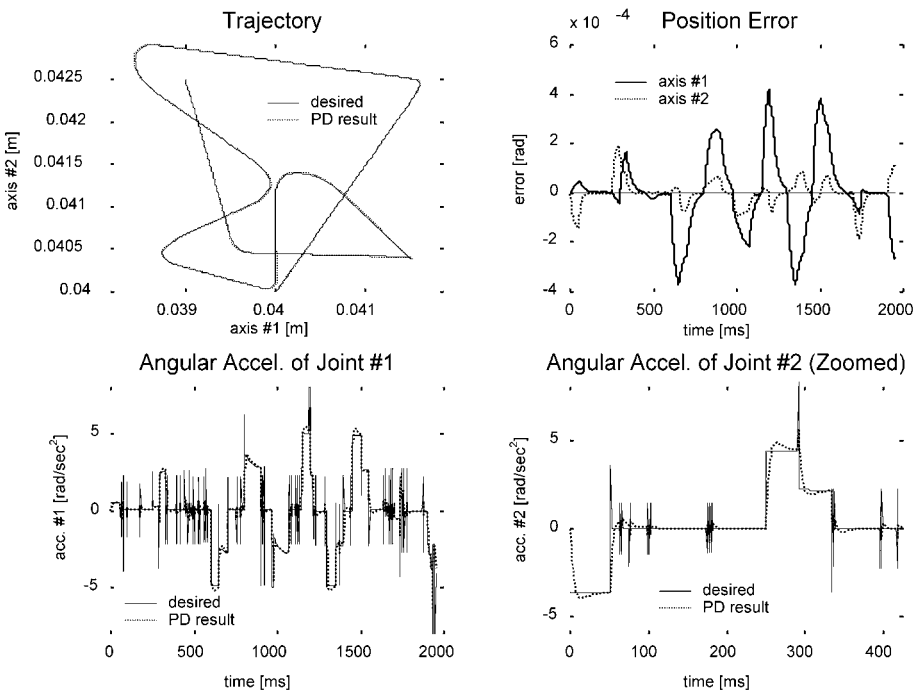

final pos error: (0.000007, -0.000016) m

stderr q1 = 0.000152 rad	; stderr q2 = 0.000053 rad	; mean1 = 0.000001 rad	; mean2 = 0.000001 rad
stderr qv1 = 0.003688 rad/s	; stderr qv2 = 0.001970 rad/s	; mean1 = -0.000013 rad/s	; mean2 = 0.000007 rad/s
stderr qa1 = 1.027570 rad/s^2	; stderr qa2 = 1.431937 rad/s^2	; mean1 = -0.003763 rad/s^2	; mean2 = 0.003370 rad/s^2

Figure 4.13 Control simulation result using trapezoidal velocity algorithm

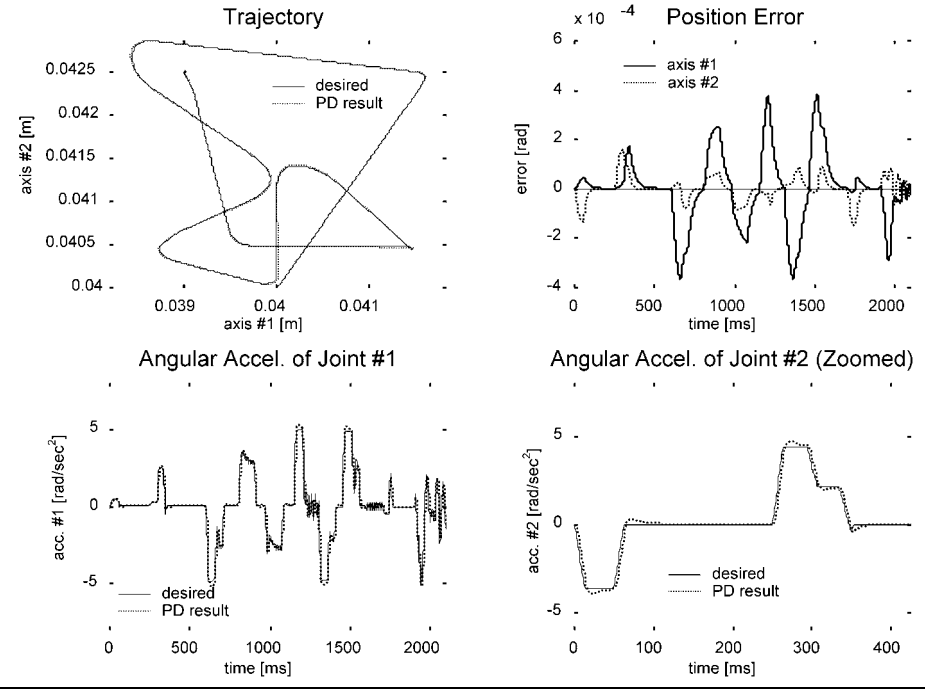

final pos error: (0.0000000379, -0.0000002579) m

stderr q1 = 0.000142 rad	stderr q2 = 0.000047 rad	; mean1 = -0.000001 rad	; mean2 = 0.000001 rad
stderr qv1 = 0.003689 rad/s	stderr qv2 = 0.002021 rad/s	; mean1 = 0.000018 rad/s	; mean2 = -0.000021 rad/s
stderr qa1 = 0.399439 rad/s^2	stderr qa2 = 0.338192 rad/s^2	; mean1 = 0.001115 rad/s^2	; mean2 = -0.001157 rad/s^2

Figure 4.14 Control simulation result using trapezoidal acceleration algorithm

Simulations on one shot point to point movement also shows different motion ends. Under the same kinematic bounds, trapezoidal velocity has a jumping termination with drastic end. Trapezoidal acceleration in other hand shows smoother ending condition with curly motions. Figure 4.15 shows the comparison.

The difference comes from different ending condition on the algorithm. The trapezoidal velocity is terminated at very high jerk when target is considerably achieved, while trapezoidal acceleration is in controlled jerk smoothly approaching the target. The figure also shows significant accuracy difference between the two algorithms.

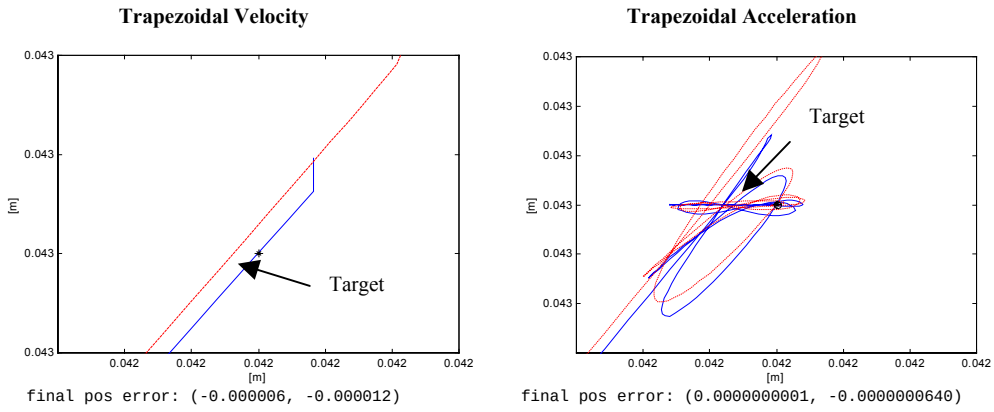

Figure 4.15 Zoomed view of typical motion ends of trapezoidal velocity (left) and trapezoidal acceleration (right). Solid line is the desired motion from the algorithm, dashed line is simulated motion of mini two links planar arm.

4.7 Collision prevention simulation

The collision prevention algorithm also has been simulated. Assuming the distance to obstacle is known from the sensory information, this simple algorithm effectively prevents collision with obstacle as in Figure 4.16. If there is enough free space to go, i.e. the distance to obstacle is larger than a safe free distance/space, the motion is continued and braked otherwise. In some cases the robot will start to brake, then notice that more free space is available while moving along the object and so continues and passes the object (Figure 4.17).

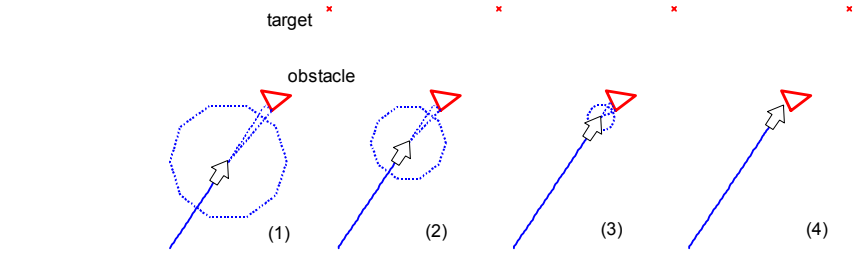

Figure 4.16 Braking is performed to prevent direct collision with blocking obstacle

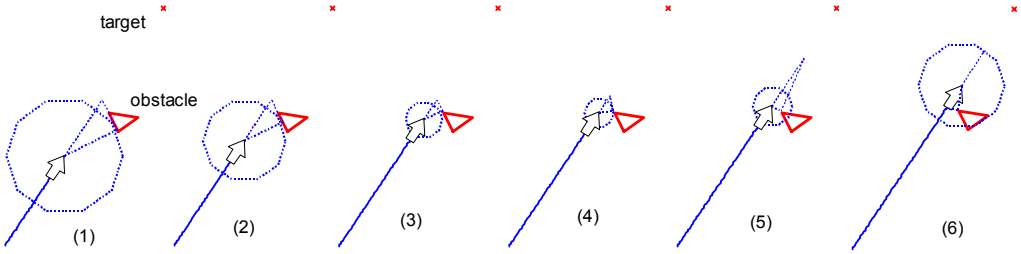

Figure 4.17 Motion is continued when available free space is confirmed.

Chaper 5

Typical Application

5.1 Point to point on two actuators

The algorithm is originally developed for a robotic assistant for microvascular surgery [70]. The surgeon's task is to stitch and join back the severed body vessels. This operation has to be performed under microscope and typically lasts for 4-6 hours. Currently, a human assistant is helping the surgeon during this tedious and exhausting operation. The assistant has to hold the vessels or handling tools precisely for long periods. Robot with its superiority in precise handling will become an effective replacement for the human assistant. The motion planning becomes important to enables the robot to efficiently perform the desired gestures and to reach sensor-guided suturing/cutting/holding location.

The manipulator designed for this application is a two link planar manipulator equipped with two mini DC motors (Faulhaber Minimotor 1016006G) capable of running at max. speed of 18400 rpm, with 2667:1 gear ratio, encoder resolution of 10 counts/rev. and controlled at 1 kHz with a Pentium 133 MHz PC. The given task simply is to realize point to point motions using simple PID joint controller. The PID parameters of the joint controller are: P = diag(13, 13) V/count, I = diag(400, 400) V/s count and D = diag(0.0001,0.0001) Vs/count.

Figure 5.1 shows a typical result of the experiment using the algorithms. The experiments show that the motion planner with trapezoidal velocity profile exhibits sudden changes of acceleration, what results in oscillations. The limited jerk of the

trapezoidal acceleration motion planning algorithm significantly suppress the oscillations and so the tracking error. This result confirms the efficiency of the jerk bound to minimize the vibrations close to the target.

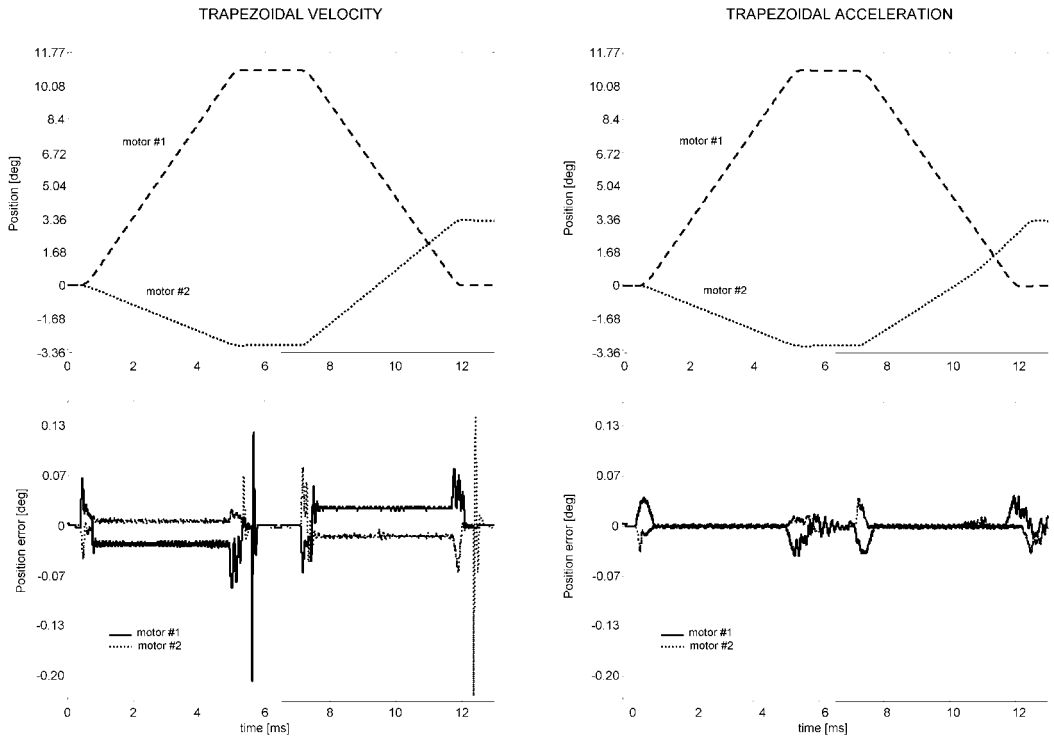

Figure 5.1 Result of point to point motion on a actuators of microsurgical assisting robot. Note the smaller error at the phase transitions of trapezoidal acceleration algorithm.

5.2 Sensor based passive visual tracking using gimbal/pitch-yaw robot

A real sensor based experiments are also conducted. The experiment realizes a passive guided visual tracking and interception of an object moving arbitrarily in Cartesian planar surface. The algorithms perform dynamic trajectory generation to reach the moving object/target subject to a set of joint actuator kinematic bounds

The equipments are a two-degree of freedom gimbal mechanism, a POLARIS^{TM} optotrack system, and a laser pointer as a virtual target pointer/trapper. The gimbal mechanism has two adjacent perpendicular rotation axis correspond to “yaw” and “pitch” axis. A laser pointer is attached adjacent to the other gimbal rotation center (i.e. align to the third axis or the “roll” axis). The laser ray points to the object position. By

swiveling right–left or up–down, the mechanism guides the laser ray for tracking the arbitrary moving object. For simplification, a white board is placed parallel to the yaw axis to allow the object moves in a parallel surface. The object location is tracked and given by the POLARIS^{TM} Optotrack System. This optical-tracking system capable to perform object tracking at refresh rate of approximately 150 ms. The object must carry an 'active device' to make it track-able. The active device emits infrared signal to the POLARIS tracking unit. Figure 5.2 below shows the experiment arrangement.

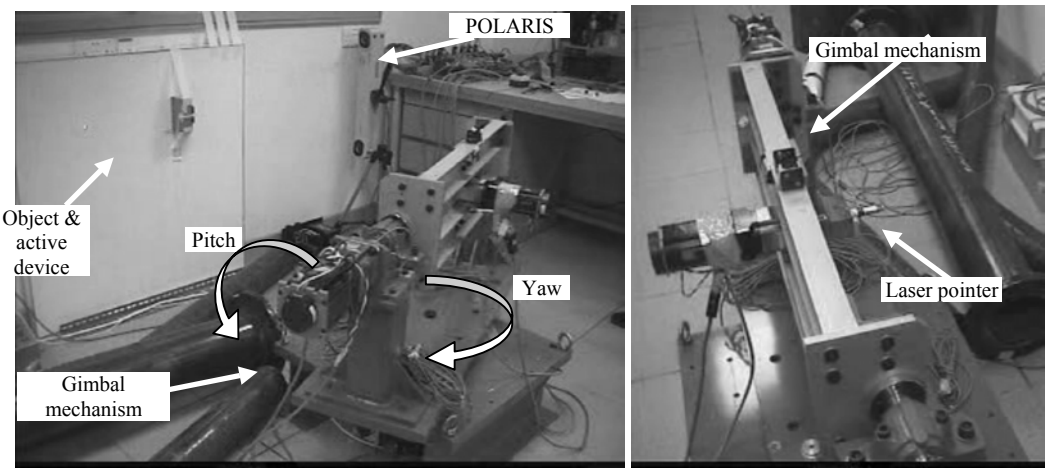

Figure 5.2 Sensor based passive visual tracking experiment setup.

The actuators of the gimbal mechanism are HATHAWAY brushless DC motors type QBO3401A00HE coupled with a 1,000 counts/rev digital encoder and 100:1 reduction gear. For safety reason the motor speed is limited to 114,000 counts/s or equal to 1710 rpm from its maximum speed, 1750 rpm.

There are two tracking test conditions, a fast object motion and slow object motion. In each condition both trapezoidal algorithms track the arbitrary object movement. To get a similar target movement for both algorithms, the object movement is recorded. The kinematic bounds setting are also different in each condition, i.e. high and low setting for each condition. Through these combinations, it is expected to see different tracking characteristics for each condition.

5.2.1. Fast object motion.

In this experiment, the object is moving on the surface up to 550 mm/s. The gimbal directs the laser ray to track and intercept the position of the object. Figure 5.3 shows the results of the tracking trajectory (in Cartesian space), the tracking trajectory (in joint space), and the tracking error of each algorithm. The tracking error is the difference between reference/desired motor position generated by the planner algorithms with the actual actuator position.

The left graphs represent trapezoidal velocity algorithm result, whereas the right represents trapezoidal acceleration. Since the tracking error is considerably small, the dotted line either in the Cartesian and joint space tracking graphs, i.e. the first and second row graphs, depict the reference and the actual position; whereas the solid line depicts the actual object position obtained form POLARIS. The actual tracking error is given in the third row graphs.

At first set of experiment, the joint kinematic bounds are set as v = 7,000 counts/s (corresponds to 6.3 º/s), a = 20,000 counts/s^2 (18 º/s^2), and for trapezoidal acceleration j = 80,000 counts/s^3 (72 º/s^3). Secondly, in Figure 5.4, the kinematic bounds is increased sixteen times to v = 114,000 counts/s (100.8 º/s), a = 20,000 counts/s^2 (288 º/s^2), and for trapezoidal acceleration j = 1,280,000 counts/s^3 (1152 º/s^3).

5.2.2 Slow object motion.

In this experiment, the object is moving up to 225 mm/s. The same experiment kinematic bounds settings and the same graphs representation are applied in this slow object movement experiment. The 20 seconds of results are given in Figure 5.5 and 5.6 respectively for low kinematic bounds (v = 7,000 counts/s,

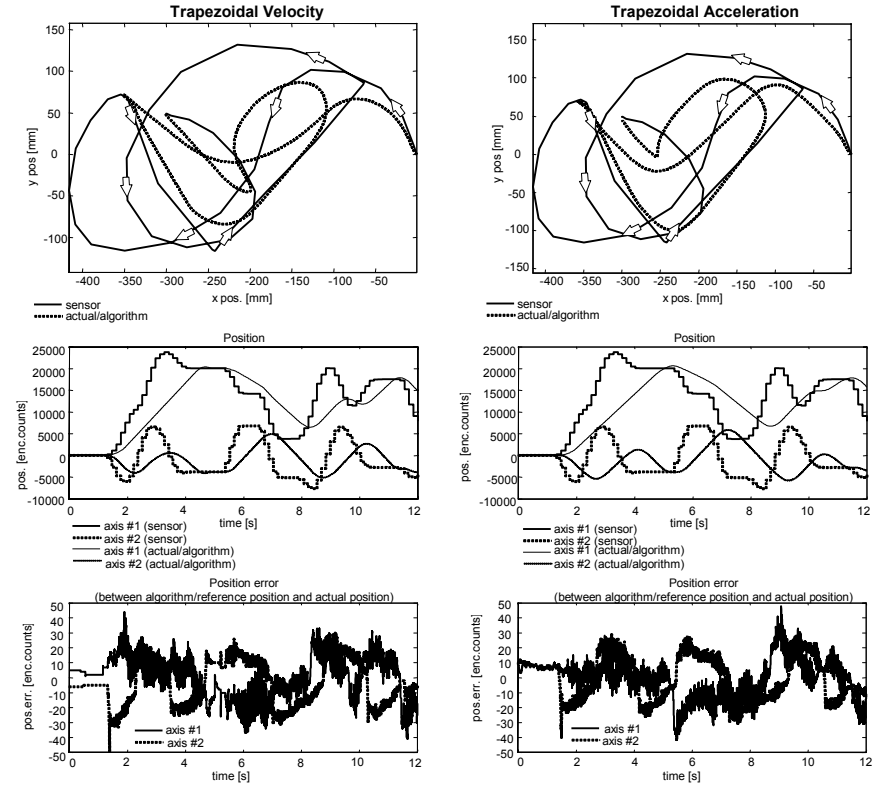

» std(err1) 13.3776
» std(err2) 15.9271

» std(err1) 13.0395
» std(err2) 15.4620

Figure 5.3 Experiment result of tracking fast moving target on low kinematic bounds. Left graphs are results of trapezoidal velocity algorithm, right graphs are trapezoidal acceleration's.

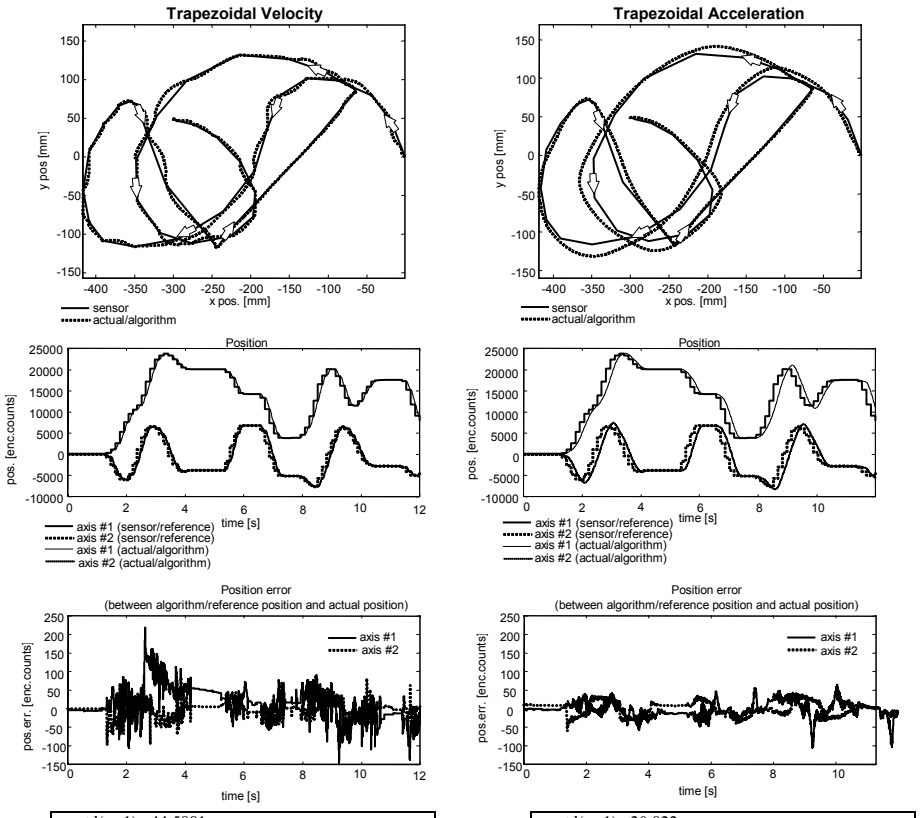

» std(err1) 44.5881
» std(err2) 20.1925

» std(err1) 20.822
» std(err2) 18.3221

Figure 5.4 Experiment result of tracking fast moving target on high kinematic bounds.

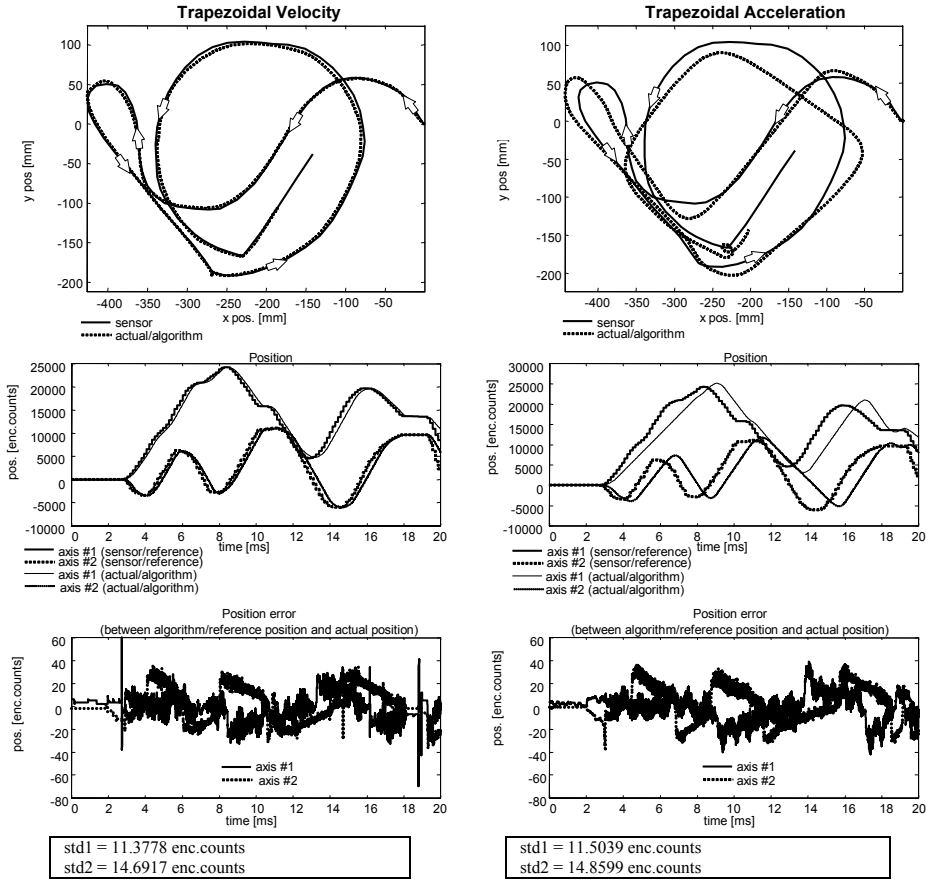

Figure 5.5 Experiment result of tracking slow moving target on low kinematic bounds.

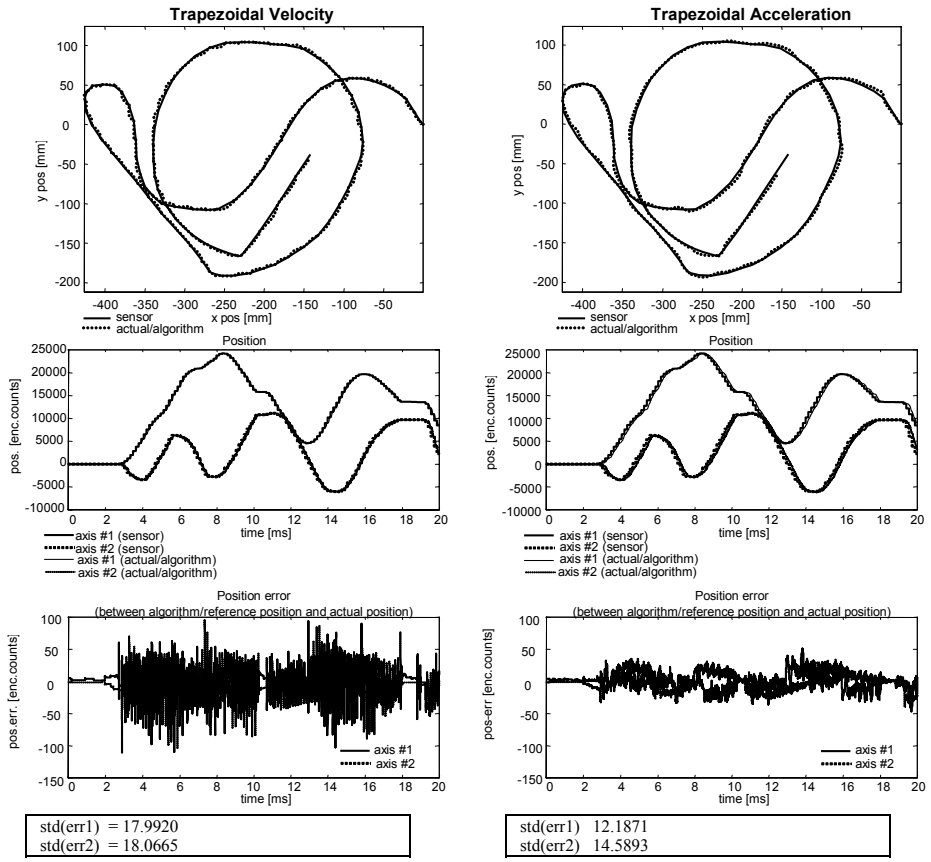

Figure 5.6 Experiment result of tracking slow moving target on high kinematic bounds.

a = 20,000 counts/s^2 and for trapezoidal acceleration j = 80,000 counts/s^3) and sixteen times higher kinematic bounds (v = 114,000 counts/s, a = 20,000 counts/s^2, and for trapezoidal acceleration j = 1,280,000 counts/s3).

5.2.3 Comparison

The algorithms are applicable satisfactorily for sensor based system. It is shown that the two algorithms are able to track arbitrary moving object. At 150 ms sensor refresh rate the algorithms dynamically generate trajectory towards the object and eventually intercept it.

At low kinematic bounds the robot experiences action lags in tracking target change either for fast or slow object movement. The lag is longer for trapezoidal acceleration as a result of the bounded jerk. Only when the object also moves slowly the trapezoidal velocity algorithm considerably can keep pace with target position changes. Therefore, trapezoidal velocity is merely sufficient for slow sensor based application. Meanwhile trapezoidal acceleration will be able to minimize the lag with higher jerk limit.

Overall, the tracking error with low kinematic bounds setting is about the same for both algorithms. Trapezoidal acceleration however is able to minimize the error spikes that are common in trapezoidal velocity applications.

More noticable tracking error suppression is shown by the trapezoidal acceleration algorithm in high kinematic bounds applications. Respectively, higher kinematic bounds also allow faster response to track the fast moving object. However, the error suppressions through the jerk limitation appear at a cost on small response lags which still can be notified at some turning points. As a consequence, in comparison to trapezoidal velocity on the same kinematic limits, the bounded jerk eventually will give bigger tracking offset between the target trail and the generated trajectory. For

fast sensor based applications trapezoidal acceleration algorithm is suitable to obtain a fast, smooth and relatively accurate tracking performance.

Chaper 6

Conclusion

6.1 Summary of work

Motion planning is an important element in robot control. Motion planning allows the robot to define the efficient and effective trajectory to achieve the goal position. Motion planning, when associated with sensor-based applications, opens new interests and challenges.

Sensor based motion planning extends system capability beyond pick and place or one shot point to point applications. Sensor based motion planning, in conjunction with the sensory information process, allows the system to accommodate input from the surrounding and perform the desirable motion response. To certain extent sensor-based motion planning advances the system intelligent.

The development of sensor based motion planning is detailed in this work. Related works, despite their particular achievements, typically and mostly are aiming on a global and task oriented solutions under dynamics considerations, which nevertheless requires very intensive computation and restricts the application scope. Here, the developed algorithms offer a simpler view and faster process while still offer optimality in kinematical consideration.

First, prior to develop sensor–based motion planning algorithm, a critical analysis is given to provide a comparison of common motion planning profiles under several performance measures. Among the critical points for sensor-based applications, are the computation cost and reliability within optimality consideration. For instance, by

offering faster computation the system is expected to allow real-time response against the changes of the requirements provided by sensory information.

Secondly, based on the analysis, the sensor based motion planner algorithms are developed. The algorithms equivalently construct the optimal trapezoidal profiles through series of conditionals, i.e. trapezoidal velocity and trapezoidal acceleration motion planning algorithms.

Third, simulations are done to find out the performance of the developed algorithms. Upon a complete analysis in one-dimensional analysis, the simulation is also done in multidimensional implementation under MATLAB and 3D graphical simulation program.

At last, typical sensor based application is also done to find out actual performance. Real-time experiments are carried out using a 2-axis gimbal mechanism with passive visual tracking using POLARIS optotrack system on actual arbitrary moving object.

6.2 Results

The critical analysis over motion planning profiles is given. It is found that polynomials, despite offering some advantages, are lacking in optimality, reliability, and flexibility especially in applications to reactive planning in sensor-based application. Cubic profile is simple; and quintic offers the best smoothness. However these two polynomial types lack in optimality as both can not control or satisfy the kinematic bounds simultaneously. A chosen criterion for characterizing a profile does not always convey reliability. Other motion parameters may not be controllable; moreover, it may still violate the selected kinematic bound criterion. Cubic, although considerably applicable with a low computation cost and comparable to trapezoidal velocity's, it still lacks on optimality. Quintic requires numerical solution to address

flexible/reactive planning, involving millions or trillions of arithmetic operations. This high computation cost may become a basic consideration when one wants to apply it for a fast reactive motion planning algorithm.

On the other hand, the developed algorithms appear to be desirable as they offer low computation cost, flexibility, reliability, and optimality with respect to actuator's kinematic bounds. Using simple series of conditionals, the algorithms offer optimality by simultaneously satisfying the given kinematic bounds as fast as possible either in one shot or reactive planning. The conditionals also make the algorithm reliable by giving fast response directly using given kinematic bounds as planning parameters. The simple conditionals are cascaded without the need of numerical solution. By implementing simple scaling method it is possible to generate coordinated motion for multidimensional sensor based applications in minimum computation cost.

The trapezoidal velocity offers a simple algorithm that is suitable for slow application. Although it is comparable to cubic, it offers better control over the trajectory generation. However, as cubic also does, it has infinite jerks in starting/turning/braking points. This lack may affect the smoothness and tracking accuracy in typical sensor based applications. However, the simulations and the experiments show that for slow applications the algorithm appears to be satisfactory.

The trapezoidal acceleration, in the other hand, offers better smoothness by controlling and limiting the jerk. However it appears that the jerk bound would give longer response lag. The jerk also should be chosen carefully as to minimize the response lag and prevent erratic oscillations. The algorithm achieves high planning accuracy as it continuously oscillates around the target until the least possible movement. Overall, as it is proven in the simulations and the experiments, for a fast dynamic target interception in sensor based application, the algorithm is suitable by offering fast

response, excellent smoothness and accuracy. The tracking error could be significantly minimized while the system is able to move fast and maintain the kinematic bounds.

6.3 Future works

It is regretful that for many reasons the author could not completely implement and apply the algorithm on what it is initially developed for, a microsurgery assisting robot. However, the actuator device in one experiment is taken from the assisting robot. Both algorithms would be suitable for the task as it has been working well in the typical sensor based simulation and experiment. By considering a real position and orientation planning, it would be desirable as a future work to implement and find out a complete performance analysis on multidimensional sensor based applications.

Although it is proven with successful result in simulation level, the collision prevention should be later intensively tested in real application. It could complement and support the intelligent feature of a system such as collision avoidance algorithms.

There also remain some points of profile analysis that are still beyond this work. Recall the mentioned points in Chapter 2, there are unsolved formulations onto which a selected criterion is still applicable. It would be helpful to know further characteristics of profiles especially in conjunction with real-time reactive motion planning.

Appendix A

A.1 Related quintic profile equations

Maximum velocity equation for nonzero to zero quintic profile

$$v = \left(-\frac{5(a_s T^2 + 6v_s T - 12q_f)\left(8a_s T^3 - 60q_f T + \left(36T^2 v_s \pm \sqrt{(-8a_s T^3 - 36v_s T^2 + 60q_f T)^2 - 4T^4 a_s (10a_s T^2 + 60v_s T - 120q_f)}\right)\right)^4}{32T^5 (10a_s T^2 + 60v_s T - 120q_f)^4} - \right.$$
$$\frac{(-3a_s T^2 - 16v_s T + 30q_f)\left(8a_s T^3 - 60q_f T + \left(36T^2 v_s \pm \sqrt{(-8a_s T^3 - 36v_s T^2 + 60q_f T)^2 - 4T^4 a_s (10a_s T^2 + 60v_s T - 120q_f)}\right)\right)^3}{4T^4 (10a_s T^2 + 60v_s T - 120q_f)^3} -$$
$$\frac{3(3a_s T^2 + 12v_s T - 20q_f)\left(8a_s T^3 - 60q_f T + \left(36T^2 v_s \pm \sqrt{(-8a_s T^3 - 36v_s T^2 + 60q_f T)^2 - 4T^4 a_s (10a_s T^2 + 60v_s T - 120q_f)}\right)\right)^2}{8T^3 (10a_s T^2 + 60v_s T - 120q_f)^2} +$$
$$\left. \frac{a_s \left(8a_s T^3 - 60q_f T + \left(36T^2 v_s \pm \sqrt{(-8a_s T^3 - 36v_s T^2 + 60q_f T)^2 - 4T^4 a_s (10a_s T^2 + 60v_s T - 120q_f)}\right)\right)}{2(10a_s T^2 + 60v_s T - 120q_f)} + v_s \right)$$

…(A.1)

Maximum acceleration equation for nonzero to zero quintic profile

$$a = \left(-\frac{\left(6a_s T^3 + 32v_s T^2 - 60q_f T - \sqrt{2}\sqrt{3a_s^2 T^4 + 42a_s v_s T^3 + 152v_s^2 T^2 - 80a_s q_f T^2 - 600q_f v_s T + 600q_f^2}\, T\right)^3}{100T^5 (a_s T^2 + 6v_s T - 12q_f)^2} - \frac{1}{50T^4 (a_s T^2 + 6v_s T - 12q_f)^2} \right.$$
$$\left(3\left(-3a_s T^2 - 16v_s T + 30q_f\right)\left(6a_s T^3 + 32v_s T^2 - 60q_f T - \sqrt{2}\sqrt{3a_s^2 T^4 + 42a_s v_s T^3 + 152v_s^2 T^2 - 80a_s q_f T^2 - 600q_f v_s T + 600q_f^2}\, T\right)^2\right) -$$
$$\left. \frac{3(3a_s T^2 + 12v_s T - 20q_f)\left(6a_s T^3 + 32v_s T^2 - 60q_f T - \sqrt{2}\sqrt{3a_s^2 T^4 + 42a_s v_s T^3 + 152v_s^2 T^2 - 80a_s q_f T^2 - 600q_f v_s T + 600q_f^2}\, T\right)}{10T^3 (a_s T^2 + 6v_s T - 12q_f)} + a_s \right)$$

…(A.2)

Maximum jerk for nonzero to zero quintic profile under using $t = 0$

$$j = -\frac{9a_s T^2 + 36T v_s - 60q_f}{T^3} \qquad \text{(A.3a)}$$

Maximum jerk for nonzero to zero quintic profile under using $t = T$

$$j = -\frac{3a_s T^2 + 24T v_s - 60q_f}{T^3} \qquad \text{(A.3b)}$$

Maximum jerk for nonzero to zero quintic profile under using its extrema root

$$j = -\frac{1800q_f^2 - 120q_f T(2a_s T + 15v_s)}{5T^3(-12q_f + a_s T^2 + 6v_s T)} + \frac{3T^2(3a_s^2 T^2 + 42a_s T v_s + 152v_s^2)}{5T^3(-12q_f + a_s T^2 + 6v_s T)} \qquad \text{(A.3c)}$$

Movement time T under maximum jerk criterion using root of (A.3a)

$$T = \frac{1}{6j}\left(-18a_s + 2^{2/3}\sqrt[3]{-1458a_s^3 + 2916 j v_s a_s + 1620 j^2 q_f + \sqrt{4(108 j v_s - 81 a_s^2)^3 + 26244(-9a_s^3 + 18 j v_s a_s + 10 j^2 q_f)^2}} + \frac{63^{2/3}(3a_s^2 - 4 j v_s)}{\sqrt[3]{-9a_s^3 + 18 j v_s a_s + 2\left(5q_f j^2 + \sqrt{j^2(-45 q_f a_s^3 - 27 v_s^2 a_s^2 + 90 j q_f v_s a_s + 48 j v_s^3 + 25 j^2 q_f^2)}\right)}}\right) \quad \text{(A.3d}$$

Movement time T under maximum jerk criterion using root of (A.3b)

$$T = \frac{1}{j}\left(-a_s + \sqrt[3]{-a_s^3 + 12 j v_s a_s + 30 j^2 q_f + \sqrt{(a_s^3 - 12 j v_s a_s - 30 j^2 q_f)^2 - (a_s^2 - 8 j v_s)^3}} + \frac{a_s^2 - 8 j v_s}{\sqrt[3]{-a_s^3 + 12 j v_s a_s + 30 j^2 q_f + \sqrt{(a_s^3 - 12 j v_s a_s - 30 j^2 q_f)^2 - (a_s^2 - 8 j v_s)^3}}}\right) \quad \text{(A.3e)}$$

Movement time T under maximum jerk criterion using jerk profile extrema is the numerical root of

$$0 = (5 j a_s T^5 - 9 a_s^2 T^4 + 30 j v_s T^4 - 60 j q_f T^3 - 126 a_s v_s T^3 - 456 v_s^2 T^2 + 240 a_s q_f T^2 + 1800 q_f v_s T - 1800 q_f^2) \quad \text{(A.3f)}$$

Total jerk measure for nonzero to zero quintic profile with $t_1 \geq 0$

$$\int_0^T |j(t)|dt = \frac{1}{25T^2(T(Ta_s + 6v_s) - 12q_f)^2}\left(-25a_s^3 T^6 + 12a_s^2\left(50q_f - 25Tv_s + \sqrt{2(3T^2a_s^2 + 42Tv_s a_s + 152v_s^2)T^2 - 80q_f(2Ta_s + 15v_s)T + 1200q_f^2}\right)T^4 - 4a_s\left(900q_f^2 + 20\left(4\sqrt{2(3T^2a_s^2 + 42Tv_s a_s + 152v_s^2)T^2 - 80q_f(2Ta_s + 15v_s)T + 1200q_f^2} - 45Tv_s\right)q_f + 3Tv_s\left(75Tv_s - 14\sqrt{2(3T^2a_s^2 + 42Tv_s a_s + 152v_s^2)T^2 - 80q_f(2Ta_s + 15v_s)T + 1200q_f^2}\right)\right)T^2 + 32\left(75q_f^2 - 75Tv_s q_f + 19T^2v_s^2\right)\sqrt{2(3T^2a_s^2 + 42Tv_s a_s + 152v_s^2)T^2 - 80q_f(2Ta_s + 15v_s)T + 1200q_f^2}\right) \quad \text{(A.4a)}$$

Total jerk measure for nonzero to zero quintic profile with $t_1 < 0$

$$\int_0^T |j(t)|dt = \left(\frac{1}{25T^2(T(Ta_s + 6v_s) - 12q_f)^2}\left(\left(6a_s T^2 + 32v_s T - 60q_f - \sqrt{2(3T^2a_s^2 + 42Tv_s a_s + 152v_s^2)T^2 - 80q_f(2Ta_s + 15v_s)T + 1200q_f^2}\right)\left(600q_f^2 - 10\left(20a_s T^2 + 3\left(24Tv_s + \sqrt{2(3T^2a_s^2 + 42Tv_s a_s + 152v_s^2)T^2 - 80q_f(2Ta_s + 15v_s)T + 1200q_f^2}\right)\right)q_f + T\left(12a_s^2 T^3 + 3a_s\left(36Tv_s + \sqrt{2(3T^2a_s^2 + 42Tv_s a_s + 152v_s^2)T^2 - 80q_f(2Ta_s + 15v_s)T + 1200q_f^2}\right)T + 16v_s\left(13Tv_s + \sqrt{2(3T^2a_s^2 + 42Tv_s a_s + 152v_s^2)T^2 - 80q_f(2Ta_s + 15v_s)T + 1200q_f^2}\right)\right)\right) - a_s\right) \quad \text{…(A.4b)}$$

Total energy (acceleration) measure for nonzero to zero quintic profile with $t_1 \geq 0$

$$\int_0^T |a(t)|^2 dt = \left(-\frac{1}{500\,T^2\,(T(T\,a_s + 6\,v_s) - 12\,q_f)^3} \right.$$
$$\left(1620000\,T\,q_f{}^4 + 27000\left(-16\,a_s\,T^3 - 104\,v_s\,T^2 + \sqrt{(8\,a_s\,T^3 + 36\,v_s\,T^2 - 60\,q_f\,T)^2 - 40\,T^4\,a_s\,(a_s\,T^2 + 6\,v_s\,T - 12\,q_f)}\right)q_f{}^3 + \right.$$
$$1800\,T\left(19\,a_s{}^2\,T^4 + 306\,a_s\,v_s\,T^3 + 1008\,v_s{}^2\,T^2 - 3\,a_s\sqrt{(8\,a_s\,T^3 + 36\,v_s\,T^2 - 60\,q_f\,T)^2 - 40\,T^4\,a_s\,(T(T\,a_s + 6\,v_s) - 12\,q_f)}\;T - \right.$$
$$\left.25\,v_s\sqrt{(8\,a_s\,T^3 + 36\,v_s\,T^2 - 60\,q_f\,T)^2 - 40\,T^4\,a_s\,(T(T\,a_s + 6\,v_s) - 12\,q_f)}\right)q_f{}^2 +$$
$$60\,T^2\left(-12\,a_s{}^3\,T^5 + 2\,a_s\,v_s\left(53\sqrt{(8\,a_s\,T^3 + 36\,v_s\,T^2 - 60\,q_f\,T)^2 - 40\,T^4\,a_s\,(a_s\,T^2 + 6\,v_s\,T - 12\,q_f)} - 1944\,T^2\,v_s\right)T + \right.$$
$$18\,v_s{}^2\left(23\sqrt{(8\,a_s\,T^3 + 36\,v_s\,T^2 - 60\,q_f\,T)^2 - 40\,T^4\,a_s\,(a_s\,T^2 + 6\,v_s\,T - 12\,q_f)} - 480\,T^2\,v_s\right) +$$
$$\left.a_s{}^2\left(7\,T^2\sqrt{(8\,a_s\,T^3 + 36\,v_s\,T^2 - 60\,q_f\,T)^2 - 40\,T^4\,a_s\,(a_s\,T^2 + 6\,v_s\,T - 12\,q_f)} - 468\,T^4\,v_s\right)\right)q_f -$$
$$T^3\left(9\,a_s{}^4\,T^6 + 36\,a_s{}^2\,v_s\left(7\sqrt{(8\,a_s\,T^3 + 36\,v_s\,T^2 - 60\,q_f\,T)^2 - 40\,T^4\,a_s\,(a_s\,T^2 + 6\,v_s\,T - 12\,q_f)} - 159\,T^2\,v_s\right)T^2 + \right.$$
$$1824\,a_s\,v_s{}^2\left(\sqrt{(8\,a_s\,T^3 + 36\,v_s\,T^2 - 60\,q_f\,T)^2 - 40\,T^4\,a_s\,(a_s\,T^2 + 6\,v_s\,T - 12\,q_f)} - 18\,T^2\,v_s\right)T +$$
$$216\,v_s{}^3\left(21\sqrt{(8\,a_s\,T^3 + 36\,v_s\,T^2 - 60\,q_f\,T)^2 - 40\,T^4\,a_s\,(a_s\,T^2 + 6\,v_s\,T - 12\,q_f)} - 256\,T^2\,v_s\right) +$$
$$\left.\left.\left.4\,a_s{}^3\left(3\,T^3\sqrt{(8\,a_s\,T^3 + 36\,v_s\,T^2 - 60\,q_f\,T)^2 - 40\,T^4\,a_s\,(a_s\,T^2 + 6\,v_s\,T - 12\,q_f)} - 62\,T^5\,v_s\right)\right)\right)\right)\right)$$

…(A.5a)

Total energy (acceleration) measure for nonzero to zero quintic profile with $t_1 < 0$

$$\int_0^T |a(t)|^2 dt = \frac{1}{125\,T^2\,(T(T\,a_s + 6\,v_s) - 12\,q_f)^3}\left(\left(\left(125\,v_s\,T^5 + 6\sqrt{(8\,a_s\,T^3 + 36\,v_s\,T^2 - 60\,q_f\,T)^2 - 40\,T^4\,a_s\,(a_s\,T^2 + 6\,v_s\,T - 12\,q_f)}\;T^3\right)a_s{}^3 + \right.\right.$$
$$18\,T^2\,v_s\left(125\,v_s\,T^2 + 7\sqrt{(8\,a_s\,T^3 + 36\,v_s\,T^2 - 60\,q_f\,T)^2 - 40\,T^4\,a_s\,(a_s\,T^2 + 6\,v_s\,T - 12\,q_f)}\right)a_s{}^2 +$$
$$12\,T\,v_s{}^2\left(1125\,v_s\,T^2 + 76\sqrt{(8\,a_s\,T^3 + 36\,v_s\,T^2 - 60\,q_f\,T)^2 - 40\,T^4\,a_s\,(a_s\,T^2 + 6\,v_s\,T - 12\,q_f)}\right)a_s +$$
$$\left.108\,v_s{}^3\left(250\,v_s\,T^2 + 21\sqrt{(8\,a_s\,T^3 + 36\,v_s\,T^2 - 60\,q_f\,T)^2 - 40\,T^4\,a_s\,(a_s\,T^2 + 6\,v_s\,T - 12\,q_f)}\right)\right)T^3 -$$
$$30\,q_f\left(\left(150\,v_s\,T^4 + 7\sqrt{(8\,a_s\,T^3 + 36\,v_s\,T^2 - 60\,q_f\,T)^2 - 40\,T^4\,a_s\,(a_s\,T^2 + 6\,v_s\,T - 12\,q_f)}\;T^2\right)a_s{}^2 + \right.$$
$$2\,T\,v_s\left(900\,v_s\,T^2 + 53\sqrt{(8\,a_s\,T^3 + 36\,v_s\,T^2 - 60\,q_f\,T)^2 - 40\,T^4\,a_s\,(a_s\,T^2 + 6\,v_s\,T - 12\,q_f)}\right)a_s +$$
$$\left.18\,v_s{}^2\left(300\,v_s\,T^2 + 23\sqrt{(8\,a_s\,T^3 + 36\,v_s\,T^2 - 60\,q_f\,T)^2 - 40\,T^4\,a_s\,(a_s\,T^2 + 6\,v_s\,T - 12\,q_f)}\right)\right)T^2 +$$
$$900\,q_f{}^2\left(3\,T\,a_s\left(20\,v_s\,T^2 + \sqrt{(8\,a_s\,T^3 + 36\,v_s\,T^2 - 60\,q_f\,T)^2 - 40\,T^4\,a_s\,(a_s\,T^2 + 6\,v_s\,T - 12\,q_f)}\right) + \right.$$
$$\left.5\,v_s\left(72\,v_s\,T^2 + 5\sqrt{(8\,a_s\,T^3 + 36\,v_s\,T^2 - 60\,q_f\,T)^2 - 40\,T^4\,a_s\,(a_s\,T^2 + 6\,v_s\,T - 12\,q_f)}\right)\right)T -$$
$$\left.13500\,q_f{}^3\left(16\,v_s\,T^2 + \sqrt{(8\,a_s\,T^3 + 36\,v_s\,T^2 - 60\,q_f\,T)^2 - 40\,T^4\,a_s\,(a_s\,T^2 + 6\,v_s\,T - 12\,q_f)}\right)\right)$$

…(A.5b)

A.2 Related modified quintic profile equations

Maximum acceleration equation for nonzero to zero modified quintic profile

$$a = \left(-\left(5\left(-\mathrm{af}\,T^2 + a_s\,T^2 + 6\,v_s\,T - 12\,q_f\right)\left(8\,\mathrm{af}\,T^3 - 12\,a_s\,T^3 - 64\,v_s\,T^2 + 120\,q_f\,T + \right.\right.\right.$$
$$\left.\left.\sqrt{(-8\,\mathrm{af}\,T^3 + 12\,a_s\,T^3 + 64\,v_s\,T^2 - 120\,q_f\,T)^2 - 4\,(10\,\mathrm{af}\,T^2 - 10\,a_s\,T^2 - 60\,v_s\,T + 120\,q_f)\,(\mathrm{af}\,T^4 - 3\,a_s\,T^4 - 12\,v_s\,T^3 + 20\,q_f\,T^2)}\right)\text{^}3\Big)\Big/$$
$$\left(4\,T^5\left(10\,\mathrm{af}\,T^2 - 10\,a_s\,T^2 - 60\,v_s\,T + 120\,q_f\right)^3\right) - \left(3\left(2\,\mathrm{af}\,T^2 - 3\,a_s\,T^2 - 16\,v_s\,T + 30\,q_f\right)\left(8\,\mathrm{af}\,T^3 - 12\,a_s\,T^3 - 64\,v_s\,T^2 + 120\,q_f\,T + \right.\right.$$
$$\left.\left.\sqrt{(-8\,\mathrm{af}\,T^3 + 12\,a_s\,T^3 + 64\,v_s\,T^2 - 120\,q_f\,T)^2 - 4\,(10\,\mathrm{af}\,T^2 - 10\,a_s\,T^2 - 60\,v_s\,T + 120\,q_f)\,(\mathrm{af}\,T^4 - 3\,a_s\,T^4 - 12\,v_s\,T^3 + 20\,q_f\,T^2)}\right)\text{^}2\Big)\Big/$$
$$\left(2\,T^4\left(10\,\mathrm{af}\,T^2 - 10\,a_s\,T^2 - 60\,v_s\,T + 120\,q_f\right)^2\right) - \left(3\left(-\mathrm{af}\,T^2 + 3\,a_s\,T^2 + 12\,v_s\,T - 20\,q_f\right)\left(8\,\mathrm{af}\,T^3 - 12\,a_s\,T^3 - 64\,v_s\,T^2 + 120\,q_f\,T + \right.\right.$$
$$\left.\left.\sqrt{(-8\,\mathrm{af}\,T^3 + 12\,a_s\,T^3 + 64\,v_s\,T^2 - 120\,q_f\,T)^2 - 4\,(10\,\mathrm{af}\,T^2 - 10\,a_s\,T^2 - 60\,v_s\,T + 120\,q_f)\,(\mathrm{af}\,T^4 - 3\,a_s\,T^4 - 12\,v_s\,T^3 + 20\,q_f\,T^2)}\right)\Big)\Big/$$
$$\left.\left(2\,T^3\left(10\,\mathrm{af}\,T^2 - 10\,a_s\,T^2 - 60\,v_s\,T + 120\,q_f\right)\right) + a_s\right)$$

…(A.6a)

Maximum velocity equation for nonzero to zero modified quintic profile

$$
\begin{aligned}
v = \Bigg(& -\frac{1}{4000\,T^5\,(12\,q_f + T\,(\mathrm{af}\,T - a_z\,T - 6\,v_z))^4}\Big(\big(-\mathrm{af}\,T^2 + a_z\,T^2 + 6\,v_z\,T - 12\,q_f\big) \\
& \Big(\big(2^{2/3}\big(\big(3\,\mathrm{af}^2\,T^2 + 3\,a_z{}^2\,T^2 + 42\,a_z\,v_z\,T - 2\,\mathrm{af}\,(2\,T\,a_z + 19\,v_z)\,T + 152\,v_z{}^2\big)\,T^2 + 40\,q_f\,(2\,\mathrm{af}\,T - 2\,a_z\,T - 15\,v_z)\,T + 600\,q_f{}^2\big)\,T^2\big)\Big/ \\
& \big(\big(-2\,\mathrm{af}^3\,T^9 - 2\,a_z{}^3\,T^9 + 2\,\mathrm{af}^2\,(2\,T\,(T\,a_z - 3\,v_z) - 15\,q_f)\,T^7 + 6\,a_z{}^2\,(5\,q_f - 7\,T\,v_z)\,T^7 - 896\,v_z{}^3\,T^6 + \\
& 12\,a_z\,v_z\,(55\,q_f - 27\,T\,v_z)\,T^6 + 2\,\mathrm{af}\,\big(2\,a_z{}^2\,T^3 + 33\,a_z\,v_z\,T^2 + 6\,v_z\,(28\,T\,v_z - 55\,q_f)\big)\,T^6 + 3600\,q_f\,v_z{}^2\,T^5 - 3600\,q_f{}^2\,v_z\,T^4 + \\
& \sqrt{2}\,\sqrt{\big(T^6\big(\big(5\,(20\,q_f + T\,(\mathrm{af}\,T - 3\,a_z\,T - 12\,v_z))\,(12\,q_f + T\,(\mathrm{af}\,T - a_z\,T - 6\,v_z)) - 2\,(30\,q_f + T\,(2\,\mathrm{af}\,T - 3\,a_z\,T - 16\,v_z)\big)^2\big)\hat{}\,3 + \\
& 2\,T^2\big(\mathrm{af}^3\,T^5 + a_z{}^3\,T^5 + \mathrm{af}^2\big(-2\,a_z\,T^2 + 6\,v_z\,T + 15\,q_f\big)\,T^3 + 3\,a_z{}^2\,(7\,T\,v_z - 5\,q_f)\,T^3 + 6\,a_z\,v_z\,(27\,T\,v_z - 55\,q_f)\,T^2 - \\
& \mathrm{af}\,\big(2\,a_z{}^2\,T^3 + 33\,a_z\,v_z\,T^2 + 6\,v_z\,(28\,T\,v_z - 55\,q_f)\big)\,T^2 + 8\,v_z\,\big(225\,q_f{}^2 - 225\,T\,v_z\,q_f + 56\,T^2\,v_z{}^2\big)\big)\hat{}\,2\big)\big)\big)\hat{}\,(1/3)\big) - \\
& 2\,(30\,q_f + T\,(2\,\mathrm{af}\,T - 3\,a_z\,T - 16\,v_z))\,T + \sqrt[3]{2}\,\big(-2\,\mathrm{af}^3\,T^9 - 2\,a_z{}^3\,T^9 + 2\,\mathrm{af}^2\,(2\,T\,(T\,a_z - 3\,v_z) - 15\,q_f)\,T^7 + 6\,a_z{}^2\,(5\,q_f - 7\,T\,v_z)\,T^7 - \\
& 896\,v_z{}^3\,T^6 + 12\,a_z\,v_z\,(55\,q_f - 27\,T\,v_z)\,T^6 + 2\,\mathrm{af}\,\big(2\,a_z{}^2\,T^3 + 33\,a_z\,v_z\,T^2 + 6\,v_z\,(28\,T\,v_z - 55\,q_f)\big)\,T^6 + 3600\,q_f\,v_z{}^2\,T^5 - 3600\,q_f{}^2\,v_z \\
& T^4 + \sqrt{2}\,\sqrt{\big(T^6\big(\big(5\,(20\,q_f + T\,(\mathrm{af}\,T - 3\,a_z\,T - 12\,v_z))\,(12\,q_f + T\,(\mathrm{af}\,T - a_z\,T - 6\,v_z)) - 2\,(30\,q_f + T\,(2\,\mathrm{af}\,T - 3\,a_z\,T - 16\,v_z)\big)^2\big)\hat{}\,3 + \\
& 2\,T^2\big(\mathrm{af}^3\,T^5 + a_z{}^3\,T^5 + \mathrm{af}^2\big(-2\,a_z\,T^2 + 6\,v_z\,T + 15\,q_f\big)\,T^3 + 3\,a_z{}^2\,(7\,T\,v_z - 5\,q_f)\,T^3 + 6\,a_z\,v_z\,(27\,T\,v_z - 55\,q_f)\,T^2 - \\
& \mathrm{af}\,\big(2\,a_z{}^2\,T^3 + 33\,a_z\,v_z\,T^2 + 6\,v_z\,(28\,T\,v_z - 55\,q_f)\big)\,T^2 + 8\,v_z\,\big(225\,q_f{}^2 - 225\,T\,v_z\,q_f + 56\,T^2\,v_z{}^2\big)\big)\hat{}\,2\big)\big)\big)\hat{}\,(1/3)\big)\hat{}\,4\Big) + \\
& \frac{1}{500\,T^4\,(12\,q_f + T\,(\mathrm{af}\,T - a_z\,T - 6\,v_z))^3}\Big(\big(2\,\mathrm{af}\,T^2 - 3\,a_z\,T^2 - 16\,v_z\,T + 30\,q_f\big)\Big(\big(2^{2/3}\big(\big(3\,\mathrm{af}^2\,T^2 + 3\,a_z{}^2\,T^2 + 42\,a_z\,v_z\,T - \\
& 2\,\mathrm{af}\,(2\,T\,a_z + 19\,v_z)\,T + 152\,v_z{}^2\big)\,T^2 + 40\,q_f\,(2\,\mathrm{af}\,T - 2\,a_z\,T - 15\,v_z)\,T + 600\,q_f{}^2\big)\,T^2\big)\Big/ \\
& \big(\big(-2\,\mathrm{af}^3\,T^9 - 2\,a_z{}^3\,T^9 + 2\,\mathrm{af}^2\,(2\,T\,(T\,a_z - 3\,v_z) - 15\,q_f)\,T^7 + 6\,a_z{}^2\,(5\,q_f - 7\,T\,v_z)\,T^7 - 896\,v_z{}^3\,T^6 + 12\,a_z\,v_z\,(55\,q_f - 27\,T\,v_z)\,T^6 + \\
& 2\,\mathrm{af}\,\big(2\,a_z{}^2\,T^3 + 33\,a_z\,v_z\,T^2 + 6\,v_z\,(28\,T\,v_z - 55\,q_f)\big)\,T^6 + 3600\,q_f\,v_z{}^2\,T^5 - 3600\,q_f{}^2\,v_z\,T^4 + \\
& \sqrt{2}\,\sqrt{\big(T^6\big(\big(5\,(20\,q_f + T\,(\mathrm{af}\,T - 3\,a_z\,T - 12\,v_z))\,(12\,q_f + T\,(\mathrm{af}\,T - a_z\,T - 6\,v_z)) - 2\,(30\,q_f + T\,(2\,\mathrm{af}\,T - 3\,a_z\,T - 16\,v_z)\big)^2\big)\hat{}\,3 + \\
& 2\,T^2\big(\mathrm{af}^3\,T^5 + a_z{}^3\,T^5 + \mathrm{af}^2\big(-2\,a_z\,T^2 + 6\,v_z\,T + 15\,q_f\big)\,T^3 + 3\,a_z{}^2\,(7\,T\,v_z - 5\,q_f)\,T^3 + 6\,a_z\,v_z\,(27\,T\,v_z - 55\,q_f)\,T^2 - \\
& \mathrm{af}\,\big(2\,a_z{}^2\,T^3 + 33\,a_z\,v_z\,T^2 + 6\,v_z\,(28\,T\,v_z - 55\,q_f)\big)\,T^2 + 8\,v_z\,\big(225\,q_f{}^2 - 225\,T\,v_z\,q_f + 56\,T^2\,v_z{}^2\big)\big)\hat{}\,2\big)\big)\big)\hat{}\,(1/3)\big) - \\
& 2\,(30\,q_f + T\,(2\,\mathrm{af}\,T - 3\,a_z\,T - 16\,v_z))\,T + \sqrt[3]{2}\,\big(-2\,\mathrm{af}^3\,T^9 - 2\,a_z{}^3\,T^9 + 2\,\mathrm{af}^2\,(2\,T\,(T\,a_z - 3\,v_z) - 15\,q_f)\,T^7 + 6\,a_z{}^2\,(5\,q_f - 7\,T\,v_z)\,T^7 - \\
& 896\,v_z{}^3\,T^6 + 12\,a_z\,v_z\,(55\,q_f - 27\,T\,v_z)\,T^6 + 2\,\mathrm{af}\,\big(2\,a_z{}^2\,T^3 + 33\,a_z\,v_z\,T^2 + 6\,v_z\,(28\,T\,v_z - 55\,q_f)\big)\,T^6 + 3600\,q_f\,v_z{}^2\,T^5 - 3600\,q_f{}^2\,v_z\,T^4 + \\
& \sqrt{2}\,\sqrt{\big(T^6\big(\big(5\,(20\,q_f + T\,(\mathrm{af}\,T - 3\,a_z\,T - 12\,v_z))\,(12\,q_f + T\,(\mathrm{af}\,T - a_z\,T - 6\,v_z)) - 2\,(30\,q_f + T\,(2\,\mathrm{af}\,T - 3\,a_z\,T - 16\,v_z)\big)^2\big)\hat{}\,3 + \\
& 2\,T^2\big(\mathrm{af}^3\,T^5 + a_z{}^3\,T^5 + \mathrm{af}^2\big(-2\,a_z\,T^2 + 6\,v_z\,T + 15\,q_f\big)\,T^3 + 3\,a_z{}^2\,(7\,T\,v_z - 5\,q_f)\,T^3 + 6\,a_z\,v_z\,(27\,T\,v_z - 55\,q_f)\,T^2 - \\
& \mathrm{af}\,\big(2\,a_z{}^2\,T^3 + 33\,a_z\,v_z\,T^2 + 6\,v_z\,(28\,T\,v_z - 55\,q_f)\big)\,T^2 + 8\,v_z\,\big(225\,q_f{}^2 - 225\,T\,v_z\,q_f + 56\,T^2\,v_z{}^2\big)\big)\hat{}\,2\big)\big)\big)\hat{}\,(1/3)\big)\hat{}\, \\
& 3\Big) - \frac{1}{200\,T^3\,(12\,q_f + T\,(\mathrm{af}\,T - a_z\,T - 6\,v_z))^2}\Big(3\big(-\mathrm{af}\,T^2 + 3\,a_z\,T^2 + 12\,v_z\,T - 20\,q_f\big) \\
& \Big(\big(2^{2/3}\big(\big(3\,\mathrm{af}^2\,T^2 + 3\,a_z{}^2\,T^2 + 42\,a_z\,v_z\,T - 2\,\mathrm{af}\,(2\,T\,a_z + 19\,v_z)\,T + 152\,v_z{}^2\big)\,T^2 + 40\,q_f\,(2\,\mathrm{af}\,T - 2\,a_z\,T - 15\,v_z)\,T + 600\,q_f{}^2\big)\,T^2\big)\Big/ \\
& \big(\big(-2\,\mathrm{af}^3\,T^9 - 2\,a_z{}^3\,T^9 + 2\,\mathrm{af}^2\,(2\,T\,(T\,a_z - 3\,v_z) - 15\,q_f)\,T^7 + 6\,a_z{}^2\,(5\,q_f - 7\,T\,v_z)\,T^7 - 896\,v_z{}^3\,T^6 + \\
& 12\,a_z\,v_z\,(55\,q_f - 27\,T\,v_z)\,T^6 + 2\,\mathrm{af}\,\big(2\,a_z{}^2\,T^3 + 33\,a_z\,v_z\,T^2 + 6\,v_z\,(28\,T\,v_z - 55\,q_f)\big)\,T^6 + 3600\,q_f\,v_z{}^2\,T^5 - 3600\,q_f{}^2\,v_z\,T^4 + \\
& \sqrt{2}\,\sqrt{\big(T^6\big(\big(5\,(20\,q_f + T\,(\mathrm{af}\,T - 3\,a_z\,T - 12\,v_z))\,(12\,q_f + T\,(\mathrm{af}\,T - a_z\,T - 6\,v_z)) - 2\,(30\,q_f + T\,(2\,\mathrm{af}\,T - 3\,a_z\,T - 16\,v_z)\big)^2\big)\hat{}\,3 + \\
& 2\,T^2\big(\mathrm{af}^3\,T^5 + a_z{}^3\,T^5 + \mathrm{af}^2\big(-2\,a_z\,T^2 + 6\,v_z\,T + 15\,q_f\big)\,T^3 + 3\,a_z{}^2\,(7\,T\,v_z - 5\,q_f)\,T^3 + 6\,a_z\,v_z\,(27\,T\,v_z - 55\,q_f)\,T^2 - \\
& \mathrm{af}\,\big(2\,a_z{}^2\,T^3 + 33\,a_z\,v_z\,T^2 + 6\,v_z\,(28\,T\,v_z - 55\,q_f)\big)\,T^2 + 8\,v_z\,\big(225\,q_f{}^2 - 225\,T\,v_z\,q_f + 56\,T^2\,v_z{}^2\big)\big)\hat{}\,2\big)\big)\big)\hat{}\,(1/3)\big)\hat{}\,2\Big) - \\
& \frac{1}{10\,(12\,q_f + T\,(\mathrm{af}\,T - a_z\,T - 6\,v_z))}\Big(a_z\,\Big(\big(2^{2/3}\big(\big(3\,\mathrm{af}^2\,T^2 + 3\,a_z{}^2\,T^2 + 42\,a_z\,v_z\,T - 2\,\mathrm{af}\,(2\,T\,a_z + 19\,v_z)\,T + 152\,v_z{}^2\big)\,T^2 + \\
& 40\,q_f\,(2\,\mathrm{af}\,T - 2\,a_z\,T - 15\,v_z)\,T + 600\,q_f{}^2\big)\,T^2\big)\Big/ \\
& \big(\big(-2\,\mathrm{af}^3\,T^9 - 2\,a_z{}^3\,T^9 + 2\,\mathrm{af}^2\,(2\,T\,(T\,a_z - 3\,v_z) - 15\,q_f)\,T^7 + 6\,a_z{}^2\,(5\,q_f - 7\,T\,v_z)\,T^7 - 896\,v_z{}^3\,T^6 + 12\,a_z\,v_z\,(55\,q_f - 27\,T\,v_z)\,T^6 + \\
& 2\,\mathrm{af}\,\big(2\,a_z{}^2\,T^3 + 33\,a_z\,v_z\,T^2 + 6\,v_z\,(28\,T\,v_z - 55\,q_f)\big)\,T^6 + 3600\,q_f\,v_z{}^2\,T^5 - 3600\,q_f{}^2\,v_z\,T^4 + \\
& \sqrt{2}\,\sqrt{\big(T^6\big(\big(5\,(20\,q_f + T\,(\mathrm{af}\,T - 3\,a_z\,T - 12\,v_z))\,(12\,q_f + T\,(\mathrm{af}\,T - a_z\,T - 6\,v_z)) - 2\,(30\,q_f + T\,(2\,\mathrm{af}\,T - 3\,a_z\,T - 16\,v_z)\big)^2\big)\hat{}\,3 + \\
& 2\,T^2\big(\mathrm{af}^3\,T^5 + a_z{}^3\,T^5 + \mathrm{af}^2\big(-2\,a_z\,T^2 + 6\,v_z\,T + 15\,q_f\big)\,T^3 + 3\,a_z{}^2\,(7\,T\,v_z - 5\,q_f)\,T^3 + 6\,a_z\,v_z\,(27\,T\,v_z - 55\,q_f)\,T^2 - \\
& \mathrm{af}\,\big(2\,a_z{}^2\,T^3 + 33\,a_z\,v_z\,T^2 + 6\,v_z\,(28\,T\,v_z - 55\,q_f)\big)\,T^2 + 8\,v_z\,\big(225\,q_f{}^2 - 225\,T\,v_z\,q_f + 56\,T^2\,v_z{}^2\big)\big)\hat{}\,2\big)\big)\big)\hat{}\,(1/3)\big) - \\
& 2\,(30\,q_f + T\,(2\,\mathrm{af}\,T - 3\,a_z\,T - 16\,v_z))\,T + \sqrt[3]{2}\,\big(-2\,\mathrm{af}^3\,T^9 - 2\,a_z{}^3\,T^9 + 2\,\mathrm{af}^2\,(2\,T\,(T\,a_z - 3\,v_z) - 15\,q_f)\,T^7 + 6\,a_z{}^2\,(5\,q_f - 7\,T\,v_z)\,T^7 - \\
& 896\,v_z{}^3\,T^6 + 12\,a_z\,v_z\,(55\,q_f - 27\,T\,v_z)\,T^6 + 2\,\mathrm{af}\,\big(2\,a_z{}^2\,T^3 + 33\,a_z\,v_z\,T^2 + 6\,v_z\,(28\,T\,v_z - 55\,q_f)\big)\,T^6 + 3600\,q_f\,v_z{}^2\,T^5 - 3600\,q_f{}^2\,v_z\,T^4 + \\
& \sqrt{2}\,\sqrt{\big(T^6\big(\big(5\,(20\,q_f + T\,(\mathrm{af}\,T - 3\,a_z\,T - 12\,v_z))\,(12\,q_f + T\,(\mathrm{af}\,T - a_z\,T - 6\,v_z)) - 2\,(30\,q_f + T\,(2\,\mathrm{af}\,T - 3\,a_z\,T - 16\,v_z)\big)^2\big)\hat{}\,3 + \\
& 2\,T^2\big(\mathrm{af}^3\,T^5 + a_z{}^3\,T^5 + \mathrm{af}^2\big(-2\,a_z\,T^2 + 6\,v_z\,T + 15\,q_f\big)\,T^3 + 3\,a_z{}^2\,(7\,T\,v_z - 5\,q_f)\,T^3 + 6\,a_z\,v_z\,(27\,T\,v_z - 55\,q_f)\,T^2 - \\
& \mathrm{af}\,\big(2\,a_z{}^2\,T^3 + 33\,a_z\,v_z\,T^2 + 6\,v_z\,(28\,T\,v_z - 55\,q_f)\big)\,T^2 + 8\,v_z\,\big(225\,q_f{}^2 - 225\,T\,v_z\,q_f + 56\,T^2\,v_z{}^2\big)\big)\hat{}\,2\big)\big)\big)\hat{}\,(1/3)\big)\Big) + v_z\Bigg\}
\end{aligned}
$$

…(A.6b)

References

[1] Yoram Koren, *Computer Control of Manufacturing Systems*, McGraw-Hill, 1985.

[2] Raven, Francis H., *Automatic Control Engineering*, McGraw-Hill, 1995.

[3] Fu, K.S, Gonzales, R.C, Lee, C.S.G, *Robotics Control, Sensing, Vision, and Intelligence*, McGraw-Hill, 1987.

[4] Sciavicco, L., Siciliano, B., *Modeling and Control of Robot Manipulator*, McGraw-Hill, 1996).

[5] Craig, J.J, *Robotics Mechanics and Control*, Addison-Wesley, 1989.

[6] Waerden, B.L.van der., "A History of Algebra, From al-Khwarizmi to Emmy Noether", Springer-Verlag, 1985.

[7] King, R. Bruce, "Beyond the Quartic Equation" Birkhauser, 1996.

[8] Pugh, A., *Robot Sensors***,** Bedford, IFS, 1985.

[9] Ruocco, S.R., *Robot Sensors and Transducers***,** Halsted Press; Milton Keynes, Open University Press , 1987.

[10] Bunke, H., Kanade, T., Noltemeier, H., "Modelling and planning for sensor based intelligent robot systems", World Scientific , 1995

[11] Crawford, L.S., "A Dextrous Master for Telesurgery," Masters thesis, UC Berkeley, December 1993

[12] Robotic Industries Association, ANSI/RIA, R15.06-1992, Standard, 1992

[13] Luthiger, J., Burdet, E., "A Modular and Sensor-Oriented Motion Planner" *Robotica* 17 : 87-95, 1999.

[14] Burdet, E., Luthiger, J, "Optimal and Flexible Motion Planning*"* internal report ETH Zurich, 1994.

[15] Burdet, E., Luthiger, J, "Coordination learning of robot movements with vision processes*" Robotica* 17 : 563-570, 1999.

[16] Bobrow, J.E., "Optimal Robot Path Planning Using the Minimum Time Criterion" *IEEE Journal of Robotics and Automation*, 4 – 4, 1988.

[17] Olomski, J, "Trajectory Planning Optimization and Control for Industrial Robots" *Proc. ICCON '89, IEEE International Conference on*, 1989.

[18] Kempkens, K., Frank, P.M., "Time-optimal Trajectory Planning – An Application to a Commercially Available Robot" *Proc. ICCON '89, IEEE International Conference on*, 1989.

[19] Heinzinger, G., Jacobs, P., Canny, J., Paden, B., "Time-optimal Trajectory for a Robot Manipulator: A Provably Good Approximation Algorithm" *Proc., IEEE International Conference on Robotics & Automation*, 1990.

[20] Gonzales, H.H.B., Gordillo, J.L., "An Algorithm for Planning Time-optimal Trajectory for Given Minimum Distance Path" *Proc., IEEE/RSJ International Conference on Intelligent Robots Systems*, 1993.

[21] Yimin, Z., "Point-to-point Robot Motion Optimization Based on the State Parametrization" *Proc., American Control Conference*, 1994.

[22] Bailin, C., Dodds, G.I., "Time-optimal and Smooth Constrained Path Planning for Robot Manipulator" *Proc., IEEE International Conference on Control*, 2 : 1122-1127,1994.

[23] Wang, Q., Zalzala, A.M.S., "Genetic Control of Near Time-optimal Motion for an Industrial Robot Arm" *Proc., IEEE International Conferece on Robotics & Automation*, 1996.

[24] Leng, D.Y., Mingkuan, C., "Robot Trajectory Planning Using Simulation" *Robotics & Computer-Integrated Manufacturing*, 13 : 121-129, 1997.

[25] Lee, Y.D., Lee, B.H., Kim, H.G., "An Evolutionary Approach for Time Optimal Trajectory Planning of Robotic Manipulator" *Information Sciences*, 113 – (3-4): 245 -260, 1999.

[26] Constantinescu, D., Croft, E.A., "Smooth and Time-optimal Trajectory Planning for Industrial Manipulators along Specified Path" *Journal of Robotic System*, 17 – 5: 233 - 249, 2000.

[27] Constantinescu, D., "Smooth and Time-optimal Trajectory Planning for Industrial Manipulators" *M.A.Sc thesis*, University of British Columbia, 1998.

[28] Singh, S.K., Leu, M.C., "Manipulator Motion Planning in the Presence of Obstacles and Dynamic Constraints" *Journal of Robotic Research*, 10 : 171 - 187, 1991.

[29] Shin, K.G., McKay, N.D., "A Dynamic Programming Approach to Trajectory Planning of Robot Manipulator" *IEEE Transaction on Automatic Control*, 13 – 6 : 491 - 500, 1986.

[30] Weimin, Y., Yugeng, X., "Optimum Motion Planning in Joint Space for Robots Using Genetic Algorithm" *Robotics and Autonomous System*, 18 : 373 - 393, 1996.

[31] Lin, C.S., Chang, P.R., Luh, J.Y.S., "Formulation and Optimization of Cubic Polynomial Trajectory for Industrial Robot" *IEEE Transaction on Automatic Control*, 28 : 1066 - 1073, 1986.

[32] MATHEMATICA™, Wolfram Research Inc., 1997

[33] Press, W.H., Teukolsky, S.A., Vetterling, W.T., Flannery, B.P., "Numerical Recipes in C: The Art of Science Computing", Cambridge 1992.

[34] Miro, J.V., White, A.S., Gill, R., "On-line time-optimal algorithm for manipulator trajectory planning", *Proc. European Control Conference'97* 1997.

[35] Latombe, J.C., *Robot Motion Planning*, Kluwer, 1991

[36] Brady, M., Hollerbach, J., Johnson, T., Lozano-Prez, T., Mason, M., "*Robot Motion: Planning and Control*", MIT Press, Cambridge, MA, 1982.

[37] Canny, J. F., "*The Complexity of Robot Motion Planning*" PhD thesis, MIT Press, Cambridge, MA, 1988.

[38] Sahar, G., Hollerbach, J. M., “Planning of Minimum-Time Trajectories for Robot Arms”, *International Journal of Robotic Research*, 5 – 3 : 90 – 100, 1986.

[39] Wapenhans, H., Holzl, J., Steinle, J., Pfeiffer, F., “Optimal Trajectory Planning with Application to Industrial Robot”, *International Journal of Advanced Manufacturing Technology*, 9 : 49 – 55, 1994.

[40] Tondu, B., Bazaz, S.A., "The three-cubic method: an optimal on-line robot joint trajectory generator under velocity, acceleration and wanderind constraints", *International Journal of Robotics Research*, 18 : 893-901, 1999.

[41] Bazaz, S.A., Tondu, B., "Minimum time on-line joint trajectory generatior based on low order spline method for industrial manipulators", *Robotics and Autonomous Systems*, 29 : 257–268, 1999.

[42] Laubach, S.L., Burdick, J.W., “An autonomous sensor-based path-planner for planetary microrovers *Proc., IEEE International Conferece on Robotics & Automation*, 1 : 347 –354, 1999.

[43] Leven, P., Hutchinson, S., Burschka, D., Färber, G., “Perception based motion planning for indoor exploration”, *Proc., IEEE International Conferece on Robotics & Automation*, 1 : 695-701, 1999.

[44] Lumelsky, V.J., “Effect of kinematics on motion planning for planar robot arms moving amidst unknown obstacles”, *IEEE Journal of Robotics and Automation,* RA3-3 : 207–223, 1987.

[45] Lozano-Perez, T., “A Simple motion planning algorithm for general robot manipulators”, *IEEE Journal of Robotics and Automation*, RA3-3 : 108-120, 1987.

[46] Wikman, T.S., Newman, W.S., “A fast, on-line collision avoidance method for kinematically redundant manipulator based on reflex control”, *Proc*., *IEEE International Conferece on Robotics & Automation*, 1 : 261-266, 1992.

[47] Croft, E.A., Fenton, R.G., Benhabib, B., “An online robot planning strategy for target interception”, *Journal of Robotic Systems*, 15-2 : 97-114, 1998

[48] Croft, E.A., Benhabib, B., Fenton, R.G., "Near-time optimal robot motion planning for on-line applications", *Journal of Robotic Systems*, 12-8 : 553-567, 1995.

[49] Hujic, D., Zak, G., Croft, E., Fenton, R.G., Mills, J.K., Benhabib, B., "Active prediction, planning and execution system for interception of moving objects", *Proc., IEEE International Symposium on Assembly and Task Planning,* 347-352, 1995.

[50] Lin, Z., Zeman, V., Patel, R.V.,"On-line robot trajectory planning for catching a moving object", *Proc., IEEE International Conference on Robotics and Automation*, 3 : 1726-1731, 1989.

[51] Mehrandezh, M., Sela, M.N., Fenton, R.G., Benhabib, B., "Proportional navigation guidance for robotic interception of moving objects", *Journal of Robotic Systems*, 17–6 : 321–340, 2000.

[52] Choi, B.K., Kim, D.W., "Bounded deviation joint path algorithms for piecewise cubic polynomial trajectories", *IEEE Transactions on Systems, Man and Cybernetics*, 20–3 : 725–733, 1990.

[53] Baillieul, J., "Kinematically redundant robots with flexible components", *IEEE Control Systems Magazine,* 13–1 : 15–21, 1993.

[54] Macfarlane, S., Croft, E.A., "Design of jerk bounded trajectories for on-line industrial robot applications", *Proc., IEEE International Conference on Robotics and Automation*, 1 : 979–984, 2001.

[55] Nam, S.H., Oh, S.Y., "Real-time dynamic visual tracking using PSD sensors and extended trapezoidal motion planning", *Applied Intelligence,* 10–1 : 53-70, 1999.

[56] Park, J. S., "Motion profile planning of repetitive point-to-point control for maximum energy conversion efficiency under acceleration conditions", *Mechatronics,* 6–6 : 649–663, 1996

[57] Guarino Lo Bianco, C., Piazzi, A., "Optimal trajectory planning with quintic G-splines", *Proc., IEEE Intelligent Vehicles Symposium*, 620–625, 2000.

[58] Piazzi, A., Visioli, A., “Interval algorithm for minimum-jerk trajectory planning of robot manipulators”, *Proc., IEEE International Conference on Decision and Control*, 2 : 1924–1927, 1997.

[59] Chand, S., Doty, K.L., “On-line polynomial trajectories for industrial robot manipulators”, *Journal of Robotic Research*, 4–2 : 38–48, 1985.

[60] Chang, Y.H.; Lee, T.T.; Liu, C.H., “On-line Cartesian path trajectory planning for robot manipulators, *Proc., IEEE International Conference on Robotics and Automation*, 1 : 62–67, 1988.

[61] Andersson, R.L., “Aggressive trajectory generator for a robot ping-pong player”, *IEEE Control Systems Magazine*, 9–2, 15–21, 1989.

[62] Buttazzo, G.; Allotta, B.; Fanizza, F.P., “Mousebuster: a robot for real-time catching”, *IEEE Control Systems Magazine*, 14–1 : 49–56, 1994.

[63] Wang, F.Y., Lever, P.J.A., ”On-line trajectory planning for autonomous robotic excavation based on force/torque sensor measurements”, *Proc., IEEE International Conference on Multisensor Fusion and Integration for Intelligent Systems*, 371–378, 1994.

[64] Allen, P.K., Timcenko, A., Yoshimi, B., Michelman, P., “Automated tracking and grasping of a moving object with a robotic hand-eye system”, *IEEE Transactions on Robotics and Automation*, 9–2 : 152–164, 1993.

[65] Burdet, E., Sosodoro, Ang, M.H, “Reactive, fast, smooth, and accurate motion planning for sensor based robotics”, *Proc., CIRAS 2001*, 2001.

[66] Kyriakopoulos, K.J., Saridis, G.N., “Minimum jerk path generation”, *Proc., IEEE International Conference on Robotics and Automation,* 1 : 364–369, 1988.

[67] MATLAB™, MathWorks, 1994.

[68] *OpenGL Programming Guide*, Silicon Graphics, 1997

[69] LabWindows/CVI 5.0, National Instruments, 1998

[70] Lee, L.Y., “A Robotic Device of Microvascular Surgeon”, B Eng Thesis, Control and Mechatronics Laboratory, Department of Mechanical Engineering, National University of Singapore, 2000.